Justus Liebig University Giessen

Inaugural Dissertation

Role of carbonic anhydrases 9 and 12 in hypoxia and non-hypoxia induced pulmonary hypertension

to obtain the academic degree of

doctor of natural sciences

- Dr. rer. nat. -

Submitted to the Faculty of Biology and Chemistry

at the Justus Liebig University Giessen

by

Aleksandar Petrovic, MSc

of Belgade, Serbia

Giessen 2024

First Supervisor and Committee Member: **Prof. Dr. Ivan Manzini**

Institute for Animal Physiology, FB 08
Justus Liebig University Giessen
Heinrich-Buff-Ring 38
35392 Giessen, Germany

Second Supervisor and Committee Member: **Prof. Dr. Ralph Schermuly**

Excellence Cluster Cardio-Pulmonary Institute (CPI), Department of Internal Medicine, FB 11 Justus Liebig University Giessen
Aulweg 130
35392 Giessen, Germany

Committee Member: **Prof. Dr. Norbert Weissmann**

Excellence Cluster Cardio-Pulmonary Institute (CPI), Department of Internal Medicine, FB 11 Justus Liebig University Giessen
Aulweg 130
35392 Giessen, Germany

Committee Member: **Prof. Dr. Katja Sträßer**

Institute of Biochemistry, FB 08
Justus Liebig University Giessen
Heinrich-Buff-Ring 17
35392 Giessen, Germany

Date of Doctoral Defence: 20.11.2024

To my parents and sister, the architects of my dreams,
whose love and guidance have shaped this dissertation.

"Science knows no country, because knowledge belongs to humanity, and is the torch which illuminates the world."

Louis Pasteur

Table of Contents

1. INTRODUCTION

1.1. Pulmonary hypertension

1.1.1. Definition and characteristics of pulmonary hypertension

Pulmonary hypertension (PH) is a severe and incurable disease portrayed by pulmonary vascular remodeling and a rise in pulmonary arterial pressure, pulmonary vascular resistance, right ventricular (RV) hypertrophy and ultimately, right heart failure[1-3]. PH represents a significant global health concern, with current estimates indicating a prevalence of approximately 1% of the worldwide population[3]. Although individuals of all age groups can be affected, prevalence tends to be higher among those aged 65 years and older, which is attributed to cardiac and pulmonary underlying factors often associated with PH[3].

During the first World Health Organization meeting on PH in Geneva in 1973, PH was characterized by a mean pulmonary arterial pressure (mPAP) of more than 25 mmHg at rest[4, 5]. At the sixth World Symposium on Pulmonary Hypertension (WSPH) in Nice 2018, the proposed threshold was lowered from 25 to 20 mmHg in accordance with the associated increase in mortality and risk of pulmonary vascular disease development[2, 6]. According to the most recent guidelines from the European Society of Cardiology (ESC) and the European Respiratory Society (ERS), pulmonary hypertension is defined by a mPAP exceeding 20 mmHg at rest[3].

While PH can arise from various underlying causes, including idiopathic factors, genetic predispositions, or secondary conditions such as heart or lung diseases, its common denominator lies in the increased pressure burden on the pulmonary circulation. As a consequence of the elevated mPAP, the right ventricular afterload increases[7]. The adaptation of right ventricular function to elevated afterload, termed RV-arterial coupling, stands as a significant prognostic factor in PH patients[7-9]. Nevertheless, assessing RV-arterial coupling is intricate and invasive, typically involving the analysis of RV pressure-volume relationships. Simplified methods, including echocardiographic and biomarker approaches, are sought-after for future establishment to facilitate easier evaluation of this crucial parameter[10-12].

1.1.2. Classification of PH

Table 1. The classification of pulmonary hypertension, ESC/ERS guidelines 2022[3].

Group 1 Pulmonary arterial hypertension (PAH)
1.1 Idiopathic PAH
1.1.1 Non-responders at vasoreactivity testing
1.1.2 Acute responders at vasoreactivity testing
1.2 Heritable PAH
1.3 Drug- and toxin-induced PAH
1.4 PAH associated with:
1.4.1 Connective tissue disease
1.4.2 HIV infection
1.4.3 Portal hypertension
1.4.4 Congenital heart disease
1.4.5 Schistosomiasis
1.5 PAH with overt features of venous/capillaries (PVOD/PCH) involvement
1.6 Persistent PH of the newborn syndrome
Group 2 PH associated with left heart disease
2.1 PH due to heart failure
2.1.1 with preserved LVEF
2.1.2 with reduced LVEF
2.2 Valvular heart disease
2.3 Congenital/acquired cardiovascular conditions leading to post-capillary PH
Group 3 PH associated with lung diseases and/or hypoxia
3.1 Obstructive lung disease or emphysema
3.2 Restrictive lung disease
3.3 Other lung disease with mixed restrictive/obstructive pattern
3.4 Hypoventilation syndromes
3.5 Hypoxia without lung disease (*e.g.* high altitude)
3.6 Developmental lung disorders
Group 4 PH associated with pulmonary artery obstructions
4.1 Chronic thromboembolic PH
4.2 Other pulmonary artery obstructions
Group 5 PH with unclear and/or multifactorial mechanisms
5.1 Haematological disorders
5.2 Systemic disorders
5.3 Metabolic disorders
5.4 Chronic renal failure with or without haemodialysis
5.5 Pulmonary tumor thrombotic microangiopathy
5.6 Fibrosing mediastinitis

Abbreviations: HIV - human immunodeficiency virus; PVOD - pulmonary veno-occlusive disease; PCH - pulmonary capillary haemangiomatosis; LVEF - left ventricular ejection fraction.

The new clinical classification of pulmonary hypertension (Table 1) was created in the fourth edition of the ESC/ERS Guidelines for diagnosing and treating PH in 2022[3]. Comprehending the complexities of PH requires a thorough understanding of its classification, which consists of five groups distinguished by underlying mechanisms and clinical features. These groups span from pulmonary arterial hypertension (PAH), predominantly impacting the small pulmonary arteries, to

PH linked with left heart disease, lung disorders and/or hypoxia, chronic thromboembolic disease, and other miscellaneous causes. While the initial pathological events may vary across different groups, mechanisms of disease progression and pathological manifestations are frequently shared among them[2]. Each group presents unique challenges in diagnosis, treatment, and prognosis, underscoring the importance of personalized approaches to patient management[13].

1.1.3. Diagnosis and current treatment of PH

The initial symptoms of pulmonary hypertension are nonspecific. They may include exertional dyspnea, fatigue, chest pain, weakness, and syncope, while manifestations like edema, ascites, and abdominal distension often appear in the later stages of the disease[14]. The right heart catheterization (RHC) is considered the gold standard for diagnosing pulmonary hypertension. Additionally, echocardiography is an important non-invasive diagnostic tool for accessing the right heart hypertrophy and hemodynamic parameters. Furthermore, other non-invasive measures, such as 6-minute walking test, chest radiography, circulating brain natriuretic peptide (BNP) and N-terminal pro-BNP (NT-proBNP) are used to predict RV overload and prognosis[14, 15].

While the mean pulmonary arterial pressure (mPAP) is pivotal for diagnosing pulmonary hypertension, additional measurements are necessary for final diagnosis and classification, which is crucial for determining risk assessment and appropriate treatment. To distinguish pre-capillary PH (PAH, group 1) from PH due to the left heart disease (post-capillary PH, group 2), the inclusion of pulmonary vascular resistance (PVR) and pulmonary arterial wedge pressure (PAWP) is essential[2, 3]. A PAWP threshold of less than 15 mmHg and a PVR exceeding 2 Wood units (WU) are recommended for defining the pre-capillary PH. Furthermore, patients are haemodynamically characterized as PAH in the absence of other causes of pre-capillary PH, such as chronic thromboembolic pulmonary hypertension (CTEPH) and PH associated with lung diseases. Post-capillary PH is defined as PAWP higher than 15 mmHg, while PVR delineates between patients with notable pre-capillary component[3].

Despite intensive research unravelling the pathogenesis of PH, the precise mechanisms underlying the disease remain elusive, highlighting the ongoing need for successful therapeutic strategies. Pharmacotherapy remains the cornerstone of PH management, with various classes of medications

targeting different pathways implicated in disease pathogenesis[13, 15, 16]. Over the years, numerous therapeutic options with vasodilatory properties have been explored, including prostacyclin analogues (treprostinil and iloprost), endothelin-receptor antagonists (bosentan and macitentan), calcium channel blockers (nifedipine and diltiazem), phosphodiesterase (PDE)-5 inhibitors (sildenafil and tadalafil) and soluble guanylate cyclase (sGC) stimulators (riociguat)[3, 16]. Combination therapies involving these agents have emerged as an effective strategy for patients with advanced disease or inadequate response to monotherapy.

Although progress in PH therapeutics leads to significantly enhanced quality of life and extended survival for patients with PH, challenges persist, including the need for early detection, individualized treatment algorithms, and novel therapeutic targets. Ongoing research endeavors continue to unravel the complex pathobiology of PH, driving the development of innovative therapies aimed at reversing progressive pulmonary vascular remodeling and right ventricular hypertrophy[3, 15].

1.2. Pulmonary arterial hypertension

1.2.1. Pathophysiology and pathohistology of PAH

At its essence, Group 1 of pulmonary hypertension represents a subset of this complex disease, characterized by elevated blood pressure within the pulmonary arteries due to a plethora of underlying causes[2, 3]. Ranging from idiopathic origins (historically labelled ‘primary’ PH) to connective tissue diseases, and from heritable (familial) manifestations, congenital heart defects to complications induced by medication, the spectrum of conditions contributing to Group 1 PH underscores its diverse nature and clinical importance (Table 1)[3]. PAH involves a multitude of various pathophysiological, molecular and histopathological events and, in many aspects, can be described as a cancer-like disease[17]. That encompasses a combination of pulmonary vascular remodeling, genetic mutations, imbalance of vasoconstrictors and vasodilators, growth factors, proinflammatory mediators, alterations of mitochondrial function, *in situ* thrombosis and the development of complex histopathological features, including neointima and plexiform lesions[17-22].

Most patients with heritable PAH and some forms of IPAH were heterozygous for a mutation in bone morphogenetic protein receptor type 2 (BMPR2), a member of the transforming growth factor (TGF)-β superfamily. Mutations in another member of the TGF-β superfamily, the activin-receptor-like kinase (ALK) 1 gene, can also trigger PH development associated with hereditary hemorrhagic telangiectasia[17, 19, 22]. Peroxisome proliferator-activated receptor gamma (PPARγ) is a transcription factor and a downstream member of the BMPR2 signaling pathway with vasodilatory, pro-apoptotic, anti-proliferative and anti-inflammatory properties and it has been shown that disrupted PPARγ signaling may play a role in the development of pulmonary hypertension[23]. Additionally, activation of various transcription factors has been described in PAH pathology, such as hypoxia-inducible factor (HIF)-1α[24, 25], HIF-2α[26-28], forkhead box protein O1 (FOXO1)[29, 30] and nuclear factor kappa-light-chain-enhancer of activated B cells (NF-κB)[31]. Furthermore, the disruption of homeostasis between vasodilators and vasoconstrictors is extensively documented in the pathophysiology of pulmonary arterial hypertension[17]. PAH patients exhibit elevated production of vasoconstrictors, such as endothelin-1, angiotensin II and thromboxane, while concurrently experiencing reduced levels of vasodilators and anti-proliferative agents, such as nitric oxide (NO) and prostacyclin[17, 32, 33].

Beyond vasoconstriction, PAH is characterized by intricate and progressive morphological transformations across all structural layers of the pulmonary arteries, highlighting pulmonary vascular remodeling as a major hallmark of PAH pathology[17, 18, 21, 34]. Dysregulated proliferation (hyperplasia), migration and resistance to apoptosis within all three layers of pulmonary vascular cells, including endothelial, smooth muscle cells and fibroblasts, contribute to this remodeling process. Furthermore, it has been reported that remodeling is characterized by elevated cell growth (hypertrophy) of vascular cells as well as recruitment and differentiation of pericytes and mononuclear cells[21]. In addition to the remodeling process primarily affecting the muscularization of normally non-muscularized peripheral arteries and arterioles, the pathogenesis of PAH involves the proliferation and hypertrophy of medial smooth muscle cells of the proximal muscular arteries[34, 35]. Furthermore, there is a proliferation of fibroblasts in the adventitia, accompanied by collagen deposition[36]. The remodeling effects of different vascular cells in pulmonary hypertension depend on factors such as the type, severity, and stage of the condition. Numerous growth factors are implicated in vascular remodeling in PAH, including platelet-derived growth

factor (PDGF), vascular endothelial growth factor (VEGF), epidermal growth factor (EGF), basic fibroblast growth factor (bFGF), and insulin-like growth factor (IGF)-1[17, 18]. For instance, in patients with idiopathic pulmonary arterial hypertension (IPAH), PDGF and its receptors (PDGFRs) are upregulated in the pulmonary vasculature[17, 37, 38]. Experimental studies have shown that the administration of tyrosine kinase inhibitors can reverse the remodeling observed in chronic hypoxia-induced PH and monocrotaline-induced PH in rats[37].

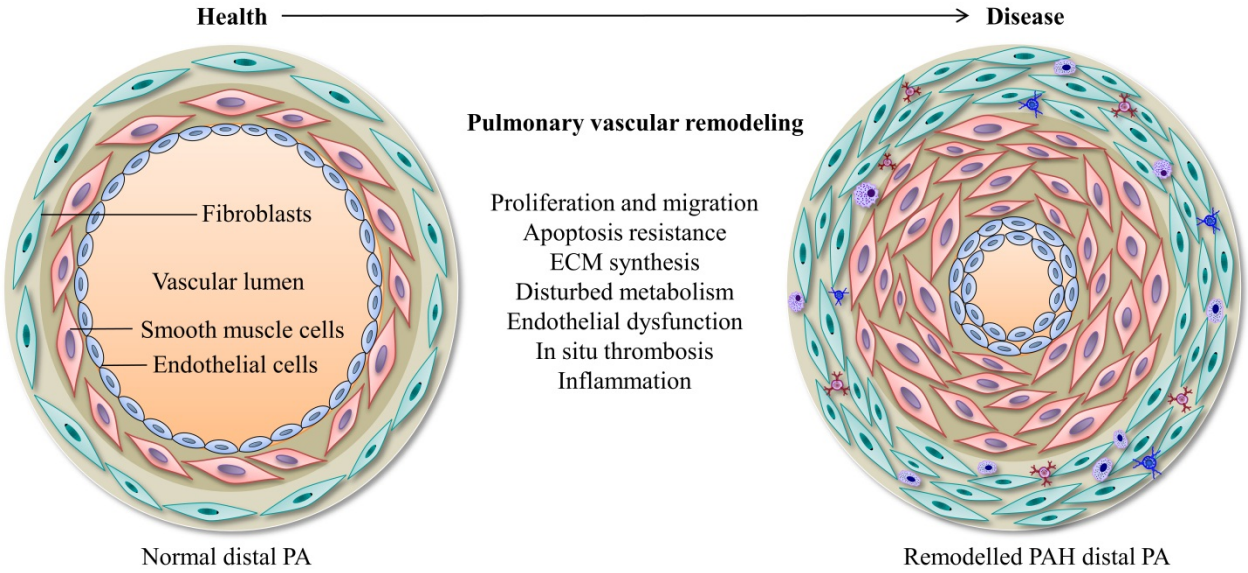

Figure 1. Pulmonary vascular remodeling in PAH.

In addition to chronic vasoconstriction, pulmonary vascular remodeling is a crucial event in the development of PAH and includes progressive morphological transformations in all structural layers of the pulmonary arteries, the intima, media and adventitia, and results in narrowing or complete obstruction of the vascular lumen and raising the blood pressure and load on the right ventricle[17, 19, 21, 34]. In PAH, pulmonary vascular cells show cancer-like features such as increased proliferation or hyperplasia, migration and resistance to apoptosis[18]. Remodeling is, besides hyperplasia, characterized by elevated cell growth or hypertrophy of vascular cells. Furthermore, genetic mutations, extracellular matrix protein synthesis, infiltration of various inflammatory cells and increased levels of proinflammatory cytokines and chemokines, activation of numerous transcription and growth factors, disturbed mitochondria metabolism and *in situ* thrombosis are contributing to the remodeling process[17, 19, 21, 39]. **Abbreviations**: PA - pulmonary artery; ECM - extracellular matrix.

In PAH patients, neointima formation serves as a pivotal pathological feature, indicative of vascular remodeling and disease progression[34, 40]. Neointima is a newly developed structural layer

within the pulmonary arteries, between the vascular endothelium and the lamina elastica interna. This layer comprises a complex interplay of vascular cells and extracellular matrix components. Research suggests that neointima formation arises from the migration and proliferation of vascular smooth muscle cells originating primarily from the media and adventitia of the arteries. Notably, the presence of α-smooth muscle actin-positive cells within the neointima highlights the involvement of specialized smooth muscle cell subpopulations in this process[41]. Although the exact cellular origins of neointima constituents remain elusive, ongoing investigations aim to decipher the intricate molecular mechanisms driving its development.

Plexiform lesions represent a significant morphologic hallmark in the pathology of pulmonary hypertension, present in approximately 80% of PAH cases[17, 40]. These lesions emerge from the dysregulated proliferation of endothelial cells in the pulmonary vasculature. Characterized by the emergence of small neovessels originating from the arteries, plexiform lesions involve a complex interplay of cellular components[40]. Besides endothelial cells, which play a central role, stroma rich in matrix proteins, apoptosis-resistant myofibroblasts and smooth muscle cells contribute to the structural integrity of plexiform lesions[42].

Emerging evidence implicates inflammation in the pathogenesis of pulmonary arterial hypertension[17, 19, 21, 39]. Increased circulating levels of monocyte chemoattractant protein (MCP)-1, tumor necrosis factor (TNF)-α, interleukin (IL)-1 and IL-6, as well as increased levels of inflammatory cell infiltrates, spanning from macrophages, dendritic and mast cells to T and B lymphocytes in remodeled pulmonary vessels, were reported in PAH patients[19, 39]. When stimulated by pathological cues, these diverse cell types release a spectrum of mediators, such as cytokines and chemokines, potentially exacerbating pulmonary vascular remodeling. This intricate interplay between inflammatory cells and their released mediators underscores the multifaceted role of inflammation in driving the progression of pulmonary hypertension.

1.2.2. The monocrotaline animal model of PAH

The monocrotaline (MCT) model is considered the classical model of group 1 PH[43, 44]. Derived from the seeds and vegetation of *Crotalaria spectabilis*, MCT, a pyrrolizidine alkaloid, has served as a fundamental tool in inducing experimental PH since its introduction in 1961 by Lalich and

Merkow[45]. The preferred and mainly used species for the study of MCT-induced PH is rat. Upon a single injection, MCT prompts the onset of severe pulmonary vascular disease in experimental animals. Despite its extensive utilization, the precise underlying mechanism driving MCT-induced PH remains elusive. Cytochrome P450 activates MCT in the liver and becomes reactive MCT pyrrole (MCTP), triggering endothelial cell death in small arterioles, a critical early event mirrored in human pulmonary hypertension[46, 47]. The lungs experience interstitial edema within hours post-injection, accompanied by extravascular protease leakage, matrix degradation, and early inflammatory response[44]. Remarkably, animals exhibit normal behavior during the initial two weeks, with no overt clinical signs. This phase precedes an escalation in reactivity to vasoconstrictors and progressive thickening of the pulmonary artery media, noticeable within 2-4 weeks post-injection. Subsequently, after 5-6 weeks, animals manifest severe PH, marked by elevated pulmonary vascular resistance and right ventricular systolic pressures, culminating in right ventricular hypertrophy[43]. In the ensuing weeks, these animals succumb to right heart failure.

Despite not fully recapitulating every aspect of human PH pathology, the MCT animal model demonstrates critical shared features, including initial endothelial injury, augmented perivascular inflammation, and the development of *de novo* muscularization in small pulmonary arteries[43, 48]. These parallels highlight the model's value for unravelling disease mechanisms and exploring and assessing novel therapeutic strategies to treat this severe and life-threatening condition.

1.3. PH associated with lung diseases and/or hypoxia

1.3.1. Pathophysiology of group 3 PH

Pulmonary hypertension associated with lung diseases and/or hypoxia constitutes the third group in the classification of PH (Table 1)[3]. Its characterization was initially established in the 2008 Dana Point classification for PH during the fourth WSPH[49]. This group encompasses numerous diseases or pathological conditions related to persistent or recurrent hypoxia, whether globally or localized within specific lung regions[50, 51]. Group 3 is the second most common form of PH, and it is characterized by elevated morbidity and mortality[52]. However, it is still not known if the developed PH is the cause of increased mortality or if it is a consequence of the severe stage of lung disease. The most common lung diseases leading to the development of PH are chronic obstructive pulmonary disease (COPD), interstitial lung disease (ILD) and obstructive sleep apnea (OSA)[50].

Additionally, it is linked to exposure to chronic hypoxia at high altitudes[53]. Pulmonary hypertension can develop in approximately 50.2% of individuals with severe COPD[54], a condition that impacts around 6% of the total population in the USA[55]. Furthermore, up to 90% of patients with Global Initiative for COPD stage IV have mPAP higher than 20 mmHg[51].

PH can occur in the healthy lung in response to low atmospheric oxygen, most commonly seen in populations who live at high altitudes[50, 53]. At an altitude of 3000m, the inspired partial pressure of oxygen (pO_2) is approximately 70% of that at sea level, while at an altitude of 5000m, the highest altitude where humans can live, the inspired pO_2 drops to around 50% of that at sea level[56]. Low alveolar oxygen (PAO_2) triggers hypoxic pulmonary vasoconstriction (HPV), redistributing pulmonary blood flow from poorly ventilated to better-ventilated lung areas to maintain the ventilation-perfusion ratio[57]. Unlike pulmonary vessels, systemic arteries dilate to enhance blood flow to hypoxic organs, thereby increasing oxygen delivery. However, a notable exception is the fetal vasculature in the placenta[58]. This process may be reversible during the initial phases by elevating oxygen concentration. In the case of chronic hypoxia, in addition to vasoconstriction, an increase in vascular endothelial growth factors, a decrease of apoptosis and activation of HIF-1α leads to pulmonary vascular remodeling and, ultimately, PH development, which is only partially reversible with oxygen[57]. Response to hypoxia varies significantly both among individuals and across different species.

1.3.2. Chronic hypoxia animal model of PH

Hypoxic exposure of mice and rats is a well-established experimental model representing group 3 of PH[43, 44, 50, 51]. Chronic hypoxia is induced either by normal air at hypobaric pressure of approximately 400 mmHg atmospheric pressure (hypobaric hypoxia) or oxygen-poor air at normal pressure with a reduction of pO_2 at sea level to approximately 10% (normobaric hypoxia). The most common pathological findings of hypoxia-induced PH in rats and mice are *de novo* muscularization of previously nonmuscularized vessels, elevation of pulmonary arterial pressure and development of RV hypertrophy[44, 59]. Hypoxia exposure triggers increased proliferation of pulmonary smooth muscle cells and adventitial fibroblasts. Although the alterations caused by hypoxia are similar in both species, the remodeling process and hemodynamic changes in rats are more severe than in mice[60, 61]. These features are reversible after the return of animals to normoxic

conditions, which is a limitation of this model in contrast to human situations where the patients do not respond to oxygen therapy.

Understanding the molecular mechanisms of hypoxic pulmonary vasculature remodeling remains a challenge. Hypoxia-inducible transcription factors play a critical role in this process[50, 62]. Investigation into the hypoxic mouse model has explored the nitric NO pathway, reactive oxygen species (ROS) and cytoskeletal architecture in PH development[63-65]. NO, a critical vasodilator and signaling molecule, acts via sGC, which shows upregulation in the remodeled smooth muscle layer of chronically hypoxic mice lungs[64]. Treatment with sGC activators significantly ameliorated PH symptoms in mice. Conversely, expression of phosphodiesterase (PDE) 1A, an endogenous inhibitor of the NO pathway, was elevated in pulmonary arterial smooth muscle cells of hypoxic mice, and its inhibition reversed PH[65]. Furthermore, reactive oxygen species are associated with increased NADPH oxidase (NOX) 4 gene expression in hypoxic lung tissue and silencing of NOX4 reduced PASMC proliferation and ROS generation[63].

1.4. The metabolic theory of pulmonary hypertension

1.4.1. The metabolic basis of PAH

When PAH was initially described in 1951[66], the pulmonary vascular bed, an entity with unique physiology and embryology compared to the systemic circulation, was considered as an exclusive organ with abnormalities in the disease pathology. Over the years, accumulating evidence has demonstrated that numerous extrapulmonary tissues and cell types are also disrupted[67, 68]. This includes immune cells, right heart cardiomyocytes and fibroblasts, skeletal muscle and bone-marrow-derived precursor cells. Based on the fact that there is a shared metabolic fingerprint among these various abnormalities in the form of mitochondrial suppression, the metabolic theory of PAH was proposed[68]. The theory suggests that we should comprehend PAH as a syndrome with multiorgan involvement and mitochondria placed at the center stage, characterized by suppressing glucose oxidation and secondary enhancement of glycolysis. Mitochondria suppression, along with its upstream and downstream signaling in PAH, shares a plethora of features with cancer pathophysiology and provides new therapeutic strategies in pulmonary hypertension[69, 70].

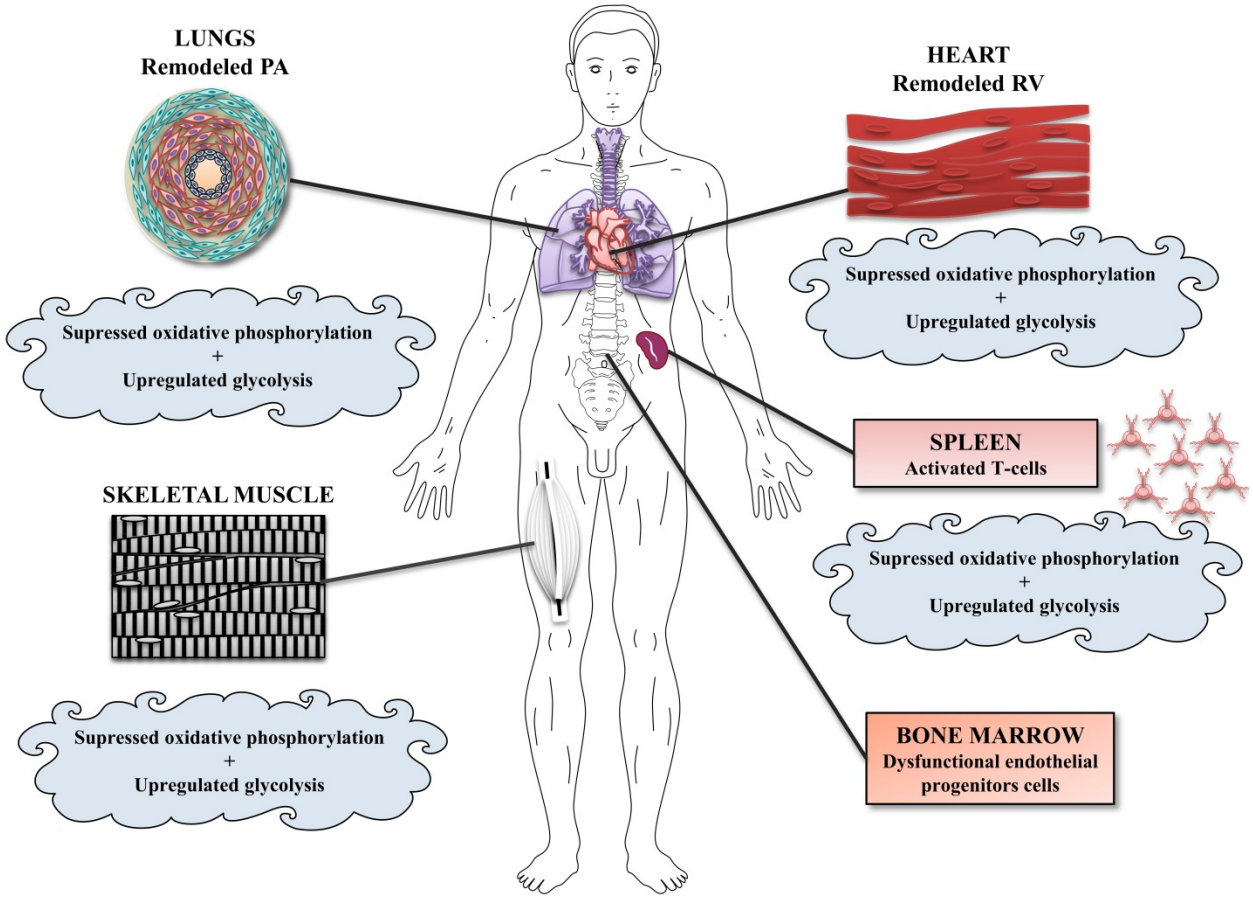

Figure 2. The multiorgan nature of pulmonary arterial hypertension.

In PAH patients, several organs are involved in disease pathophysiology, in addition to remodeling small pulmonary arteries in the lung. This gave the basis for the metabolic theory of pulmonary hypertension, which describes PAH as a syndrome with multiorgan involvement[67, 68]. Additional extrapulmonary tissues involved in disease development include remodeled RV and cardiomyocytes, skeletal muscle and activated immune cells with similar abnormalities in the form of mitochondria oxidative phosphorylation suppression and secondary increase of glycolysis. PAH patients have shared features with metabolic syndrome, such as insulin resistance[71, 72] and lipid depositions in skeletal muscle of PH mice have been described[73]. PAH is characterized by various activated immune cells and increased proinflammatory cytokines contributing to pulmonary vascular remodeling. Activated T cells are characterized by mitochondrial suppression[74]. Furthermore, bone-marrow-derived precursor cells, specifically dysfunctional endothelial progenitor cells, could contribute to pulmonary artery endothelial cells with described suppressed mitochondria[75].

Abbreviations: PA - pulmonary artery; RV - right ventricle.

PASMC mitochondria is a well-described oxygen sensor responsible for producing mitochondria-derived reactive oxygen species (mROS)[57, 76]. mROS can diffuse to the cytoplasm and cell

membrane and influence redox-sensitive targets, such as Kv channels and components of the HIF-1α pathway, leading to PASMC contraction[76]. Regulation of mitochondria function is downstream from various molecular signaling pathways, from oncogenes and tumor suppressor proteins to hypoxia, inflammation and endoplasmatic reticulum (ER) stress[77-79]. Conversely, mROS, such as α ketoglutarate (αKG), regulates nuclear factor of activated T cells (NFAT) and HIF-1α transcription factors, known molecular hallmarks of the pulmonary vascular remodeling process[80]. In addition, αKG and citrate have an important role in epigenetic mechanisms, such as histone methylation and acetylation, known features of PAH. Finally, mitochondria represents one of the critical regulators of apoptosis, and it has been demonstrated that mitochondria-induced apoptosis in PAH is decreased[80].

Pyruvate dehydrogenase (PDH) is crucial in regulating glucose oxidation in mitochondria[81, 82]. PDH catalyzes the conversion of pyruvate into acetyl coenzyme A (acetyl-CoA) in the mitochondria, a necessary step for starting the citric acid (TCA, Krebs) cycle. PDH kinase (PDK) inhibits PDH, leading to attenuation of the pyruvate metabolism into the mitochondria and, consequently, inhibition of TCA cycle and electron transport chain (ETC) complexes. HIF-1α, on the other hand, is responsible for activating PDK[83-85]. PDK inhibition by dichloroacetate diminished PH development *in vivo* and normalized PASMC phenotype[86, 87]. In addition, PDH is a calcium-dependent enzyme, and recent research demonstrated that ER stress, a well-described feature in PAH, can decrease mitochondrial calcium and, consequently, PDH inhibition[88, 89].

PAH patients have shared features with type 2 diabetes patients, reflected in similar insulin resistance[71, 72]. In PAH patients, this metabolic dysfunction comes in lack of obesity or diabetes and is associated with a worse prognosis. Recent studies have shown that insulin resistance precedes pulmonary vascular remodeling in mice and that insulin resistance is associated with skeletal muscle pathology[73]. Therefore, the role of skeletal muscle would explain insulin resistance in PAH patients. In addition, characteristic lipid deposition of the classic metabolic syndrome is also observed in PH mice skeletal muscle[73]. Interestingly, patients with type 2 diabetes have some features of the metabolic shift in skeletal muscle[90]. Moreover, increasing evidence suggests impact of ER stress on insulin signaling, which results in insulin resistance[91].

The hypertrophied RV is another extrapulmonary organ characterized by metabolic shift and glycolytic phenotype in PAH[92, 93]. PDK inhibition by dichloroacetate enhanced RV function in pulmonary artery banding (PAB) experimental model, excluding the drug's effect on the pulmonary vasculature[92, 94]. Even though there was a beneficial effect of activating mitochondrial oxidation, it is still unclear if the metabolic shift is a sustained feature of the compensating and the transition to the decompensating phase of RV remodeling. Further research is necessary to answer these questions and provide new biomarkers of the RV function in the future. Moreover, immune cells involved in PAH pathophysiology are also characterized by glycolytic phenotype upon activation[95, 96]. Activated T cells are characterized by mitochondrial suppression and enhanced glycolysis[74] while circulating immune cells have reported ER stress accompanied by elevated cytokines production[97]. Finally, pulmonary artery endothelial cells also exhibit glycolytic phenotype[98]. Some PH hypotheses proposed that these cells originate from bone marrow-derived endothelial progenitor cells. In diabetes, mitochondria disrupted progenitor endothelial cells have been described[75].

1.4.2. The Warburg effect

Approximately a hundred years ago, Otto Warburg demonstrated that cultured cancer tissues are characterized by high glucose uptake and lactate extraction, even in the presence of oxygen[99]. Those three features, termed aerobic glycolysis, define the Warburg effect. Long ahead of Warburg, Pasteur showed that hypoxia leads to glucose conversion to lactate[100]. Even though this can be applied to hypoxic tumors, Warburg proved that the metabolic shift to glycolysis in tumor tissues will occur even in the presence of sufficient oxygen necessary to convert glucose to carbon dioxide in oxidative phosphorylation.

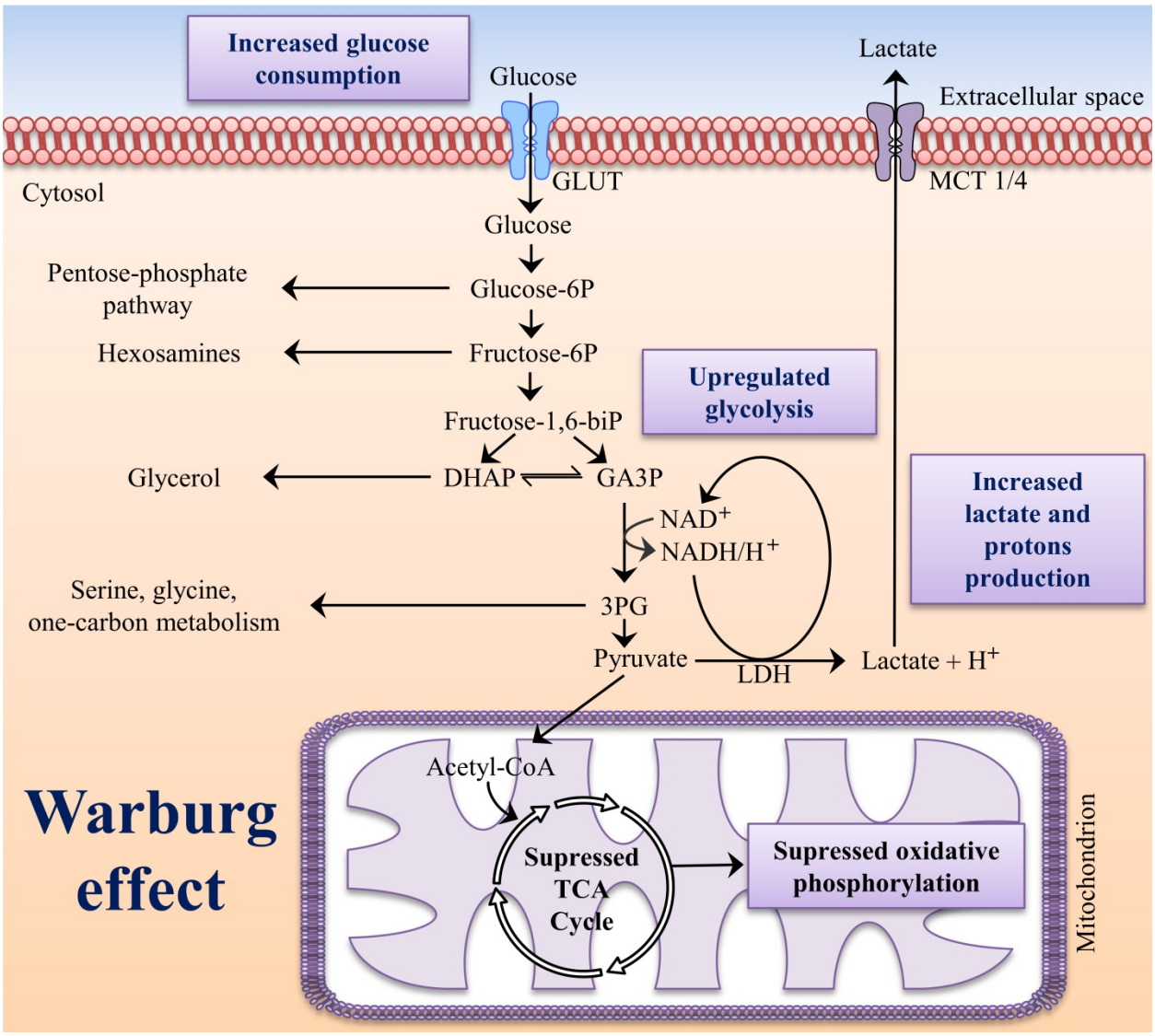

Figure 3. The Warburg effect in tumor cells.

In 1924, Otto Warburg demonstrated a metabolic shift in glucose metabolism from oxidative phosphorylation to glycolysis as a primary source of energy production in the form of adenosine triphosphate (ATP) in highly proliferative cancer cells, even in the presence of oxygen[99]. Warburg suggested that impaired mitochondria function is the cause of malignant transformation. Pyruvate, the end-product of glycolysis, is fermented into lactic acid by lactate dehydrogenase, producing lactate and protons in cancer cells. As a primary source of ATP production, glycolysis has a few advantages for proliferative cancer cells[101]. Despite yielding only 2 ATP molecules per glucose molecule, compared to 32 ATP molecules in oxidative phosphorylation, glycolysis is favorable due to its speed rate, which allows cancer cells to increase glucose consumption. In addition, increased glycolysis produces an abundance of non-mitochondria metabolites, which are necessary for macromolecule synthesis and, subsequently, cell proliferation, such as Glucose-6P for the pentose-phosphate

pathway, Fructose-6P for the hexosamines pathway, 3PG for the serine-glycine-one carbon pathways and DHAP for the glycerol synthesis[102, 103].

Abbreviations: GLUT - glucose transporter; MCT 1/4 - monocarboxylate transporter 1 and 4; Glucose-6P - glucose-6-phosphate; Fructose-6P - fructose-6-phosphate; Fructose-1,6.biP - fructose-1,6-biphosphate; DHAP - dihydroxyacetone phosphate; GA3P - glyceraldehyde 3-phosphate; 3PG - 3-phosphoglycerate; LDH - lactate dehydrogenase; NAD^+ - oxidized form of NAD (nicotinamide adenine dinucleotide), $NADH/H^+$ - reduced form of NAD plus hydrogen proton; TCA Cycle - tricarboxylic acid cycle (Krebs, the citric acid cycle).

Today, we know that besides tumor cells, the Warburg effect is the main hallmark of various highly proliferating cells because upregulated glycolysis brings several advantages to these cells[104, 105]. Even though glycolysis will produce noticeably fewer ATP molecules than oxidative phosphorylation (2 versus 32 ATP molecules), it occurs at a much higher speed rate, allowing rapid glucose uptake of the proliferating cells. Furthermore, increased glycolysis provides the cells with several non-mitochondrial metabolites crucial for macromolecular synthesis[102, 103]. These include glycerol synthesis, pentose-phosphate (PPT), hexosamine and serine-glycine-one carbon (SGOC) pathways. Glycerol is building block of complex lipids, while PPT produces ribose, necessary for nucleotide synthesis, and nicotinamide adenine dinucleotide phosphate (NADPH), which is crucial for cholesterol and fatty acid synthesis. The hexosamine pathway is required for protein glycosylation, while SGOC feeds glutathione, nucleotides and methylation reactions.

1.5. Carbonic anhydrases

1.5.1. Structure and function of carbonic anhydrases

Carbonic anhydrases (CAs) are a family of metalloenzymes that catalyze the reversible carbon dioxide (CO_2) hydration to bicarbonate (HCO_3^-) and protons (H^+) (Figure 4)[106]. Carbonic anhydrase was discovered in 1933 by two independent groups, Meldrum and Roughton in Cambridge and Stadie and O'Brien from the University of Pennsylvania, in an effort to find a catalyst that rescues the body's carbon dioxide from bicarbonate in the blood[107]. After decades of research, today we know that CAs are assorted into eight genetically distinct classes: α-, β-, γ-, δ-, ζ-, η-, θ- and ι-CAs with different metal ions preferences used as cofactors within the active site of the enzyme[108]. The α-CA class, characterized by zinc ion (Zn^{2+}) at the catalytic site, is found mainly in vertebrates and represents the only CA class in mammals. CAs have ancient origins, as

evident by their diverse presence in the evolution tree. The β-CA class is characteristic for higher plants and prokaryotes, γ-CA class is exclusive for archaebacteria, η-CA class is identified in Plasmodium, while δ-, ζ- and θ-CA classes are found in phytoplanktons.

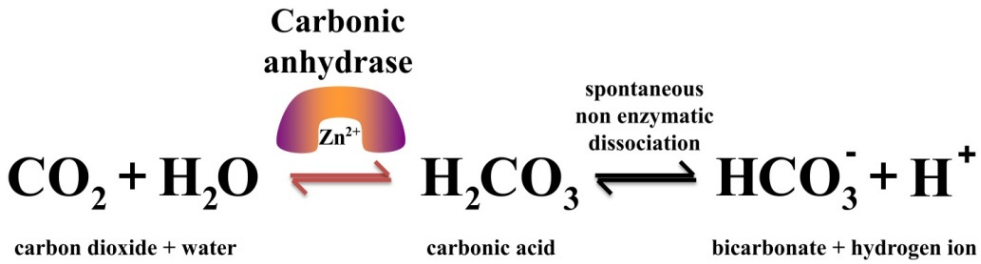

Figure 4. Carbonic anhydrase catalysis of carbon dioxide hydration.

Except for three acatalytic α-CA isoforms (CA8, 10 and 11), α-CAs actively catalyze the reversible hydration of carbon dioxide to bicarbonate ion and a proton in a two-step reaction process[109]. CAs also catalyze many other reactions, including the conversion of aldehydes to alcohols, cyanamide to urea and cyanate to carbamic acid[108]. At the bottom of the CAs active site cavity, the catalytic zinc ion (Zn^{2+}) is coordinated in a tetrahedral manner, binding to three conserved histidine residues (His 94, 96 and 119) and one water molecule[110].

Accumulating discoveries over the years have implicated CAs essential roles in a broad range of physiological processes, such as ion transport, acid-base regulation, gas exchange, secretion of electrolytes, bone resorption and calcification, signal transduction, photosynthesis and CO_2 fixation, among many others[110, 111]. CAs can be involved in a diverse array of functions due to the existence of specific CA isoforms with different molecular features, tissue distribution and responses to inhibitors. In the α-CA class, sixteen isoforms have been described. Based on their cellular localization, they are divided into cytosolic (CA1, 2, 3, 7, 8, 10, 11 and 13), mitochondrial (CA5A and B), secreted (CA6), transmembrane (CA9, 12 and 14) and glycosylphosphatidylinositol (GPI)-anchored (CA 4 and 15). Three of the cytosolic CA isoforms (CA8, 10 and 11) do not have catalytic activity due to the absence of histidine residues, which are responsible for the coordination of zinc ions to the enzyme's catalytic pocket[108].

1.5.2. Role of carbonic anhydrase 9 and 12 in cancer pathophysiology

CAs, especially transmembrane isoforms CA9 and 12, have recently become one of the highly intriguing topics in the cancer research field due to the fact that they are overexpressed in many types of tumors and often associated with disease progression[112-117]. Extensive research has depicted the role of CA9 and 12 in various functional properties of cancer cells, such as cancer cell adhesion, migration, invasion and metastasis[118]. In addition, CA9 and 12 are the essential part of the cancer cell's pH regulation system[112, 119-122]. Furthermore, the main feature of CA9 and 12, which makes them promising therapeutic targets, is their rare expression in non-cancerous tissues[123-125]. CA9 expression is limited to epithelia of the stomach, gallbladder, pancreas and intestine, while CA12 expression is present in the kidney, intestine, reproductive epithelia and eye. CA9-deficient mice have only mild phenotypic changes, most prominently gastric hyperplasia, where CA9 protects gastric epithelia from acid load[126, 127].

CA9 gene is located in the p12-p13 region of chromosome 9 and consists of 11 exons, covering approximately 11 kb of DNA[128, 129]. The highly inducible CA9 gene is transcribed into a single 1.5 kb mRNA, which is further translated into two transmembrane proteins with 54 and 58 kDa molecular weights. CA9 protein structural domains include N-terminal proteoglycan-like region (PG) encoded by exon 1, catalytic domain (CA) encoded by exons 2-8, transmembrane region (TM) and intracellular tail (IC) encoded by exon 10 and 11, respectively[110, 130]. CA12 gene is located in the q22 region of chromosome 15 and comprises 13 exons[131]. CA12 protein has 44 kDa molecular weight and does not possess a PG structural domain. CA9 and 12 are dimeric composed of two monomeric proteins, with CA9 disulfide bonds and CA12 hydrogen bonds mediating the dimerization[110]. Transcription of the CA9 gene, one of the most sensitive sensors of HIF-1α activity, is much better described than the CA12 gene[132].

CA9 gene transcription is a complex action predominantly driven by the binding of HIF-1α to the hypoxia responsive element (HRE), localized just in front of the transcription initiation site in the CA9 promoter[133, 134]. In addition to HRE, the CA9 core promoter contains five cis-acting elements (PR1-5)[133, 135]. Constitutive binding of SP1 and SP3 transcription factors to PR1 and PR5 elements is crucial for the HIF-1α transcriptional activation of CA9[136, 137]. In addition, PR2, an AP1-binding site, and PR3 act as CA9 transcription amplifiers, while PR4 regulatory element has a negative

effect on CA9 transcription[135, 137]. Even though it has been demonstrated by chromatin immunoprecipitation that both HIF-1α and HIF-2α bind to the CA9 HRE[138], in all the cell types investigated so far, CA9 is exclusively responsive to HIF-1α[132]. Numerous studies have investigated the effects of various stimuli on CA9 transcription, and the overwhelming evidence points to the critical role of the HIF-1α pathway in regulating CA9 transcription. Besides known oncogenes such as phosphoinositide 3-kinase (PI3K) and extracellular signal-regulated kinase (ERK)[139, 140], some inflammatory and growth factor stimuli, such as IL-1, IL-6, TNF-α and TGF-β also positively influence CA 9 transcription[141-144]. Some of these stimuli show a hypoxia-independent induction and stabilization of HIF-1α. In addition, several post-translational modifications have been described, such as protein kinase A phosphorylation of the cytoplasmic tail[145, 146], N-glycosylation in the catalytic domain and O-glycosylation in the PG domain[147, 148]. The role of this modifications on the functional properties of CA9 remains to be investigated[149].

Besides expression in tumor tissues, soluble CA9 is detectable in cancer patients' plasma and is often a sign of poor prognosis. Almost twenty years ago, Zatovicova et al. showed that the extracellular domain of CA9 is shed in tumor cells by a disintegrin and metalloprotease (ADAM) 17[150]. A more recent study demonstrated additional involvement of ADAM 10 in CA9 ectodomain shedding[151]. Circulating CA9 has been thoroughly investigated in various types of cancer, and some of these studies are summarized in Table 2[152-167]. In more detail, in patients with clear cell renal cell carcinoma (CCRCC) soluble CA9 levels correlated with tumor size and stage[166, 167]. Studies performed in gastric cancer patients showed that circulating CA9 levels were higher in the metastatic compared to the non-metastatic group[163]. Furthermore, in patients with hepatocellular carcinoma (HCC) and liver cirrhosis, serum CA9 levels significantly correlated with different stages of HCC, and patients with CA9 levels above 400 pg/ml had an increased mortality risk[162]. High CA9 circulating levels were associated with shorter overall survival in non-small cell lung cancer[152], head and neck cancer[156] and castration-resistant prostate cancer patients[165].

Table 2. Circulating levels of CA9 in various types of cancer[152-167].

Type of cancer	Publication	CA9 concentration (pg/ml)		
		Healthy (n)	Disease (n)	Difference
Non-small cell lung cancer (NSCLC)	Ilie et al, 2010	**2.48** (0-16.65), (n=58)	**45.4** (0-372,89), (n=209)	P<0.001
	Ostheimer et al, 2013		**105** (22-420), (n=55)	
Breast cancer	Schütze et al, 2013	**199** (26-1133), (n=48)	**296** (56-1500), (n=140)	NS
	Brown-Glaberman et al, 2016	**20.5** (8.8-41.2), (n=10)	LABC: **34**, MBC: **90.7** (LABC: n=57, MBC: n=23)	P<0.001
Head and neck cancer	Rosenberg et al, 2016	Complete remision: **74.07** (0-393.72), (n=16) Persistent disease: **153.91** (0-1933.4), (n=32)		NS
Testicular germ cell tumors (TGCTs)	Kalavska et al, 2016	**249.6**±100 (n=35)	**405.2**±90.1 (n=83)	p=0.007
Ovarian cancer	Woelber et al, 2010		**269** (104-1202), (n=37)	
Vulvar cancer	Kock et al, 2010		**237** (56-879), (n=31)	
Locally advanced rectal cancer (LARC)	Hektoen et al, 2015	Baseline: **63** (17-591), (n=66) Post-NACT: **213** (n=66) Post-CRT: **309** (n=54), Evaluation: **80** (n=50)		
Cervical cancer	Woelber et al, 2011		**104** (mean **137**) (23-499), (n=46)	
Hepatocellular carcinoma (HCC) and liver cirrhosis	Finkelmeier et al, 2018	**41** (5-169), (n=43)	HCC: **370** (median) (10-5080), (n=215) Cirrhosis: **482** (11-1921), (n=65)	p<0.01
Gastric cancer	Fidan et al, 2013	**47.3** ± 32.2 (n=34)	**182.5** ± 212.4 (n=50)	p<0.0001
Oral cancer	Yang et al, 2014	**41.98**±28.57 (n=100)	**85.37**±67.65 (n=191)	P<0.001
Prostate cancer	Smith et al, 2016	HRLPC baseline: **147** (n=48), **114** (n=20) CRPC before: **148**, after chemotherapy: **116** (n=20)		
Clear cell renal cell carcinoma (CCRCC)	Zhou et al, 2010	CCRCC: **126.1** (n=18) non-CCRCC renal tumors: **2.1** (n=14)		p=0.013
	Takacova et al, 2012	CCRCC: **209.22** (n=57) non-CCRCC renal tumors: **28.78** (n=13)		p=0.002

Abbreviations: CRT - chemoradiotherapy; CRPC - Castration-resistant prostate cancer; HRLPC - High-risk localized prostate cancer; LABC - locally advanced breast cancer; MBC - metastatic breast cancer; NACT - neoadjuvant chemotherapy; NS - non-significant.

Since the discovery of CA9 and 12 as potential therapeutic targets in cancer pathobiology, much effort has been put into developing targeted therapies, including monoclonal antibodies and small molecular inhibitors (CAIs) for the catalytic activity of CA9 and 12[108, 125, 130, 168]. Girentuximab (G250) is an anti-CA9 monoclonal antibody and the first drug to enter the clinical trial for treating

renal cell carcinoma (RCC) patients[169-171]. G250 has shown initial clinical success, but in the phase 3 trial (ARISER), nonmetastatic RCC patients showed no overall or disease-free survival improvement[169]. One of the biggest challenges in designing CAIs has been selectivity for tumor-related extracellular CAs without inhibiting intracellular CAs[115, 125]. CAIs, such as sulfonamides, benzene sulfonamides or cyclic sulfonamides attached to saccharide tails, are characterized by membrane impermeability due to high molecular weight and inclusion of sugar moiety. SLC-0111 is a ureido-benzenesulfonamide CA9 and 12 inhibitor which showed promising anti-proliferative effects *in vitro* and *in vivo* models[172, 173] and has successfully completed a phase I clinical trial for the treatment of CA9 overexpressing solid tumors[174]. Another promising CAI is S4[175, 176], a ureidosulfamate with a high affinity for CA9 and 12 and a low affinity for CA1 and 2[177]. S4 inhibited the proliferation and migration of MDA-MB-231 cells *in vitro*, and treatment with S4 significantly reduced the metastatic tumor burden in the lungs of mice bearing orthotropic eGFP-MDA-MB-231 tumors[175].

1.5.3. Role of CA9 and 12 in the pH regulation system

Among many functions, CAs are an essential part of cancer cell's intracellular pH regulation system[112, 119-122]. Besides CAs, this system consists of Na^+/H^+ exchanger (NHE)-1, monocarboxylate transporter (MCT) 1 and 4, H^+-pump (V-ATPase), aquaporin (AQP) 1 and bicarbonate transporters such as Cl^-/HCO_3^- anion exchanger (AE) and Na^+-dependent HCO_3^- cotransporter (NBC) (Figure 5)[112]. The metabolic shift towards glycolysis in highly proliferative cancer cells leads to abnormally increased production of lactate and protons, the end-products of glycolysis. Proton accumulation inside the cell would result in a decrease of intracellular pH value below the optimal range and, subsequently, the inability of the cell to continue to proliferate[178]. It has been reported that a decrease of intracellular pH below the optimum range can affect a variety of proteins and enzymes and, through proposed conformational changes, interfere with their normal functional properties, such as phosphorylation and, finally, their activation or inactivation[178-180]. pH-sensitive targets affect a plethora of cellular functions, such as ion homeostasis, signal transduction, cell shape, contractility and, interestingly, metabolism[178]. Several studies have demonstrated that the activity of hexokinase and phosphofructokinase, two crucial enzymes for glycolysis initiation, is pH-dependent[181, 182].

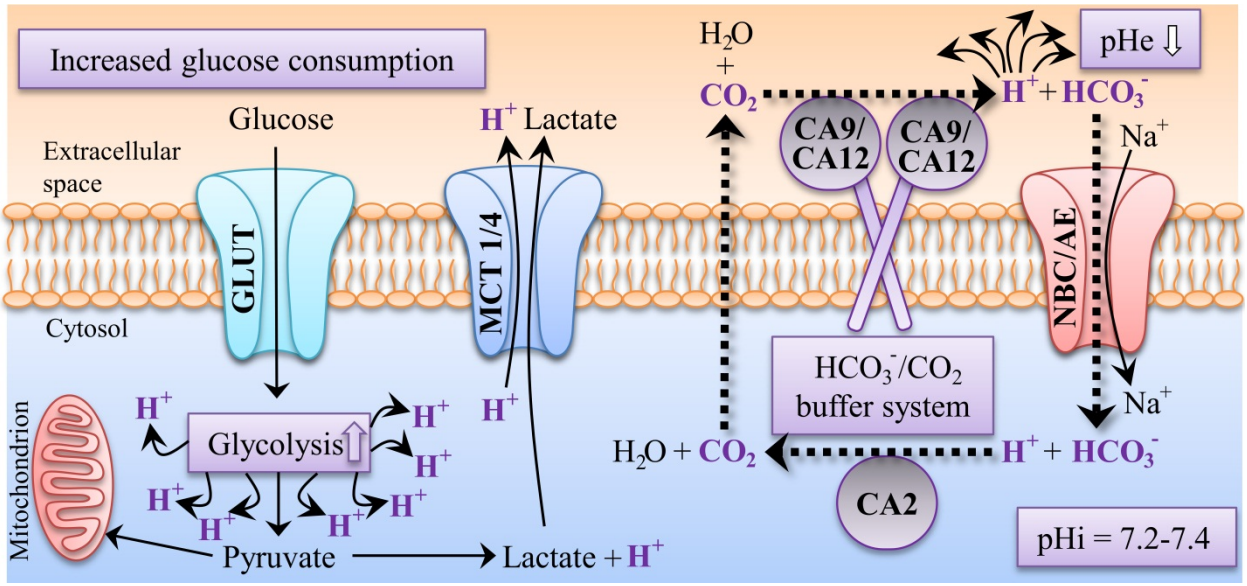

Figure 5. CA9 and 12 role in the pH regulation system in cancer cells.

The metabolic shift from oxidative phosphorylation to glycolysis is a hallmark of malignant cell transformation and results in an abnormal production of lactate and protons, the end products of glycolysis. Proton accumulation would challenge intracellular pH homeostasis, and cancer cells respond by activating their pH regulation system[112, 119-122]. HIF-1α mediated upregulation of CA9 and 12 have a crucial role in this process. CA9 and 12, through the bicarbonate-carbon dioxide buffer system, extrude protons outside the cell, leading to extracellular acidification, favoring cancer cell invasiveness and spreading. Additionally, lactate is extruded together with protons through monocarboxylate transporters 1 and 4. As a result, cancer cells maintain intracellular pH homeostasis, increased glucose consumption and glycolysis and highly proliferative phenotype.

Abbreviations: GLUT - glucose transporter; MCT 1/4 - monocarboxylate transporter 1 and 4; NBC - Na^+-dependent HCO_3^- cotransporter; AE - Cl^-/HCO_3^- anion exchanger; pHe - extracellular pH; pHi - intracellular pH.

Cancer cells adapt to this challenge by activating their pH regulation system[112, 119-122]. In more detail, intracellular ubiquitously expressed CA2 initially catalyze the conversion of protons and bicarbonate to CO_2, which passes the cell membrane freely or through the AQP1 channels and is immediately converted to H^+ and HCO_3^- by membrane-bound CA9 and 12, CA isoforms with extracellular catalytic domain. Bicarbonate is rapidly transferred back into the cell through AE or NBC bicarbonate transporters. At the same time, the accumulation of extruded protons eventually results in acidification of the extracellular milieu, favoring cancer cell invasiveness and spreading. CAs can form structural and functional complexes with bicarbonate transporters, termed ‘transport

metabolon'[183]. Essentially, CA9 and 12, through a carbon dioxide-bicarbonate buffer system, play a role in maintaining intracellular pH homeostasis, which has several biological implications.

1.5.4. Carbonic anhydrases in pulmonary hypertension

Even though elevated CA9 protein expression as a marker of activated HIF1-α has been reported in pulmonary hypertensive endothelial cells[184], no studies investigated the specific role of CA9 and 12 in pulmonary hypertension. On the other hand, several publications depict the effect of acetazolamide (ACZ), a non-selective CA inhibitor, on the pathophysiology of PH[185-190]. ACZ is a drug used to treat acute mountain sickness, glaucoma, epilepsy and idiopathic intracranial hypertension[191].

It has been demonstrated that treatment with ACZ reduces hypoxic pulmonary vasoconstriction in isolated perfused rabbit lungs[186] and conscious, spontaneously breathing dogs[187]. In another study, the effect of preventive and curative ACZ treatment was investigated in rats exposed to chronic hypoxia[188]. Acetazolamide ameliorated the effects of chronic hypoxia on PVR and CO, but it did not affect the hemodynamic properties of the investigated animals. In addition, recently, it has been shown that ACZ ameliorates inflammation and experimental PH in the Sugen 5416/hypoxia model in rats[185]. In this study, Hudalla et al. focused on the importance of CA2 isoform in alveolar macrophages. However, when interpreting the results of CA inhibition with ACZ, we have to consider studies which demonstrated that the effects of ACZ on vasodilatation during hypoxia and inhibition of hypoxia-induced calcium responses are independent of CA enzymatic activity[189, 190].

1.6. Aims of the study

Pulmonary vascular remodeling as a hallmark of pulmonary hypertension (PH) has been characterized by several cancer-like features, including dysregulated proliferation and migration of pulmonary vascular cells and suppression of glucose oxidation accompanied by the secondary enhancement of glycolysis. Elevated expressions of membrane-bound carbonic anhydrases 9 and 12 isoforms have been reported in various types of cancer. CA9 and 12 are the critical pH regulators responsible for maintaining the proliferative state of cancer cells. Therefore, we hypothesize that CA9 and 12 play an essential role in the pathogenesis of hypoxia and non-hypoxia induced PH and may subsequently represent novel therapeutic targets.

In light of the background provided, the following investigations were conducted to address the research questions:

1) mRNA and protein expression profile of CAs in IPAH patients, mouse PASMCs after hypoxia exposure and human PASMCs upon hypoxia and non-hypoxia stimulation
2) role of HIF-1α and HIF-2α transcription factors on expression profile of CA9 and 12 in human PASMCs after hypoxia stimulation
3) effect of CA9 and 12 inhibition or silencing on the proliferation of mouse and human PASMCs upon hypoxia and non-hypoxia stimulation
4) effect of CA9 and 12 inhibition on the migration of human PASMCs upon hypoxia and non-hypoxia stimulation
5) effect of CA9 and 12 inhibition on the pH homeostasis of human PASMCs
6) effect of CA9 and 12 inhibition on the activation of human PASMCs protein kinases after hypoxia exposure
7) effect of CA9 and 12 inhibition on hemodynamics, RV hypertrophy, structure and function and pulmonary vascular remodeling in experimental PH induced by MCT injection in rats and chronic hypoxia exposure in mice
8) CA9 circulating levels in PH patients

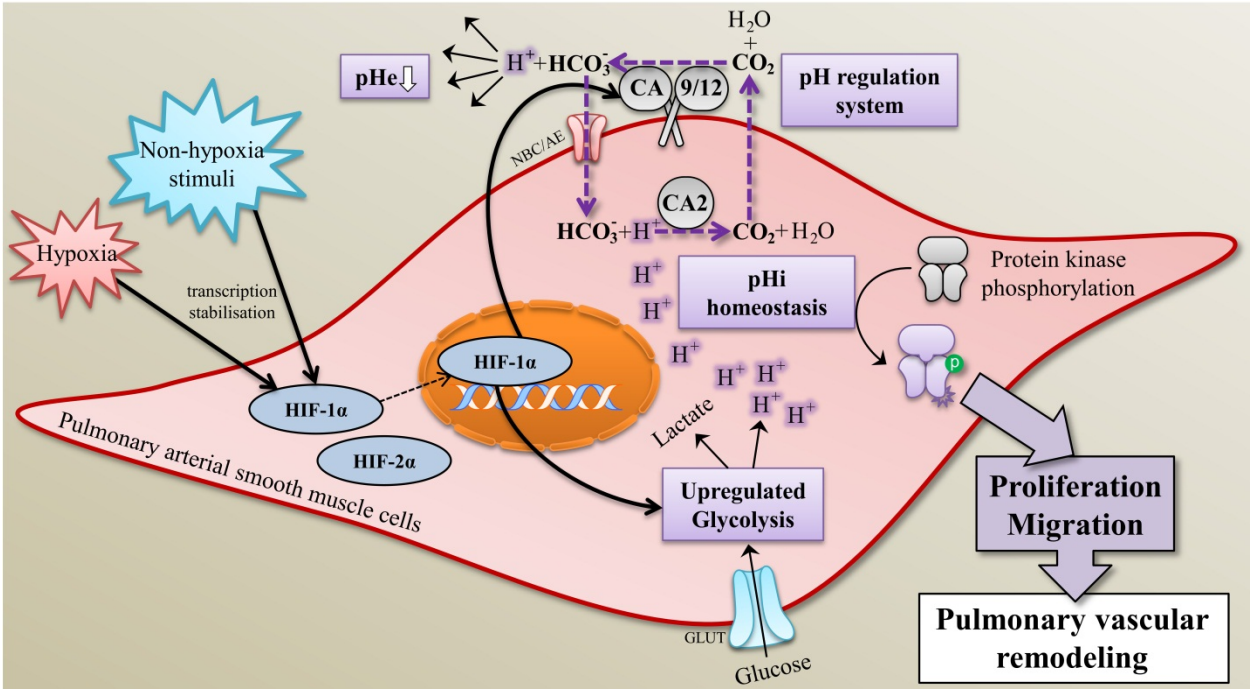

Figure 6. Aims of the study.

Are CA9 and 12 expression profiles upregulated in IPAH patients? Will hypoxia and non-hypoxia stimuli affect the expression of CA9 and 12 in PASMCs? If so, is it driven by HIF-1α or HIF-2α transcription factor? Do CA9 and 12 have a role in the increased proliferation and migration of PASMCs upon hypoxia and non-hypoxia stimulation? If so, which isoform has a higher impact? Are CA9 and 12 involved in intracellular pH homeostasis and extracellular acidification of highly proliferative human PASMCs? Do CA9 and 12 inhibition affect the activation of protein kinases in human PASMCs upon hypoxia stimulation? Will CA9 and 12 pharmacological inhibition have a beneficial therapeutic effect in experimental models of PH induced by MCT injection in rats and chronic hypoxia exposure in mice? Can CA9 become a prognostic circulating biomarker in PH patients?

Abbreviations: GLUT - glucose transporter; HIF-1α - hypoxia-inducible factor 1 alpha; NBC - Na^+-dependent HCO_3^- cotransporter; AE - Cl^-/HCO_3^- anion exchanger; pHe - extracellular pH; pHi - intracellular pH.

2. MATERIAL AND METHODS

2.1. Material

2.1.1. Equipment

Equipment	Company
Automated microtome (Leica RM 2165)	*Leica Microsystems GmbH, Wetzlar, Germany*
Balance for substances (Mettler Toledo PB303 Delta Range®)	*Mettler Toledo GmbH, Greifensee, Switzerland*
Cell incubator HERAcell 150	*Thermo Fisher Scientific Inc., Waltham, MA, USA*
Centrifuge Mikro 200R	*Andreas Hettich GmbH & Co. KG, Tuttlingen, Germany*
ChemiDocTM Touch Imaging System	*Bio-Rad Laboratories GmbH, Hercules, CA, USA*
ChemiDocTM XRS^{+}	*Bio-Rad Laboratories GmbH, Hercules, CA, USA*
Culture Hood	*Heraeus GmbH, Hanau, Germany*
Flattening bath for paraffin sections (Leica HI 1210)	*Leica Microsystems GmbH, Wetzlar, Germany*
Heating Block	*VWR, Bruchsal, Germany*
Heating chamber	*Memmert GmbH & Co. KG, Schwabach, Germany*
Heating Plate Hi 1220	*Leica Microsystems GmbH, Wetzlar, Germany*
Hotplate/Stirrer (371)	*VWR International GmbH, Bruchsal, Germany*
Ice flake machine (Icematic F100 Compact)	*Castelmac SPA, Castelfranco, Italy*
IncuCyte ZOOM	*Essen BioScience Ltd., Ann Arbor, MI, USA*
InnoScan is900	*Innopsys Inc., Chicago, IL, USA*
Ismatec® roller-pump	*Cole-Parmer GmbH, Wertheim Germany*
Light microscope (DMLA)	*Leica Microsystems GmbH, Wetzlar, Germany*
Low Voltage Power Supplies Power pack P25T	*Biometra GmbH, Jena, Germany*
Microplate reader Infinite M200	*Tecan Trading AG, Männedorf, Switzerland*

Mini-PROTEAN® electrophoresis cells	*Bio-Rad Laboratories GmbH, Hercules, CA, USA*
Mx3000 qPCR System	*Agilent Stratagene, Santa Clara, CA, USA*
NanoDrop (ND-1000)	*Kisker-Biotech, Steinfurt, Germany*
Oxy Cycler A84 XOV	*BioSpherix, Parish, NY, USA*
Paraffin cooling station Leica EG 1150C	*Leica Microsystems GmbH, Wetzlar, Germany*
Paraffin embedding station Leica EG 1140H	*Leica Microsystems GmbH, Wetzlar, Germany*
PCR Plate sealer PX1	*Bio-Rad Laboratories GmbH, Hercules, CA, USA*
766 Laboratory pH Meter, Calimatic	*Knick Elektronische Messgeraete GmbH & Co. KG, Berlin, Germany*
PowerLab system	*AD Instruments GmbH, Spechbach, Germany*
Precelly® 24 Homogenizer	*PeqLab Biotechnologie GmbH, Erlangen, Germany*
QIAxcel Advanced System	*Qiagen GmbH, Hilden, Germany*
PamStation®12 platform	*PamGene International, s-Hertogenbosch, Netherlands*
Real-time polymerase chain reaction (PCR) Detection System (CFX Connect™)	*Bio-Rad Laboratories GmbH, Hercules, CA, USA*
Rectal thermometer	*Indus Instruments, Houston, TX, USA*
Roller mixer LLG - uniROLLER 10	*Lab Logistics Group GmbH, Meckenheim, Germany*
Rotary microtome cryostat (CM1520)	*Leica Microsystems GmbH, Wetzlar, Germany*
Shaking table Swip	*Edmund Bühler GmbH, Bodelshausen, Germany*
SPR - 671 Mikro-Tip® mouse pressure catheter, REF 8406719	*Millar Instruments Inc., Houston, TX, USA*
SPR - 320 Mikro-Tip® rat pressure catheter, REF 8408160	*Millar Instruments Inc., Houston, TX, USA*
Table Centrifuge Mikro 200R	*Andreas Hettich GmbH & Co. KG, Tuttlingen, Germany*
Thermocycler, T3000	*Biometra GmbH, Jena, Germany*
Thermoregulation plate TCAT-2LV controller	*Physitemp Instruments Inc., Clifton, NJ, USA*

Trans-Blot® SD Semi -dry Cell	*Bio-Rad Laboratories GmbH, Hercules, CA, USA*
Trans-Blot® Turbo Semi -dry Cell	*Bio-Rad Laboratories GmbH, Hercules, CA, USA*
Ultrapure Milli-Q®	*Merck KGaA, Darmstadt, Germany*
Vevo® 2100 high-resolution Imaging System	*FUJIFILM VisualSonics Inc., Toronto, Canada*
Vortexer MS1 Minishaker	*IKA GmbH, Staufen, Germany*
Water bath	*Memmert GmbH & Co. KG, Schwabach, Germany*

2.1.2. Chemicals and consumables

Chemicals and consumables	**Company**
25 Culture-Inserts 2 Well for self-insertion (80209)	*Ibidi, Gräfelfing, Germany*
Acetone (32201)	*Merck KGaA, Darmstadt, Germany*
Adenosine (A9251)	*Merck KGaA, Darmstadt, Germany*
Agarose (11406)	*SERVA Electrophoresis GmbH, Heidelberg, Germany*
Agarose, low-gelling temperature (6351)	*Carl Roth GmbH & Co. KG, Karlsruhe, Germany*
Alkaline Phosphatase (AP) Polymer System (POLAP-100)	*Zytomed Systems GmbH, Berlin, Germany*
Amersham ECL Plus Western Blotting Detections System (29018903)	*GE Healthcare, Little Chalfont, UK*
Ammonium persulfate (APS, A3678)	*Promega GmbH, Madison, WI, USA*
Ampuwa® water (3478.1)	*Carl Roth GmbH & Co. KG, Karlsruhe, Germany*
Antibody Diluent (ZUC025-100)	*Zytomed Systems GmbH, Berlin, Germany*
Automatic pipettes (100-1000 µl, 10-100 µl, 1-10 µl)	*Eppendorf AG, Hamburg, Germany*
Background punisher (BP974)	*Biocare Medical LLC, Pacheco, CA, USA*
Bovine serum albumin (BSA, A7030)	*Merck KGaA, Darmstadt, Germany*
Bradford assay (5000114)	*Bio- Rad Laboratories GmbH, Hercules, CA, USA*
Buffer RLT (79216)	*Qiagen GmbH, Hilden, Germany*

Human Carbonic Anhydrase IX Quantikine ELISA Kit (DCA900)	*R&D systems, Minneapolis, MN, USA*
Cannulas (16G, 18G)	*BD Microlance, Franklin Lakes, NJ, USA*
Carboxy SNARF-1	*Thermo Fisher Scientific Inc., Waltham, MA, USA*
CAT Hematoxylin (CATHE-M)	*Biocare Medical LLC, Pacheco, CA, USA*
Cell culture dishes (35er, 60er, 100er)	*Sarstedt AG & Co. KG, Nümbrecht, Germany*
Cell culture plates (6, 12, 24, 96 well)	*Greiner Bio-One GmbH, Frickenhausen, Germany*
Cell proliferation ELISA kit, Bromodeoxyuridine (BrdU, colorimetric, 11647229001)	*Sigma Aldrich, St. Louis, MO, USA*
Cell scrapers	*Greiner Bio-One GmbH, Frickenhausen, Germany*
Collagenase type IV	*Sigma Aldrich, St. Louis, MO, USA*
Combtips advanced (5 ml, 10 ml, 25 ml)	*Eppendorf AG, Hamburg, Germany*
Comp-Beads	*BD Biosciences, San Jose, CA, USA*
Conical centrifuge tubes (15 ml, 50 ml)	*Greiner Bio-One GmbH, Frickenhausen, Germany*
Coverslips 24x36 mm	*Menzel GmbH & Co. KG, Braunschweig, Germany*
Cryo Tubes	*Sarstedt AG & Co. KG, Nümbrecht, Germany*
Dimethyl-sulfoxide (DMSO, D4540)	*Merck KGaA, Darmstadt, Germany*
Disodiumhydrogenphosphate dihydrate (Na_2HPO_4, 106580)	*Merck KGaA, Darmstadt, Germany*
Distilled Water (3478.1)	*Carl Roth GmbH & Co. KG, Karlsruhe, Germany*
Distilled Water (dH_2O, DNAse/RNAse-free, 10977023)	*Invitrogen™, Thermo Fisher Scientific Inc., Waltham, MA, USA*
DMEM-F12 (11320-033)	*GIBCO™, Thermo Fisher Scientific Inc., Waltham, MA, USA*
DNAse (04536282001)	*Roche Diagnostics GmbH, Mannheim, Germany*
Dulbecco's Modified Eagle Medium (DMEM, 31885023)	*GIBCO™, Thermo Fisher Scientific Inc., Waltham, MA, USA*
Embedding cassettes	*Leica Microsystems GmbH, Wetzlar, Germany*

Enrofloxacine (Baytril 2.5%®)	*Bayer Vital GmbH, Leverkusen, Germany*
Ethanol (pure) for molecular biology (108543)	*Merck KGaA, Darmstadt, Germany*
Ethanol 100% (27694)	*Otto Fischar GmbH, Saarbrücken, Germany*
Ethanol 70% (ETO-5000-70-1)	*SAV Liquid Production GmbH, Flintsbach am Inn, Germany*
Ethanol 96% (27695)	*Otto Fischar GmbH, Saarbrücken, Germany*
Ethylenediaminetetraacetic acid (EDTA, 8043)	*Carl Roth GmbH & Co. KG, Karlsruhe, Germany*
Fetal bovine serum (FBS, F0804)	*Merck KGaA, Darmstadt, Germany*
Fe_3O_4 (Iron particles)	*Sigma Aldrich, St. Louis, MO, USA*
Filtered tips (10 µl, 100 µl, 1000 µl)	*Nerbe plus GmbH & Co. KG, Winsen, Germany*
Filtopur S 0.2 µm (83.1826.001)	*Sarstedt AG & Co. KG, Nümbrecht, Germany*
Fluoro Care Anti-Fade Mountant (FP001G10)	*Biocare Medical LLC, Pacheco, CA, USA*
Formaldehyde (3,5–3,7%, stabilized with methanol, 27244)	*Otto Fischar GmbH, Saarbrücken, Germany*
GeneRuler™ 100bp DNA Ladder (SM0313)	*Thermo Fisher Scientific Inc., Waltham, MA, USA*
Gibson Assembly® Cloning Kit (E5510S)	*New England Biolabs, Ipswich, MA, USA*
Glass bottles, beakers, cylinders	*DURAN Group Holding GmbH, Wertheim, Germany*
Glass bottles, beakers, cylinders	*VWR International LLC, Bruchsal, Germany*
Gloves (Nitra-Tex®)	*Ansell Ltd., Tamworth, UK*
Hand towels	*Essity Hygiene and Health, Stockholm, Sweden*
Hank's Balanced Salt Solution (HBSS, 14025050)	*GIBCO™, Thermo Fisher Scientific Inc., Waltham, MA, USA*
Heparin (Heparin-Natrium 5000 I.U.)	*Ratiopharm GmbH, Ulm, Germany*
Histological glass slides 25x75x1 mm (SuperFrost UltraPlus®)	*R. Langenbrinck GmbH, Emmendingen, Germany*
Recombinant Human IL-1 beta/IL-1F2 Protein (201-LB)	*R&D systems, Minneapolis, MN, USA*
Recombinant Human IL-6 Protein (206-IL)	*R&D systems, Minneapolis, MN, USA*

Recombinant Human PDGF-BB, Biotinylated Protein, (BT220)	*R&D systems, Minneapolis, MN, USA*
Recombinant Human TGF-beta 1, Biotinylated Protein, CF, (BT7754)	*R&D systems, Minneapolis, MN, USA*
Recombinant Human TNF-alpha, Biotinylated Protein (BT210)	*R&D systems, Minneapolis, MN, USA*
Hydrochloride (HCl, 37%, 4625.1)	*Carl Roth GmbH & Co. KG, Karlsruhe, Germany*
Hydrogen-peroxide (30%, 107209)	*Merck KGaA, Darmstadt, Germany*
Intracellular pH Calibration Buffer Kit (P35379)	*Thermo Fisher Scientific Inc., Waltham, MA, USA*
iScript complementary DNA (cDNA) Synthesis Kit (1708890)	*Bio-Rad Laboratories GmbH, Hercules, CA, USA*
Isoflurane (HDG9623)	*Baxter Deutschland GmbH, Unterschleissheim, Germany*
Isopropyl-alcohol (99.8%, 190764)	*Merck KGaA, Darmstadt, Germany*
iTaq Universal SYBR® Green Supermix (1725124)	*Bio-Rad Laboratories GmbH, Hercules, CA, USA*
Ketamine (Ursotamin®)	*Serumwerk Bernburg AG, Bernburg, Germany*
Laemmli protein sample buffer (4x) for SDS - PAGE (4x, 1610747)	*Bio-Rad Laboratories GmbH, Hercules, CA, USA*
L-Glutamine (P04-80100)	*GIBCO™, Thermo Fisher Scientific Inc., Waltham, MA, USA*
Lipofectamine™ 2000	*Thermo Fisher Scientific Inc., Waltham, MA, USA*
Lipofectamine™ 3000	*Thermo Fisher Scientific Inc., Waltham, MA, USA*
Live Cell Imaging Solution (A59688DJ)	*Thermo Fisher Scientific Inc., Waltham, MA, USA*
lumox® multiwell, 96-well	*Sarstedt AG & Co. KG, Nümbrecht, Germany*
Medical adhesive bands	*3M Health Care, St.Paul, MN, USA*
Medium 199 (M199, 31150022)	*GIBCO™, Thermo Fisher Scientific Inc., Waltham, MA, USA*
Methanol (99.8%, 32213)	*Merck KGaA, Darmstadt, Germany*
Micro tubes (0.5 ml, 1.5 ml, 2.0 ml)	*Sarstedt AG & Co. KG, Nümbrecht, Germany*
Microfil® (MV122 Yellow)	*Flow Tech Inc., Carver, MA, USA*

Microtome blades (MX35 Premier)	*Thermo Fisher Scientific Inc., Waltham, MA, USA*
Monocrotaline (Crotaline®)	*Sigma Aldrich, St. Louis, MO, USA*
M-PER lysis buffer (78501)	*Thermo Fisher Scientific Inc., Waltham, MA, USA*
Multipette E3x	*Eppendorf AG, Hamburg, Germany*
MultiplateTM PCR Plate 96-Well, clear	*Bio-Rad Laboratories GmbH, Hercules, CA, USA*
Nano-Glo® Dual-Luciferase® Reporter Assay System	*Promega GmbH, Madison, WI, USA*
Needles (BD Microlance 3®) (18G/1.2 mm x 40 mm, 20G/0.9 mm x 40 mm, 26G/0.45 mm x 13 mm)	*Becton Dickinson GmbH, Heidelberg, Germany*
Neubauer counting chamber	*Paul Marienfeld GmbH & Co. KG, Lauda-Königshofen, Germany*
Non-tissue culture treated Petri dishes	*Sarstedt AG & Co. KG, Nümbrecht, Germany*
Nuclear Fast Red (Kernechtrot Aluminiumsulfat, 2E-012)	*Waldeck GmbH & Co. KG, Münster, Germany*
Opti-MEM™, Reduced Serum Medium (31985062)	*GIBCO™, Thermo Fisher Scientific Inc., Waltham, MA, USA*
Parafilm®	*Merck KGaA, Darmstadt, Germany*
Paraformaldehyde (PFA, sc-281692)	*Santa Cruz Biotechnology Inc., Dallas, TX, USA*
Paraplast Plus® for tissue embedding (P3683)	*Merck KGaA, Darmstadt, Germany*
Penicillin/Streptomycin (15070-063)	*GIBCO™, Thermo Fisher Scientific Inc., Waltham, MA, USA*
pGL3 Luciferase Reporter Vectors (E1751)	*Promega GmbH, Madison, WI, USA*
Phenylmethansulfonylfluorid (PMSF, P7626)	*Merck KGaA, Darmstadt, Germany*
Phenylmethylsulfonyl Fluoride (PVDF) - membrane	*Pall Deutschland Holding GmbH & Co. KG, Dreieich, Germany*
Phosphate-buffered saline (D-PBS, P04-53500)	*PAN-Biotech GmbH, Aidenbach, Germany*
Picrosirius red staining kit (ab150681)	*Abcam, Cambridge, UK*
Pierce™ BCA Protein Assay Kits (23225)	*Thermo Fisher Scientific Inc., Waltham, MA, USA*
Pierce Protease and Phosphatase Inhibitor Mini Tablets (A32959)	*Thermo Fisher Scientific Inc., Waltham, MA, USA*

Polyethylenglycol 400 (PEG, B21992.30)	*Thermo Fisher Scientific Inc., Waltham, MA, USA*
Potassium chloride (KCl, 6781.1)	*Merck KGaA, Darmstadt, Germany*
Potassiumdihydrogenphosphate (KH_2PO4, 104873)	*Merck KGaA, Darmstadt, Germany*
Precision Plus Protein Dual Color Standards (1610374)	*Bio-Rad Laboratories GmbH, Hercules, CA, USA*
Primers (listed below)	*Metabion International AG, Planegg, Germany*
Promoter-Driven Control NanoLuc® Luciferase Vectors, CMV (N1091)	*Promega GmbH, Madison, WI, USA*
Protease-Inhibitor-Cocktail cOmplete™ Mini EDTA-free	*Roche Diagnostics GmbH, Mannheim, Germany*
RIPA Lysis Buffer System (sc-24948A)	*Santa Cruz Biotechnology Inc., Dallas, TX, USA*
RNeasy Micro Kit (74004)	*Qiagen GmbH, Hilden, Germany*
RNeasy Mini Kit (74106)	*Qiagen GmbH, Hilden, Germany*
RPMI medium 1640 (P04-16500)	*PAN-Biotech GmbH, Aidenbach, Germany*
S4 (5577)	*Tocris Bioscience, Bristol, UK*
Saline solution (0,9% NaCl, 3570160)	*B.Braun Melsungen AG, Melsungen, Germany*
Serological pipette (5 ml, 10 ml, 25 ml, 50 ml)	*BD Falcon, Heidelberg, Germany*
Skimmed milk powder (T145.3)	*Carl Roth GmbH & Co. KG, Karlsruhe, Germany*
SmBM™ Smooth Muscle Cell Growth Basal Medium, (CC-3181)	*Lonza*, *Basel, Switzerland*
SmGM™-2 Smooth Muscle Cell Growth Medium-2 BulletKit™ (CC-3182)	*Lonza, Basel, Switzerland*
SmGM™-2 Smooth Muscle Cell Growth Medium-2 SingleQuots™ Supplements and Growth Factors (CC-4149)	*Lonza, Basel, Switzerland*
Smooth Muscle Cell Growth Medium 2 (C-22062)	*PromoCell GmbH, Heidelberg, Germany*
Sodium dodecyl sulfate (SDS, AM9820)	*Invitrogen™, Thermo Fisher Scientific Inc., Waltham, MA, USA*
SureTag DNA Labelling Kit (5190-3400)	*Agilent Technologies Inc. Santa Clara, CA, USA*

Surgical instruments	*Fine Science Tools GmbH, Heidelberg, Germany*
SYBR® Safe DNA gel stain (S33102)	*Invitrogen™, Thermo Fisher Scientific Inc., Waltham, MA, USA*
Syringes (Injekt®-F) (1 ml, 2 ml, 5 ml, 20 ml)	*Carl Roth GmbH & Co. KG, Karlsruhe, Germany*
Tetramethylethylenediamine (TEMED, 2367.3)	*Carl Roth GmbH & Co. KG, Karlsruhe, Germany*
Thiazolyl Blue Tetrazolium Blue (MTT), (M5655-1G)	*Sigma Aldrich, St. Louis, MO, USA*
Thread, black no.16	*Coats GmbH, Kenzingen, Germany*
Tips for automatic pipettes (200 µl, 1000 µl, 10 µl)	*Sarstedt AG & Co. KG, Nümbrecht, Germany*
TRIS (4855.2)	*Carl Roth GmbH & Co. KG, Karlsruhe, Germany*
Tris-buffered saline 20x (TBS, ZUC052-500)	*Zytomed Systems GmbH, Berlin, Germany*
TRIS-HCl (9090.2)	*Carl Roth GmbH & Co. KG, Karlsruhe, Germany*
TritonX-100 (X100)	*Merck KGaA, Darmstadt, Germany*
Trypsin/EDTA (10x, P10-024100)	*PAN-Biotech GmbH, Aidenbach, Germany*
Tween® 20 (P1379)	*Merck KGaA, Darmstadt, Germany*
Water, sterile (00088992)	*B.Braun Melsungen AG, Melsungen, Germany*
Whatman Gel Blotting Paper	*GE Healthcare, Little Chalfont, UK*
Xylazine 20 mg/ml	*Serumwerk, Bernburg, Germany*
Xylol (9713.2)	*Carl Roth GmbH & Co. KG, Karlsruhe, Germany*
β-Mercaptoethanol (4227.3)	*Carl Roth GmbH & Co. KG, Karlsruhe, Germany*

2.1.3. Software

Software	**Company**
Analyze Pro software	*Mayo Clinic, Rochester, MI, USA*
Adobe Illustrator	*Adobe Inc., San José, CA, USA*
Adobe Photoshop	*Adobe Inc., San José, CA, USA*
Bionavigator	*PamGene International, s-Hertogenbosch, Netherlands*

CFX Manager™ Software	*Bio-Rad Laboratories GmbH, Hercules, CA, USA*
Evolve 12	*PamGene International, s-Hertogenbosch, Netherlands*
GraphPad Prism Version 8	*GraphPad Software Inc., La Jolla, CA, USA*
IncuCyte Software	*Essen BioScience Ltd., Ann Arbor, MI, USA*
Image Lab Version 4.1	*Bio-Rad Laboratories GmbH, Hercules, CA, USA*
Tecan i-control™ Microplate Reader Software	*Tecan Trading AG, Männedorf, Switzerland*
Microsoft Office 2016	*Microsoft Corporation, Redmond, WA, USA*
Qwin software	*Leica Microsystems GmbH, Wetzlar, Germany*
VisualSonics Vevo LAB	*FUJIFILM VisualSonics Inc., Toronto, Canada*

2.1.4. Primer sequences

Gene abbreviation	Sequence
Human CA1	Forward: 5’ TGTTCCATCCTGTAGGCTGATCC 3’
	Reverse: 5’ TGCTCCATTGTTCAGGACCATTTT 3’
Human CA2	Forward: 5’ ATGCTGCAGAACTTCACTTGGTT 3’
	Reverse: 5’ ACAACTTTCTGAAGGCCCGGT 3’
Human CA3	Forward: 5’ GCAGCGGAGCTTCATTTGGT 3’
	Reverse: 5’ GGAACTCGCCATTCTCATGTCC 3’
Human CA4	Forward: 5’ TTTGCTGTCCCGCAAGATGC 3’
	Reverse: 5’ AGGACTCGGCTTGAACCTCG 3’
Human CA5	Forward: 5’ GTTTTTAAAGCTCGGGGCCCAT 3’
	Reverse: 5’ GCAGAGTGGAGGGGTCGAAG 3’
Human CA6	Forward: 5’ TGTCAAGCTCTCCAGGACACA 3’
	Reverse: 5’ TGGCCCTTGCCCTGATTCG 3’
Human CA7	Forward: 5’ GCCGGCACTACTGGACCTAC 3’
	Reverse: 5’ TCCCCATCTGCCTTTCAGAGATG 3’
Human CA8	Forward: 5’ CGCCATCATTGCTCTGTTTGTTC 3’
	Reverse: 5’ CGCAGCAGAGGGTCTGGTAA 3’
Human CA9	Forward: 5’ CACCGCCTTTGCCAGAGTTG 3’
	Reverse: 5’ CTCTGAGCCTTCCTCAGCGA 3’

Human CA10	Forward: 5’ TCGTCTGCATATCAGCTCAACAGA 3’
	Reverse: 5’ CCGTTTCCCCACAGAGCAAAG 3’
Human CA11	Forward: 5’ CACATCGGACCAGCACCTGA 3’
	Reverse: 5’ ACACAGACTCCACGCTGCAT 3’
Human CA12	Forward: 5’ GCCCCAGTGAACGGTTCCAA 3’
	Reverse: 5’ GCAGGTCTATGGGGGACTGC 3’
Human CA13	Forward: 5’ CGAGGCTCAGCTGGGGATAC 3’
	Reverse: 5’ AGTGGTCGGAGGGAAGAGTCA 3’
Human CA14	Forward: 5’ GCTGCAGATGGGGGTCAACA 3’
	Reverse: 5’ TGGGCGACTGGGCATTGTTT 3’
Human PBGD	Forward: 5’ CAGCTTGCTCGCATACA 3’
	Reverse: 5’ GAATCTTGTCCCCTGTGGTG 3’
Mouse CA2	Forward: 5’ GCAACCGGATGGATTGGCTG 3’
	Reverse: 5’ CGCACGCTTCCCCTTTGTTT 3’
Mouse CA3	Forward: 5’ GCACACCGTGGACGGAGTAAA 3’
	Reverse: 5’ CCTTTCTCCCGTCCTATCTTCAGG 3’
Mouse CA4	Forward: 5’ GGCAGCGTCTTTCCCCTCAA 3’
	Reverse: 5’ CTTCTCAGGCCCCAAGCAACT 3’
Mouse CA5A	Forward: 5’ GTGGACGGCCATACCTACCC 3’
	Reverse: 5’ GATGCGCCCCGAGCTTCA 3’
Mouse CA9	Forward: 5’ CCTTTCTGCAGGAGAGCCCA 3’
	Reverse: 5’ GTAGTAGCGGCTGAGGTCCG 3’
Mouse CA12	Forward: 5’ TCGCCAGGACAAAGATGCCT 3’
	Reverse: 5’ TTTCCCCAGCAGGACCAACA 3’
Mouse β2M	Forward: 5’ CGGTGACCGTGATCTTTCTG 3’
	Reverse: 5’ AGGAAGTTGGGCTTCCCATT 3’

2.1.5. siRNAs

siRNA	Catalog ID	Company
ON-TARGETplus Non-targeting siRNA Control#1	D-001810-01-20	*Dharmacon, Lafayette, CO, USA*
SMARTpool: ON-TARGETplus Human CA9 siRNA	L-005244-00-0010	*Dharmacon, Lafayette, CO, USA*
SMARTpool: ON-TARGETplus Human CA12 siRNA	L-003634-00-0010	*Dharmacon, Lafayette, CO, USA*
SMARTpool: ON-TARGETplus Human EPAS1 siRNA	L-004814-00-0010	*Dharmacon, Lafayette, CO, USA*

SMARTpool: ON-TARGETplus Human HIF1A siRNA	L-004018-00-0010	*Dharmacon, Lafayette, CO, USA*

2.1.6. Carbonic anhydrase 9 promoter sequences

CA9 promoter	Sequence
WT	CCCCGATAACCTTCTGCCTGTGCACACACCTGCCCCTCA CTCCACCCCCATCCTAGCTTTGGTATGGGGGAGAGGGC ACAGGGCCAGACAAACCTGTGAGACTTTGGCTCCATCT CTGCAAAAGGGCGCTCTGTGAGTCAGCCTGCTCCCCTCC AGGCTTGCTCCTCCCCCACCCAGCTCTCGTTTCCAATGC ACGTACAGCCCGTACACACCGTGTGCTGGGACACCCC
HRE-mut	CCCCGATAACCTTCTGCCTGTGCACACACCTGCCCCTCA CTCCACCCCCATCCTAGCTTTGGTATGGGGGAGAGGGC ACAGGGCCAGACAAACCTGTGAGACTTTGGCTCCATCT CTGCAAAAGGGCGCTCTGTGAGTCAGCCTGCTCCCCTCC AGGCTTGCTCCTCCCCCACCCAGCTCTCGTTTCCAATGC TTTTACAGCCCGTACACACCGTGTGCTGGGACACCCC

2.1.7. Antibodies

Antibody	Host species	Company
Anti-α-smooth muscle actin antibody, clone 1A4 (A5228)	Mouse	*Sigma Aldrich, St. Louis, MO, USA*
Anti-beta-actin antibody (ab8226)	Mouse	*Abcam, Cambridge, UK*
Anti-CA9 antibody (11071-1-AP)	Rabbit	*Proteintech, Sankt Leon-Rot, Germany*
Anti-CA12 antibody (15180-1-AP)	Rabbit	*Proteintech, Sankt Leon-Rot, Germany*
Anti-HIF-1α (10006421)	Rabbit	*Cayman Chemical Company, MI, USA*
Anti-HIF-2α (AF2997-SP)	Rabbit	*R&D systems, Minneapolis, MN, USA*
Anti-Mouse IgG, horseradish-peroxidase-labelled (secondary) antibody (W4011)	Goat	*Promega GmbH, Madison, WI, USA*
Anti-Rabbit IgG, horseradish-peroxidase-labelled (secondary) antibody (W4021)	Goat	*Promega GmbH, Madison, WI, USA*

Anti-von Willebrand factor (vWF) antibody (A0082)	Rabbit	*Dako Deutschland GmbH, Hamburg, Germany*

2.2. Methods

2.2.1 Experimental animals and human samples

We have used the following animal species obtained from Charles River Laboratories, Sulzfeld, Germany for this study: adult male 1) Sprague-Dawley rats (Species: *Rattus norvegicus*) (300-350g of body weight (BW)) and 2) C57BL/6 J mice (Species: *Mus musculus*) (20-22g BW). Rats and mice were maintained under controlled temperature conditions (22 ± 2ºC), day and night cycle (14/10 hours), relative humidity (55 ± 10%) and food and water was provided ad libitum. All *in vivo* studies were performed according to the guidelines of the University of Giessen and were approved by the local ethical authorities (Regierungspräsidium Giessen, reference number - GI 20/10 Nr. G35/2017). All human lung tissue and plasma samples investigated in this study were provided by the UGMLC Giessen Biobank. From each subject informed consent was obtained in a written form. The study complied with the Declaration of Helsinki, and the protocol was approved by the Ethics Committee of the faculty of medicine at Justus-Liebig University of Giessen, Germany, for lung tissue (No. 111/08 and 58/15) and plasma (No. 100/2013) samples.

2.2.2. Monocrotaline (MCT)-induced pulmonary hypertension in rats

A pyrrolizidine alkaloid monocrotaline (MCT) is the main toxic substance isolated from the plant *Crotalaria spectabilis*. MCT is frequently used to induce experimental pulmonary hypertension, as we have previously published[37, 192, 193]. Basically, the experimental PH in this study was induced in adult male Sprague-Dawley rats (300-350g BW) via single subcutaneous (s.c.) administration of MCT at the dose of 60mg/kg in the area of animal neck. Fully established pulmonary vascular disease usually develops 5 weeks after the MCT injection. According to our developed protocol, MCT solution was freshly prepared by dissolving this alkaloid in 1N HCl and 1N NaOH. In details, 250mg of MCT was dissolved in 3ml of 1N HCl and 2ml of 1N NaOH with final adjustment of pH at 7.4. An s.c. injection was administered at day 0, while the healthy control rats received only the vehicle (HCl and NaOH) according to BW. In order to avoid possible infections, animals were receiving an antibiotic solution (2.5% baytril) from day 1 to 15 after the MCT injection. This antibiotic was dissolved in the drinking water, at a concentration of 2ml of baytril in 500ml of water.

2.2.3. Chronic hypoxia-induced pulmonary hypertension in mice

C57BL/6 J mice were exposed to chronic hypoxic (Hox) conditions (10% O_2) in duration of 5 weeks in order to develop PH, as we have previously described[37, 192-195]. In general, the mice were kept in ventilated hypoxic chambers under the temperature range from 22-24°C and the constant level of hypoxia was held by an autoregulatory control unit (Oxy Cycler A84 XOV). Mice exposed to normoxic (Nox) conditions (21% O_2) in a ventilated chamber served as a healthy control.

2.2.4. *In vivo* studies: experimental design

In order to investigate the effects of CA9 and 12 inhibition on development of experimental PH, we have used S4 inhibitor at the doses of 10 mg/kg (Figure 7a) and 100 mg/kg BW (Figure 7b) for rats and mice, respectively. In general, 3 weeks upon the MCT injection or chronic hypoxia exposure, animals started receiving the S4 inhibitor (Tocris Bioscience, Bristol, UK) via the *i.p.* application once per day for the next 2 weeks. Placebo groups received only the vehicles (PEG 400 (37,5%), Ethanol (12,5%), NaCl 0,9% (50%)). Echocardiographic assessment of the right ventricular structure and function was performed 2 times, as indicated in the scheme below (Figure 7). At the end of experiments (5 weeks), both rats and mice underwent the hemodynamic measurements, followed by determination of right ventricular hypertrophy (Fulton´s index), pulmonary vascular morphometry and tissue harvesting.

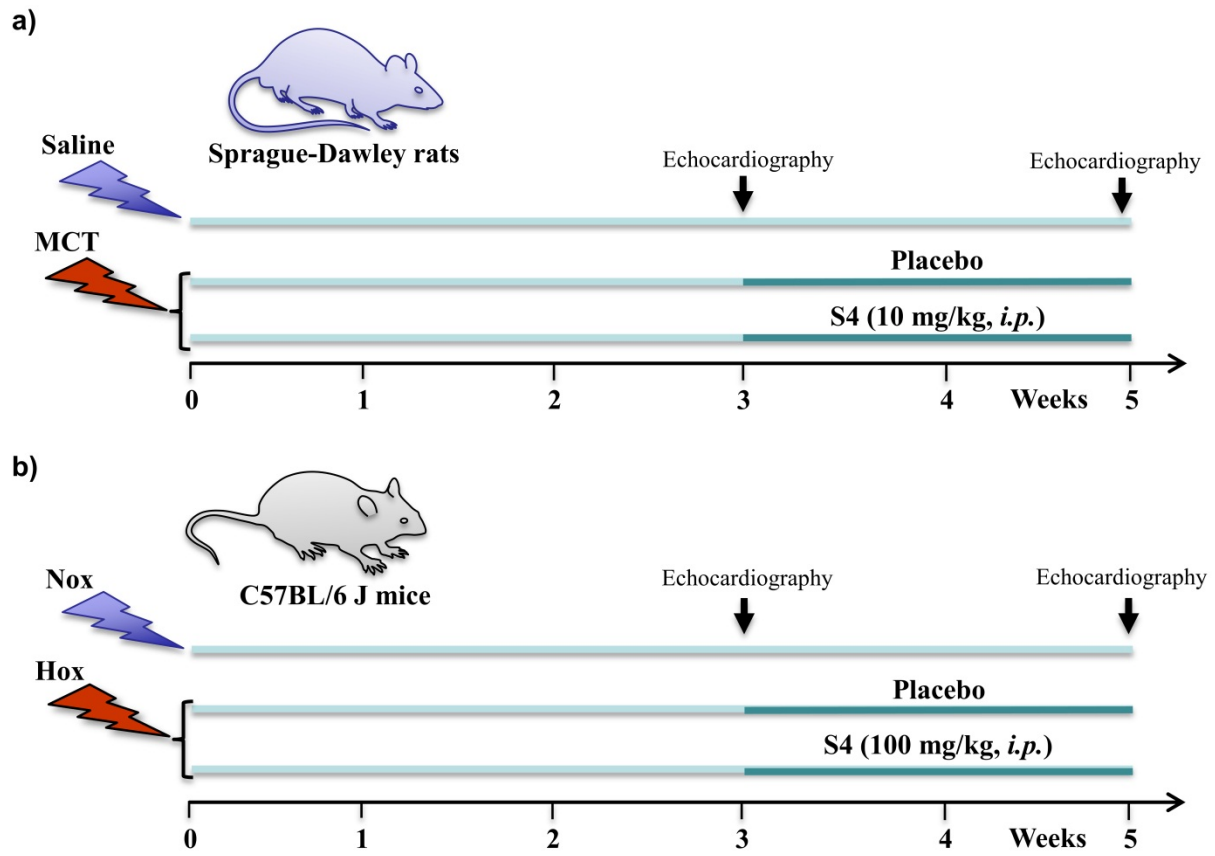

Figure 7. Experimental design of the S4 treatment study.

Schematic representation of the experimental design for investigation of CA9 and 12 inhibitor (S4) in **a**) monocrotaline-induced pulmonary hypertension in rats and **b**) chronic hypoxia-induced pulmonary hypertension in mice.

Abbreviations: Nox - normoxia; Hox - hypoxia; MCT - monocrotaline; *i.p.* - intraperitoneal administration.

2.2.5. Non-invasive echocardiography

We have performed the echocardiography as the leading non-invasive diagnostic imaging technique to obtain data on function and morphology of the right heart, as we have previously reported in the literature[196-199]. In this project, the images were acquired with a VEVO2100 high resolution imaging system (VisualSonics, Toronto, Canada) using the MicroScan linear array transducer MS250 (13-24 Mhz) for MCT rat and the MS550D (22-55 Mhz) for chronic Hox mice models of PH. Calculations were performed offline with the according software Vevo LAB provided by VisualSonics. The following parameters were assessed in our study: right ventricular internal diameter (RVID), right ventricular wall thickness (RVWT), tricuspid annular plane

systolic excursion (TAPSE), Pulsed tissue Doppler-derived right ventricular annular systolic excursion velocity (S´RV) and cardiac index (CI).

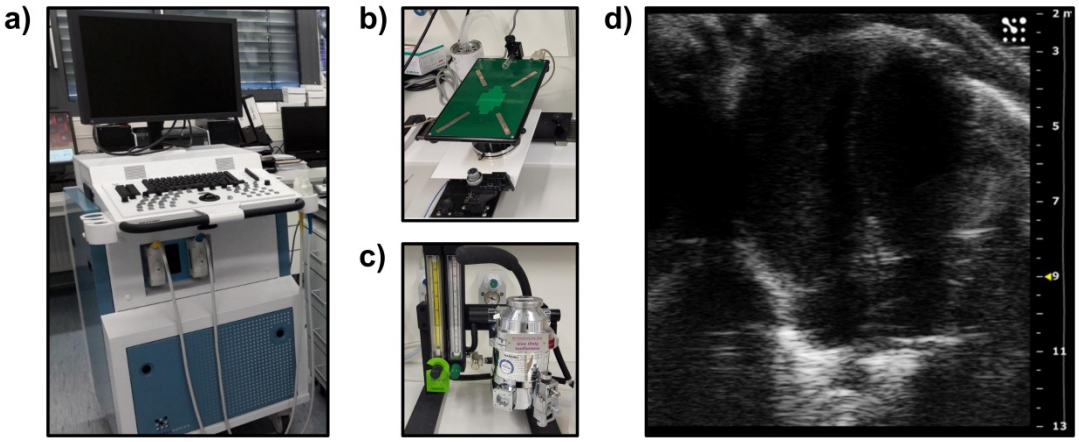

Figure 8. Echocardiography diagnostic imaging.

a) VEVO2100 high resolution imaging system, **b**) heating platform with electrocardiogram electrodes, **c**) isoflurane anesthesia system, **d**) example of echocardiography imaging in small animal rodents.

2.2.6. Hemodynamic and right ventricular hypertrophy (RVH) measurements

At the end of 5 weeks upon the MCT injection in rats and chronic hypoxia exposure in mice, we have used the Millar catheters for the invasive measurements of the systemic arterial pressure (SAP) and right ventricular systolic pressure (RVSP), similarly as we have described previously[196-199]. Briefly, during inhaled anesthesia and introduction of the mechanical ventilation, the right jugular vein was exposed, and the Millar catheter was forwarded through this vessel to the right ventricle for the measurement of RVSP. In the case of SAP measurement, we have used the left carotid artery.

Upon the completion of hemodynamics, the hearts of both animal models were extracted and dissected to separate right ventricle (RV) from the left ventricle and septum (LV+S).The weight ratio of these two components (RV/(LV+S)) was calculated as a measure of right ventricular hypertrophy (RVH), as we have previously described[196, 198, 199].

2.2.7. Lung tissue processing

After the completion of the hemodynamic measurements, the abdomen and thoracic cavity of animals were opened and both heart ventricles were incised in order to allow the removal of blood. Briefly, the right ventricle was initially incised at approximately 5mm below the base of pulmonary artery and the lungs were flushed out of blood by a cannula connected to a reservoir with saline solution, which was inserted into the pulmonary artery through the right ventricle. Once the flushing was finalized, the right lung lobes were snap frozen in liquid nitrogen and stored for further analyses, while the left lungs were prepared for histology using a cannula inserted into the pulmonary artery and connected to a reservoir filled with 3.5-3.7% formalin solution. After the formalin fixation, the lungs were later placed in histological cassettes, dehydrated in an automatic dehydration machine and then embedded in paraffin. For different staining procedures, the sections of 3μm in diameter were cut from the paraffin blocks using a microtome.

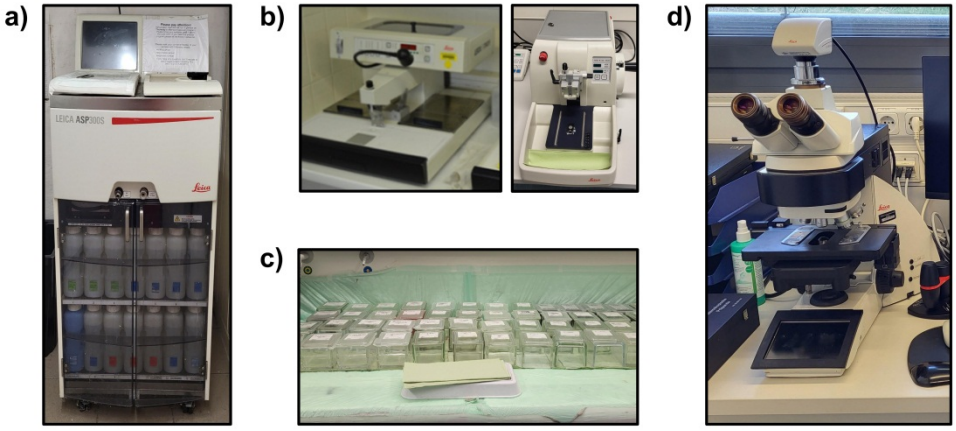

Figure 9. Immunohistochemistry: lung tissue processing and morphometry.
a) Dehydration machine, **b**) embedding machine and microtome, **c**) immunostaining procedure, **d**) histological morphometry.

2.2.8. Histological assessment of the pulmonary vascular remodeling: degree of muscularization

The assessment of pulmonary vascular remodeling was performed by the morphometric determination of the degree of muscularization of the rats and mice small peripheral pulmonary vessels, as we have published before[200-202]. Initially, the sections of formalin-fixed and paraffin embedded lung tissues were obtained as mentioned above, and double immunostaining was performed with an anti-α-smooth muscle actin (αSMA) and anti-von Willebrand factor antibodies.

The degree of muscularization was analyzed by categorizing the small pulmonary vessels (20-50μm in size for MCT rat model and 20-70μm in size for chronic Hox mice model) into 3 groups: fully muscularized, partially muscularized and non-muscularized. All morphometric analyses were done in a blinded fashion manner.

2.2.9. Isolation of mouse pulmonary artery smooth muscle cells (PASMCs)

Mouse PASMCs were isolated from pulmonary precapillary arteries as previously described[203]. In detail, the pulmonary artery was cannulated and 3 ml of Medium 199 (M199) containing 5mg/ml Fe_3O_4, 5mg/ml low melting point agarose, 1% penicillin and 1% streptomycin was injected into mice. Because iron particles do not pass through capillaries, only precapillary arteries were filled with the rapidly solidifying agarose and iron. Next, lung tissue was minced with scissors in 1ml phosphate buffered saline (PBS) and mixture was suspended in 10ml PBS in a magnetic holder, attracting the pulmonary arteries containing the iron particles and agarose. The supernatant was aspirated and the arteries, after washing 3 times with PBS, were moved into Petri dishes containing 10ml of M199 with 80U/ml collagenase. and incubated at 37°C for one hour. Upon incubation, tissue mixture was disrupted by drawing it through 15- and 18-gauge needles. The resulting suspension was washed 3 times with M199 containing 10% fetal bovine serum (FBS) in the magnetic holder. Pulmonary artery medial layer was resuspended in medium, transferred to culture flasks and incubated at 37°C in the cell incubator for approximately 5 days. Cells were split upon reaching 80% confluence and cultured for two passages in human medium for SMC (PromoCell, Heidelberg, Germany) with 15% FBS. For this study, experimental procedures included PASMCs exposure to hypoxic (1% O_2) or normoxic (21% O_2) conditions for different duration of time (6 hours, 1, 3 and 5 days), and subsequently analysis for CAs mRNA and protein expression. In addition, mouse PASMCs were treated with either S4 inhibitor or dimethyl sulfoxide (DMSO) and exposed to hypoxic (1% O_2) or normoxic (21% O_2) conditions for 72 hours, followed by proliferation measurements.

2.2.10. Human pulmonary artery smooth muscle cell *in vitro* culture, RNA isolation and real-time polymerase chain reaction (PCR)

Donor human PASMCs were purchased from Lonza, Basel, Switzerland and cultured in Smooth Muscle Growth Medium-2 (Lonza, Basel, Switzerland) containing supplement-mix. Supplements include recombinant human fibroblast growth factor-B (rhFGF-B), recombinant human epidermal growth factor (rhEGF), insulin and antibiotics gentamicin and amphotericin. Human PASMCs passage 7 were incubated at 37°C in a humidified atmosphere of 5% CO_2 in either normoxic (21% O_2) or hypoxic (1% O_2) conditions for a period of 24 and 48 hours. In experiments investigating non-hypoxia stimuli hPASMC were cultured in Smooth Muscle Cell Basal Medium in the presence of antibiotics, which served as unstimulated control. Furthermore, cells were stimulated with either 30 ng/ml of human transforming growth factor beta (TGF-β), 30 ng/ml of human tumor necrosis factor alpha (TNF-α) or 50 ng/ml of human platelet-derived growth factor (PDGF-BB) for a period of 24, 48 and 72 hours. In both experimental designs, after the incubation period cell lysates were prepared for the qPCR measurement. Briefly, cells were washed once with 500 µl of ice-cold PBS before adding 300 µl/well of RLT lysis buffer (Qiagen GmbH, Hilden, Germany) completed with 10µl/ml of mercaptoethanol.

Total RNA (1µg) was extracted from isolated PASMCs or lung homogenates from human IPAH patients and donors using RNeasy Mini Kit (Qiagen GmbH). Complementary DNA (cDNA) was produced by reverse transcriptase polymerase chain reaction via iScript cDNA Synthesis Kit (Bio-Rad, Hercules, CA, USA). Real-time PCR was performed in Mx3000P (Agilent Stratagene, Santa Clara, CA, USA) or CFX Connect™ (Bio-Rad) qPCR system using the iTaq Universal SYBR Green Supermix (Bio-Rad). List of primers used is listed above (**2.1.4. Primer sequences).** Porphobilinogen deaminase (PBGD) served as a housekeeping gene. The cycling protocol was 1x(95°C, 10 min) and 45x(95°C, 5s; 62°C, 5s, 72°C, 10s). Each gene was measured in duplicate. In order to confirm specific amplification of the expected PCR product, melting curve analysis and agarose gel electrophoresis with SYBR® Safe DNA gel stain (Invitrogen, Waltham, MA, USA) were performed. The ΔCt values were calculated by subtracting the Ct values of the target gene from the endogenous control (ΔCt = Ct [endogenous control] - Ct [target]) and the fold change $2^{\Delta\Delta Ct}$ was calculated as described previously[204].

2.2.11. RNA interference by synthetic siRNA

Selective targeting of HIF-1α, HIF-2α, CA9 and 12 was performed using a pool of specific small interfering RNA (siRNA). Scrambled siRNA sequence (SCR siRNA) which does not target any gene was used as a control. SiRNAs used are listed above (**2.1.5. siRNAs**). Transfection was performed in Smooth Muscle Cell Basal Medium without antibiotics when PASMCs have reached approximately 60 % confluence. The medium was changed four hours prior to transfection performed using a Lipofectamine™ 2000 Transfection Reagent (Thermo Fisher Scientific Inc., Waltham, MA, USA). SiRNA was used at concentration of 100 nM and both siRNA and transfection reagent were diluted in Opti-MEM™ medium (GIBCO™, Waltham, MA, USA). Following five hours upon transfection, the medium was changed to Smooth Muscle Growth Medium-2 containing antibiotics.

2.2.12. Dual-luciferase reporter assay

Human lung epithelial cell line (A549) were co-transfected with either wild-type (WT) or hypoxia responsive element (HRE) mutated (HRE-mut) CA9 promoter cloned into pGL3 firefly luciferase reporter vector and promoter driven pNL1.1.CMV[Nluc/CMV] NanoLuc® control vector (Promega GmbH, Madison, WI, USA). Cloning was accomplished by Gibson Assembly® Cloning Kit (New England Biolabs, Ipswich, MA, USA). WT and HRE-mut CA9 promoter sequences are listed above (**2.1.6. Carbonic anhydrase 9 promoter sequences**). Co-transfection was performed by Lipofectamine™ 3000 (Thermo Fisher Scientific Inc., Waltham, MA, USA) with 1.5 µg of total DNA (1485 ng of firefly and 15 ng of NanoLuc DNA) following the manufacturer's instructions. Following the transfection, A549 cells were exposed to normoxia (21% O_2) or hypoxia (1% O_2) conditions for 24 hours. Subsequently, Nano-Glo® Dual-Luciferase® Reporter Assay System (Promega GmbH) was performed following the manufacturer's instructions. Firefly and NanoLuc luciferase luminescence were measured by Infinite M200 microplate reader (Tecan Trading AG, Männedorf, Switzerland) and the results were calculated as a Firefly/NanoLuc RLU ratio.

2.2.13. Western blot analysis

Human donor PASMCs passage 7 were incubated at 37°C in a humidified atmosphere of 5% CO_2 in either normoxic (21% O_2) or hypoxic (1% O_2) conditions for a period 48 hours. In experiments

investigating stimulation with non-hypoxia stimuli, including TGF-β, TNF-α, PDGF-BB, IL-1 and IL-6, hPASMC were cultured in Smooth Muscle Cell Basal Medium in the presence of antibiotics for a period of 48 hours. Used concentration of non-hypoxia stimuli were described above, except IL-1 and IL-6 which were used at 10 ng/ml.

Proteins from PASMCs were extracted using a cell scraper. Proteins from lung tissue samples of chronic hypoxia-induced PH mice were extracted by Precelly®24 Homogeniser (PeqLab Biotechnologie GmbH, Erlangen, Germany). RIPA lysis buffer (Santa Cruz Biotechnology Inc., Dallas, TX, USA) completed with phenylmethylsulfonyl fluoride (PMSF), sodium orthovanadate and protease inhibitor cocktail was added to the PASMCs or homogenized tissue. Following incubation on ice, samples were centrifuged (20,000xg, 15 minutes, 4°C) and Pierce™ BCA Protein Assay (Thermo Fisher Scientific Inc., Waltham, MA, USA) was used to determine protein concentration in the supernatant. Protein quantity of 20μg/μL was used for Western blotting. Protein extracts were separated on a 12% or 15% sodium dodecyl sulfate (SDS) polyacrylamide gel, followed by electrotransfer to a 0.45 μm polyvinylidene fluoride membrane (PVDF, Pall Corporation, Dreieich, Germany). Next, membrane was blocked with 5% non-fat dry milk in TBS-T buffer (Tris Buffer Saline + 0.1% Tween 20) for one hour and subsequently incubated overnight at 4°C with anti-CA9 (1:1000 dilution), CA12 (1:1000 dilution), HIF-1α (1:1000 dilution), HIF-2α (1:1000 dilution) or anti-β-actin (1:50000 dilution) antibodies. Details of all the antibodies used are listed above (**2.1.7. Antibodies**). Following membrane washing in TBS-T buffer three times for 10 min, specific immunoreactive signals were detected by enhanced chemiluminescence (GE Healthcare, Little Chalfont, UK) using an appropriate secondary antibody coupled to horseradish-peroxidase.

2.2.14. Measurement of PASMCs proliferation and cell viability

Proliferation of human and mouse PASMCs was assessed by 5-bromo-2′-deoxyuridine (BrdU) assay (Sigma Aldrich, St. Louis, MO, USA). In more details, 5000/well of human PASMCs were seeded into 24-well plates and following the 24 hours starvation period PASMCs were incubated at 37°C in a humidified atmosphere of 5% CO_2 in either normoxic (21% O_2) or hypoxic (1% O_2) conditions for 72 hours. PASMCs were cultured in Smooth Muscle Growth Medium-2 and treated with different concentrations of S4 (10 and 50μM). BrdU labeling reagent was added 18 hours

towards the end of the incubation period. The absorbance of the substrate reaction was measured at 370nm (reference wavelength 492nm) by Infinite M200 microplate reader. Same conditions were applied for mouse PASMCs. In case of the experiments investigating non-hypoxia stimuli, human PASMCs were cultured in Smooth Muscle Cell Basal Medium containing antibiotics and stimulated with 50 ng/ml of PDGF-BB. In addition, same experimental design (hypoxia and PDGF-BB induced proliferation) was coupled with siRNA-driven specific knockdown of CA9 and 12.

Assessment of human and mouse PASMCs cell viability was performed by Thiazolyl Blue Tetrazolium Blue (MTT) assay (Sigma Aldrich, St. Louis, MO, USA). Briefly, 5000/well of mouse or human PASMCs were seeded into 96-well plates and following the recovery period PASMCs were incubated at 37°C in a growth medium containing various concentration of S4 for 24 hours. Subsequently, growth medium was changed with 0.5 mg/ml of MTT dissolved in RPMI 1640 medium (PAN-Biotech GmbH, Aidenbach, Germany) in darkness for four hours. Next, MTT was replaced with acidic isopropanol and following 15 minutes of room temperature incubation on shaker, MTT conversion to MTT formazan absorbance was measured at 570 nm (reference wavelength 690 nm) by Infinite M200 microplate reader.

2.2.15. Measurement of PASMCs migration

Human PASMCs were seeded in a 2 well silicone inserts with a defined cell-free gap (Ibidi, Gräfelfing, Germany) placed in a 24-well plate at a density of 7500 cells per insert well. Following the recovery period the inserts were removed from the plates. After washing one time with warm PBS, cells were treated with medium containing either 50μM S4 or DMSO control and transferred to IncuCyte ZOOM Live-Cell microscopy imaging system (Essen BioScience Ltd., Ann Arbor, MI, USA). PASMCs were incubated for a period of 12 hours under hypoxia conditions (1% O_2, 5% CO_2) or 24 hours upon PDGF-BB stimulation (21% O_2, 5% CO_2), at 37° in water saturated incubator. Images were taken every 10 (hypoxia) or 15 (PDGF-BB) minutes and analysed by IncuCyte Software (Essen BioScience Ltd). Results are presented as percent of initial wound surface covered by migrated cells (wound confluence %).

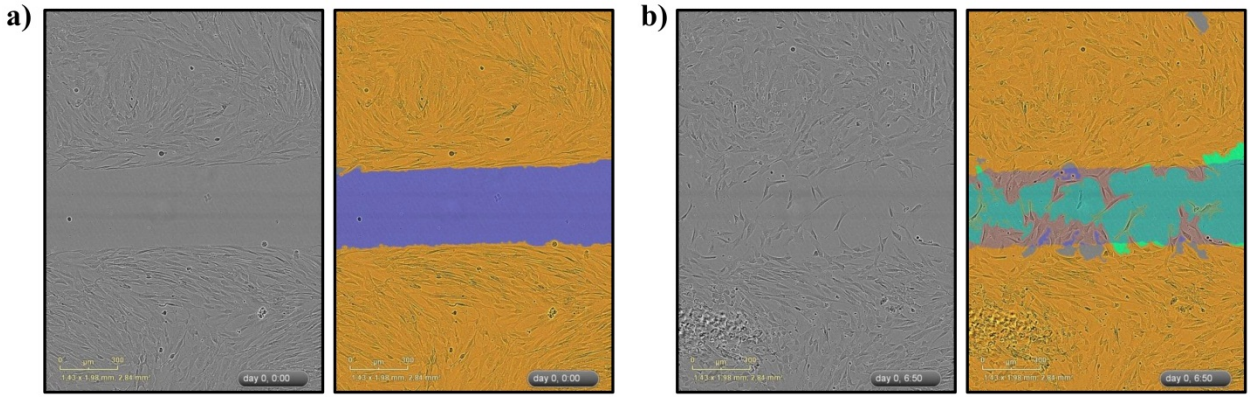

Figure 10. IncuCyte ZOOM Live-Cell microscopy imaging system.
Representative images of **a**) initial wound surface and **b**) wound surface covered with migrated PASMCs analyzed by IncuCyte Software. Scale bars=300µm.

2.2.16. PASMCs intracellular and extracellular pH measurements

For assessment of intracellular pH, 5-(and-6)-Carboxy SNARF-1 Acetoxymethyl Ester, Acetate (Thermo Fisher Scientific Inc., Waltham, MA, USA) was used. Carboxy SNARF-1 is a long-wavelength fluorescent dye with pH-dependent emission. In more details, passage 7 of human PASMCs were cultured at 37°C in a humidified atmosphere of 5% CO_2 in either normoxic (21% O_2) or hypoxic conditions (1% O_2) for a period of 48 hours and stimulated with 50µM S4 inhibitor or DMSO. Upon 48 hours cells were washed with Live Cell Imaging Solution (LCIS, Thermo Fisher Scientific Inc., Waltham, MA, USA) and incubated with 5 µM Carboxy SNARF-1 at 37°C for 30 minutes. Following two more washings with LCIS, cells were incubated at 37°C for 10 minutes in either LCIS or cell loading solution. In order to quantify intracellular pH, Intracellular pH Calibration Buffer Kit was used (Thermo Fisher Scientific Inc., Waltham, MA, USA) for preparation of cell loading solutions. In details, three different calibration buffers with fixed pH of 5.5, 6.5 and 7.5 were used with addition of 10µM Nigericin and 10 µM Valinomycin. Carboxy SNARF-1 fluorescence was measured with 514nm excitation and 580nm and 640nm emission wavelengths by Infinite M200 microplate reader.

In order to estimate changes of human PASMCs extracellular pH, cell culture medium was collected after incubation and pH measurements were immediately performed by 766 Calimatic pH meter (Knick Elektronische Messgeraete GmbH & Co. KG, Berlin, Germany). In details, human PASMCs passage 7 were cultured in normoxic and hypoxic or basal and PDGF-BB

stimulated conditions in the presence of 50μM S4 inhibitor or DMSO control for a period of 72 hours.

2.2.17. Measurement of PASMCs tyrosine and serine/threonine protein kinase activity

Human PASMCs were cultured at 37°C in a humidified atmosphere of 5% CO_2 in normoxia (21% O_2) or hypoxia (1% O_2) conditions for 72 hours. In hypoxia conditions, cells were treated with either 50μM S4 inhibitor or DMSO control. Upon incubation cells were placed on ice, washed twice with ice-cold PBS and scraped from the dishes in 200 μl of M-PER lysis buffer (Thermo Fisher Scientific Inc., Waltham, MA, USA) containing Pierce protease and phosphatase inhibitor cocktails. The cell lysate was incubated for one hour at 4°C, followed by centrifugation at 16,000g for 15 min at 4°C. Supernatant was immediately frozen and stored at -80°C in aliquots for subsequent peptide-based kinase activity assay by PamStation®12 platform (PamGene International, s-Hertogenbosch, Netherlands) with Evolve 12 software, as previously described[200].

1 μg of protein lysate was dissolved in protein kinase buffer and placed on the array of the PamChip PTK (protein tyrosine kinase) and STK (serine/threonine kinase). Bionavigator software (PamGene) performed analysis of the obtained data and prediction of upstream activated kinases, based on the phosphorylation of their distinct substrates placed on the peptide array chip. Data are visualized on the log-transformed y-axis in a heat map depicting the degree of phosphorylation for each peptide.

2.2.18. Enzyme-linked immunosorbent assay (ELISA)

EDTA plasma samples were obtained from pulmonary artery during the conductance right heart catheterization, for assessing of RV-arterial coupling in PH patients. Based on the ratio of end-systolic to arterial elastance (Ees/Ea), subjects were affiliated with the coupled (Ees/Ea>0.8) or uncoupled (Ees/Ea<0.8) group, as previously described[205, 206]. Demographic and clinical data of PH patients are presented in Table 4. In order to analyze circulating CA9 levels in described subjects, CA9 ELISA assay (R&D systems, Minneapolis, MN, USA) was performed following the manufacturer's instructions. Calculation of the results was achieved by using the five parameter logistic curve. Results are presented as pg per ml of plasma.

2.2.19. Statistical analysis

Values are presented as means ± SEM. The statistical significance of the data was assessed using Student's t test with Welsh's correction or analysis of variance (one-way ANOVA) with Tukey or Dunnett post-hoc test, as appropriate. For multiple comparisons involving more than four groups, a two-way ANOVA with Sidak post-hoc test was conducted. In cases of variables association, linear regression analysis with Spearman correlation was performed. A p-value below 0.05 was considered as statistically significant.

3. RESULTS

3.1. Carbonic anhydrases (CAs) mRNA expression profile

3.1.1. IPAH patients' CAs gene analysis

Lung tissue samples obtained from IPAH patients and donors were analyzed for mRNA expression for all members of the CA family of enzymes, as described above. Our data showed a significant increase of CA1, 9 and 12 mRNA expression in lung tissue samples of IPAH patients compared to donors (Figure 11).

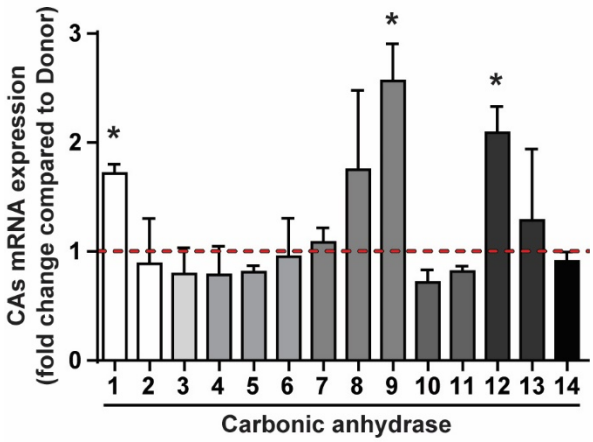

Figure 11. CAs gene expression profile in IPAH patients compared to donors.
mRNA expression of 14 carbonic anhydrase family isoforms in IPAH patients compared to donors is shown. Data are given as a fold change of IPAH patients' CAs mRNA expression compared to donors (depicted by the red dotted line in the figure). Data are presented as mean ± SEM (n=7-9). *p<0.05 compared to donor.

Demographic and clinical characteristics of involved human subjects, such as age, gender ratio and mPAP are depicted in Table 3. The mean pulmonary arterial pressure for the IPAH patients group measured by right heart catheterization was 49.7 ± 4.2 mmHg.

Table 3. Demographic and clinical data of IPAH patients and donors.

	Age (Years)	Gender ratio m/f (%)	mPAP (mmHg)	SAP (mmHg)	6MWD (m)
Donor	51.2 ± 5.3	37.5/62.5	N/A	N/A	N/A
IPAH	36.1 ± 4.9	33.3/66.7	49.7 ± 4.2	81.5 ± 12.8	319 ± 17.8

Abbreviations: f – female; m – male; mPAP – mean pulmonary arterial pressure; SAP – systolic arterial pressure; 6MWD – six-minute walk distance. Data are presented as mean ± SEM (n=8 (Donor), 9 (IPAH), 4 (mPAP, SAP), 6 (6MWD)).

3.1.2. CAs mRNA expression in mouse PASMCs after chronic hypoxic incubation

Mouse PASMCs were exposed to hypoxia conditions for five days, and gene expression levels for different CA isoforms were analyzed, as mentioned in the methods section. Our results showed that there was a visible tendency in increased mRNA levels for CA3 and 12 (Figure 12a).

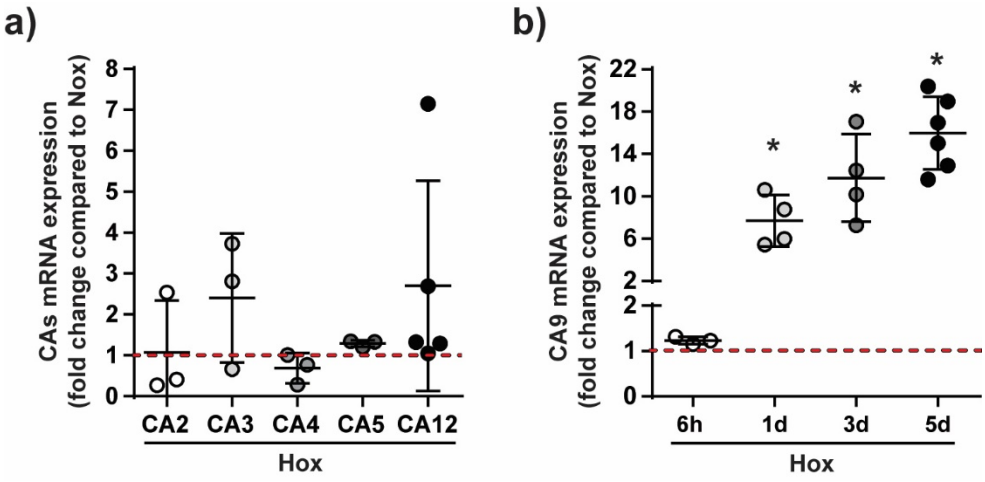

Figure 12. CAs gene expression profile in mouse PASMCs after hypoxia exposure.

a) mRNA expression of CAs in mPASMCs after five days of 1% O_2 chronic hypoxia and **b**) CA9 mRNA expression in mPASMC after 6 hours (6h), one (1d), three (3d) and five (5d) days of 1% O_2 hypoxia incubation are shown. Data are given as fold change compared to appropriate normoxia (Nox) control (portrayed by a red dotted line). Data are presented as mean ± SEM (n=3-4). *$p<0.05$ compared to appropriate normoxia control.

Notably, there was a significant, time-dependent enhancement in the mRNA expression of CA9 in mPASMCs exposed to different durations of hypoxia (Figure 12b).

3.1.3. CA9 and 12 mRNA expression in human PASMCs after chronic hypoxic incubation

As described in the methods paragraph, human PASMCs were cultured in hypoxia conditions for different durations of time and analyzed for CA9 and 12 mRNA expression levels.

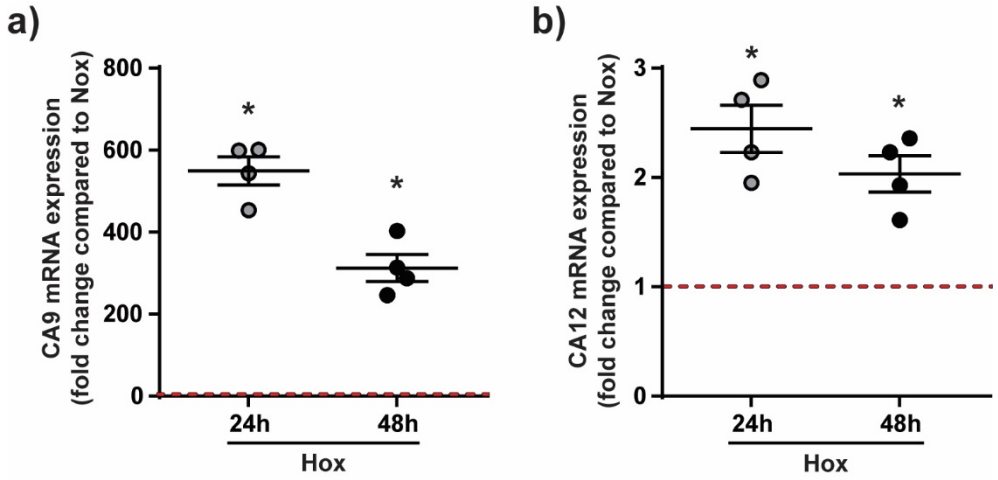

Figure 13. CA9 and 12 gene expression in hPASMCs after hypoxia exposure.

a) CA9 and **b**) CA12 mRNA expression in hPASMCs after 24 (24h) and 48 (48h) hours of hypoxia (1% O_2) incubation (Hox) are shown. Data are given as fold change compared to appropriate normoxia (Nox) control (depicted by the red dotted line in the figure). Data are presented as mean ± SEM (n=4). *$p<0.05$ compared to appropriate normoxia control.

Our investigation revealed a significant increase of both CA9 (Figure 13a) and 12 (Figure 13b) mRNA expression levels in hPASMCs after hypoxia exposure. In both cases, the most prominent increase was observed after 24 hours of hypoxia incubation.

3.1.4. Human PASMCs CA9 and 12 mRNA expression after TNF-α, PDGF-BB and TGF-β stimulation

Human PASMCs were stimulated with various inflammatory stimuli and growth factors, such as TNF-α, PDGF-BB and TGF-β for 24, 48 and 72 hours and subsequently investigated for CA9 and 12 mRNA expression levels, as described previously.

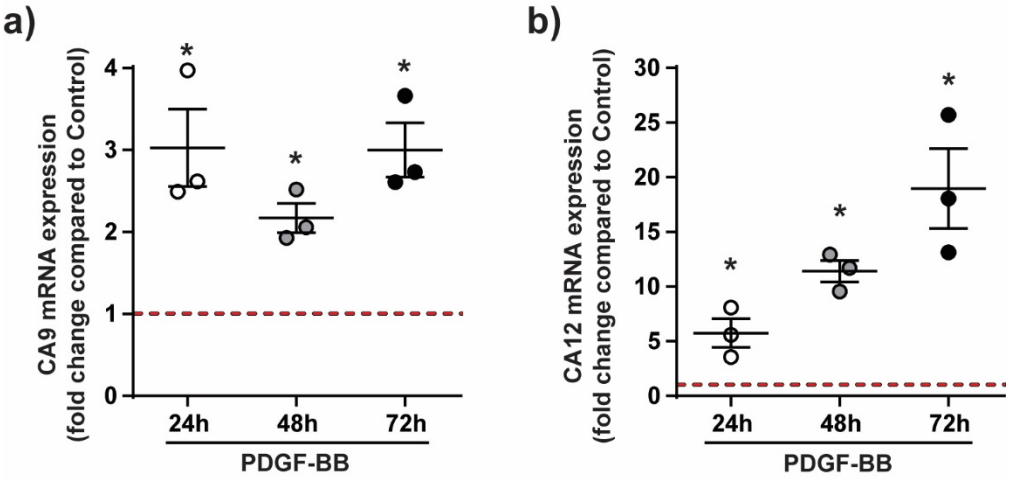

Figure 14. CA9 and 12 gene expression profile in human PASMCs after PDGF-BB stimulation.

a) CA9 and **b**) 12 mRNA expression in hPASMCs after 24 (24h), 48 (48h) and 72 (72h) hours of platelet-derived growth factor-BB (PDGF-BB) stimulation are shown. Data are given as fold change compared to control (depicted by the red dotted line in the figure) and presented as mean ± SEM (n=3). *p<0.05 compared to control.

Our results revealed that all investigated stimuli led to a significant increase of mRNA expression levels of both CA9 and 12 (Figures 14-16). In more detail, PDGF-BB stimulation resulted in significant CA9 and 12 gene level increases after all investigated time points, with the most prominent change observed in CA12 mRNA levels after PDGF-BB stimulation for 72 hours (Figure 14a-b).

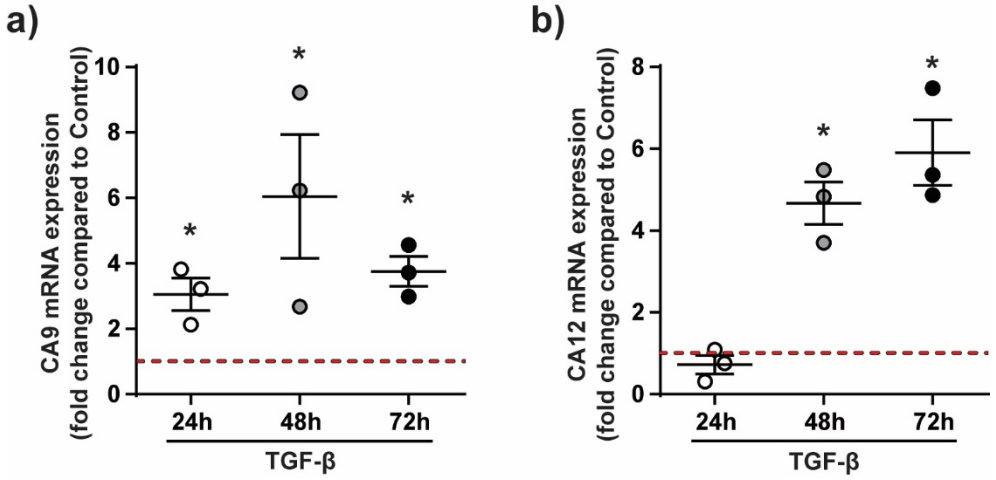

Figure 15. mRNA expression of CA9 and 12 in human PASMCs after TGF-β stimulation.

a) CA9 and **b**) 12 mRNA expression in hPASMCs after 24 (24h), 48 (48h) and 72 (72h) hours of transforming growth factor beta (TGF-β) stimulation are shown. Data are given as fold change compared to control (portrayed by the red dotted line in the figure) and presented as mean ± SEM (n=3). *p<0.05 compared to control.

Similarly, TGF-β stimulation of hPASMCs led to a significant increase of CA9 mRNA after all experimental conditions (Figure 15a). In the case of CA12 mRNA levels, the effect was observed after 48 and 72 hours of TGF-β stimulation (Figure 15b). Furthermore, TNF-α stimulation of hPASMCs significantly increased CA9 and 12 mRNA expression after 48 and 72 hours (Figure 16a-b).

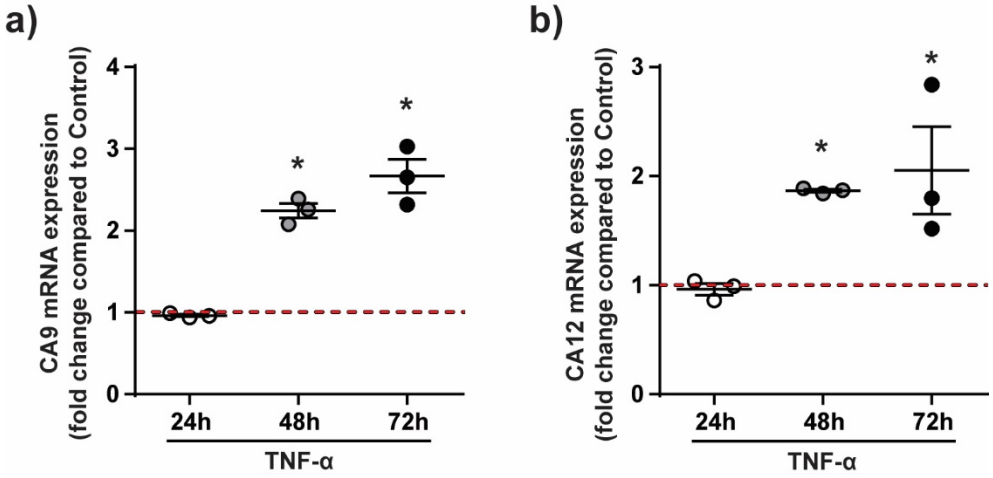

Figure 16. CA9 and 12 gene expression profile in human PASMCs after TNF-α stimulation.
a) CA9 and **b**) 12 mRNA expression in hPASMCs after 24 (24h), 48 (48h) and 72 (72h) hours of tumor necrosis factor-alpha (TNF-α) stimulation are shown. Data are given as fold change compared to control (portrayed by the red dotted line in the figure) and presented as mean ± SEM (n=3). *p<0.05 compared to control.

3.2. CA9 and 12 protein expression profile

3.2.1. CA9 and 12 protein expression in the lungs of mice with chronic hypoxia-induced PH

Lung tissue samples obtained from chronic hypoxia-induced PH mice and respective normoxia control were analyzed for CA9 and 12 protein expression, as described in the methods section.

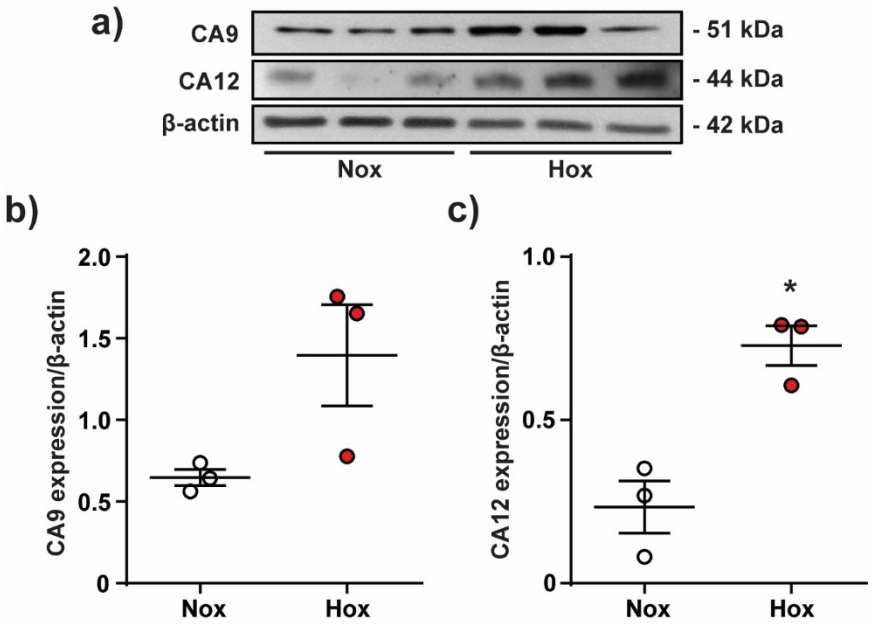

Figure 17. The protein expression of CA9 and 12 in the lungs of mice with chronic hypoxia-induced pulmonary hypertension.

a) Representative blots of CA9 and 12 protein expression in lung tissue (homogenate) of mice exposed to 5 weeks of 10% O_2 chronic hypoxia (Hox) compared to normoxia control (Nox) and respective densitometric analysis of **b**) CA9 and **c**) 12 protein expression are shown. Data are given as the ratio of CA9 or 12 to β-actin expression and presented as mean ± SEM (n=3). *$p<0.05$ compared to Nox.

The obtained data showed a significant augmentation of CA12 protein expression in the lungs of mice with chronic hypoxia-induced PH compared to normoxia control (Figure 17c) and a noticeable trend in augmented CA9 levels (Figure 17b).

3.2.2. Mouse PASMCs CA9 and 12 protein expression under chronic hypoxia

As previously described, precapillary PASMCs isolated from healthy mice were exposed to different durations of hypoxia, and subsequently, protein expression levels for CA9 and 12 were investigated.

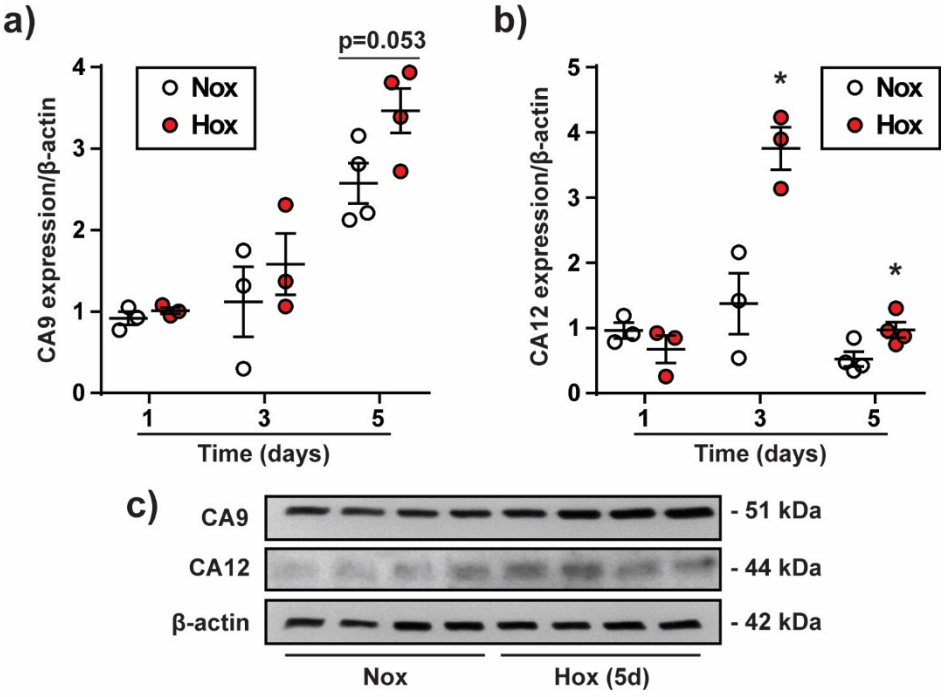

Figure 18. CA9 and 12 protein expression profile in mPASMCs after hypoxia exposure. Densitometric analysis of **a**) CA9 and **b**) 12 protein expression in mPASMCs after one, three and five days of 1% O_2 hypoxia incubation (Hox) or respective normoxia control (Nox) are shown. **c**) Representative blots of CA9 and 12 protein expression in mPASMCs after five days (5d) of 1% O_2 hypoxia incubation are presented. Data are given as the ratio of CA9 or 12 to β-actin expression and displayed as mean ± SEM (n=3-4). *p<0.05 compared to Nox.

Our results showed a significant increase of CA12 protein expression after three and five days of hypoxia exposure (Figure 18b), while the rise in CA9 protein expression was approaching significance after five days of hypoxia exposure (Figure 18a).

3.2.3. CA9 and 12 protein expression in human PASMCs after chronic hypoxic incubation

PASMCs isolated from healthy donors were cultured in hypoxia for 48 hours and, as described above, analyzed for CA9 and 12 protein expression levels. Our data showed a significant increase of both CA9 and 12 protein expression profiles after hypoxia exposure, compared to normoxia control (Figure 19b-c).

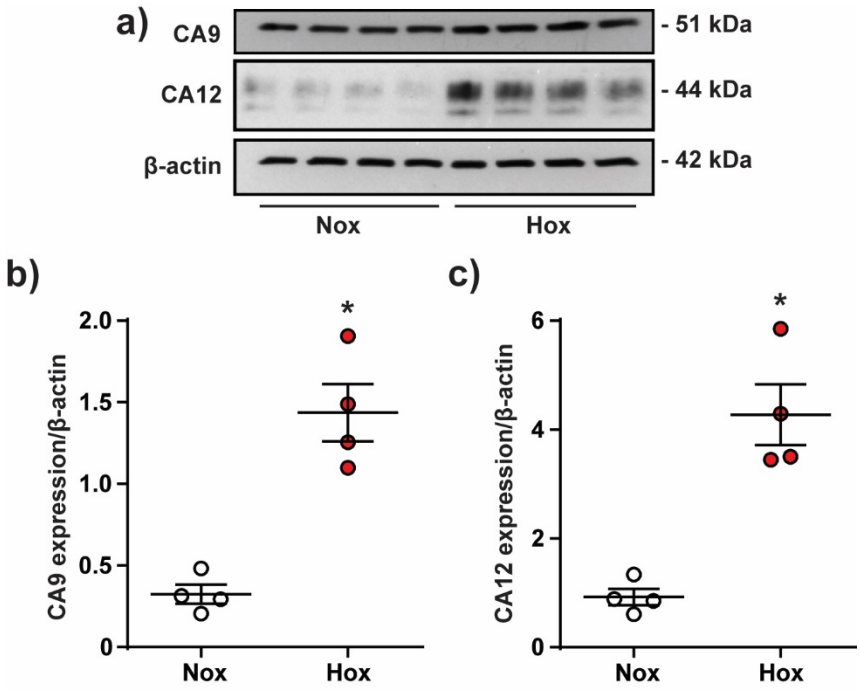

Figure 19. The protein expression of CA9 and 12 in hPASMCs after hypoxia exposure.

a) Representative blots of CA9 and 12 protein expression in hPASMCs after 48 hours of 1% O_2 chronic hypoxia incubation (Hox) compared to normoxia control (Nox) and densitometric analysis of **b**) CA9 and **c**) 12 protein expression are shown. Data are given as the ratio of CA9 or 12 to β-actin expression and presented as mean ± SEM (n=4). *p<0.05 compared to Nox.

3.2.4. Human PASMCs CA9 and 12 protein expression after TNF-α, PDGF-BB, TGF-β, IL-1 or IL-6 stimulation

As mentioned above, human PASMCs were stimulated with various inflammatory stimuli and growth factors, such as TNF-α, PDGF-BB, TGF-β, IL-1 and IL-6 for 48 hours and subsequently investigated for CA9 and 12 protein expression levels. CA9 expression analysis showed a significant increase upon TGF-β stimulation and a notable trend in augmentation after TNF-α and PDGF-BB stimulation (Figure 20a). Additionally, our results demonstrated a significant increase of CA9 protein expression upon IL-1 and IL-6 stimulation (Figure 21a, d).

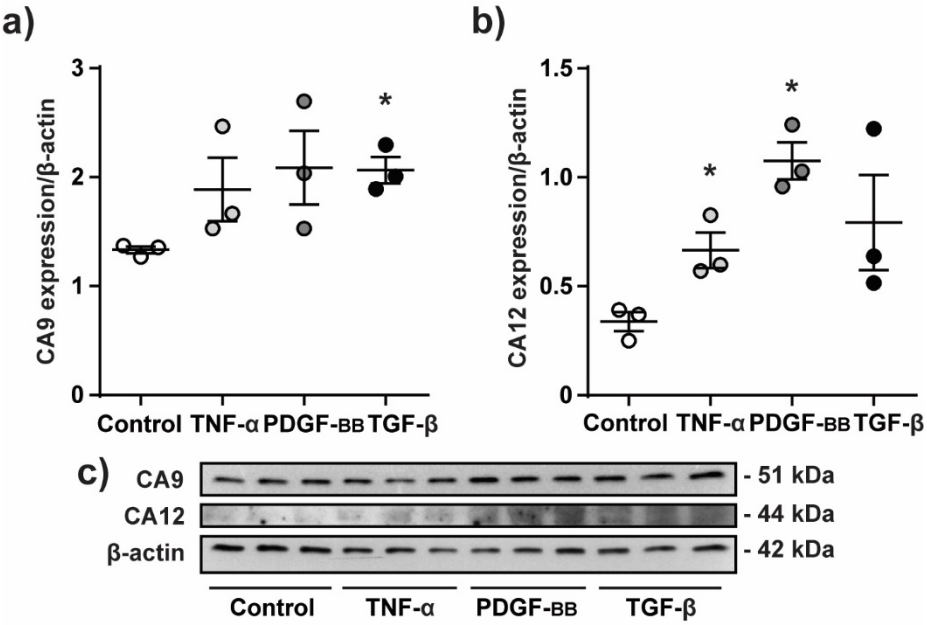

Figure 20. CA9 and 12 protein expression in human PASMCs after TNF-α, PDGF-BB and TGF-β stimulation.

Densitometric analysis of **a**) CA9 and **b**) 12 protein expression in hPASMCs after 48 hours of tumor necrosis factor-alpha (TNF-α), platelet-derived growth factor-BB (PDGF-BB) and transforming growth factor beta (TGF-β) stimulation compared to unstimulated control (Control) and **c**) respective representative pictures are shown. Data are given as the ratio of CA9 or 12 to β-actin expression and presented as mean ± SEM (n=3). *p<0.05 compared to Control.

Regarding the CA12 protein expression profile, our investigation showed significant augmentation upon PDGF-BB and TNF-α stimulation and a visible tendency in increased levels after TGF-β stimulation (Figure 20b). In addition, IL-1 and IL-6 stimulation of hPASMCs led to a prominent effect and significantly increased CA12 protein expression (Figure 21c, e).

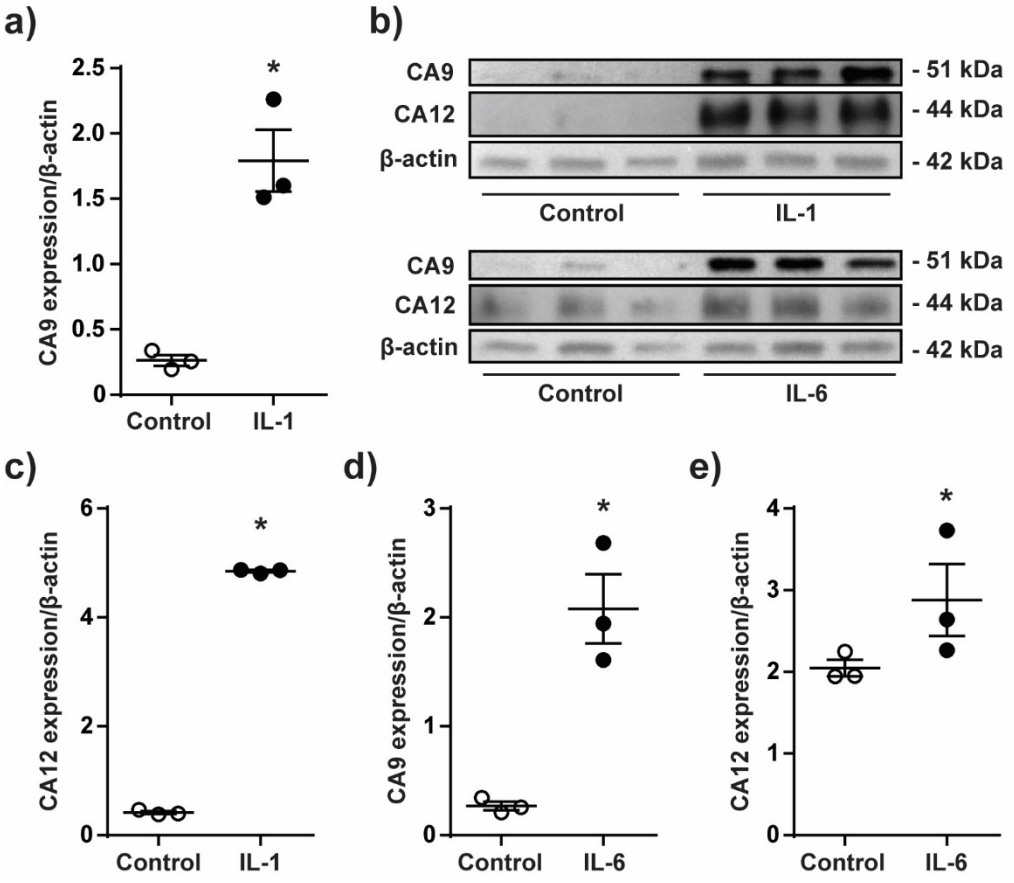

Figure 21. The protein expression of CA9 and 12 in hPASMCs after IL-1 and IL-6 stimulation.

Densitometric analysis of **a**) CA9 and **c**) 12 protein expression in hPASMCs after 48 hours of interleukin-1 (IL-1) or **d, e**) interleukin-6 (IL-6) stimulation compared to unstimulated control (Control) and **b**) respective representative blots are shown. Data are given as the ratio of CA9 or 12 to β-actin expression and presented as mean ± SEM (n=3). *$p<0.05$ compared to Control.

3.3. Role of HIF-1α and HIF-2α on CA9 and 12 expression profile in PASMCs

3.3.1. Importance of HIF-1α binding to the HRE in CA9 promoter region

In order to investigate the role of HIF-1α in CA9 transcriptional activation via binding to the hypoxia-responsive element (HRE) in the CA9 promoter, we have transfected a human lung epithelial cell line (A549) with a plasmid vector containing either wild-type or HRE-mutated promoter region of the CA9 gene, as previously described (Figure 22a). Subsequently, A549 transfected cells were exposed to normoxia or hypoxia conditions for 24 hours. CA9 promoter activity was assessed by dual-luciferase assay, and our results demonstrated that mutation in HRE

significantly decreased CA9 promoter activity in hypoxia compared to wild-type control (Figure 22b).

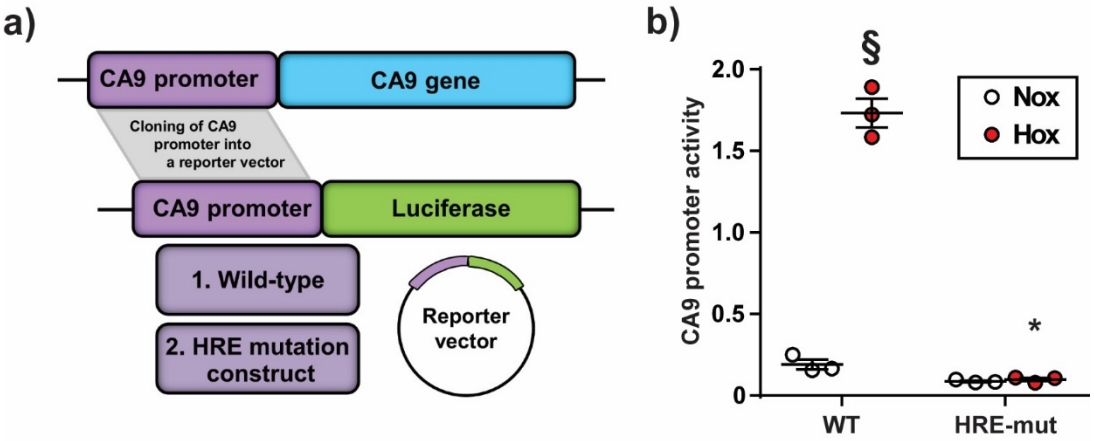

Figure 22. CA9 promoter activity in the A549 cell line exposed to hypoxia.

a) Schematic representation of luciferase promoter plasmids co-transfected into A549 cell line as described in the methods section, followed by 24 hours of 1% O_2 hypoxia exposure (Hox), compared to normoxia control (Nox) and **b**) dual-luciferase measurement of wild-type (WT) and hypoxia-responsive element mutation construct (HRE-mut) CA9 promoter activity are shown. Data are given as firefly and NanoLuc relative luciferase unit (RLU) ratio and presented as mean ± SEM (n=3). §$p<0.05$ compared to Nox WT, *$p<0.05$ compared to Hox WT.

3.3.2. Impact of HIF-1α knockdown on the increased CA12 protein expression in human PASMCs under chronic hypoxia incubation

Furthermore, to examine the role of the HIF-1α transcription factor in the upregulation of hPASMCs CA12 in hypoxia, we have performed siRNA-based silencing of HIF-1α and examined the effects on CA12 protein expression in human PASMCs after hypoxia exposure (Figure 23). Silencing of HIF-1α success was evident by significantly decreased protein expression of HIF-1α in normoxia and hypoxia conditions (Figure 23a). Hypoxia resulted in significant upregulation of CA12 protein expression compared to normoxia control. Notably, our results showed a significant decrease in CA12 protein expression upon HIF-1α knockdown in both normoxia and hypoxia conditions (Figure 23b).

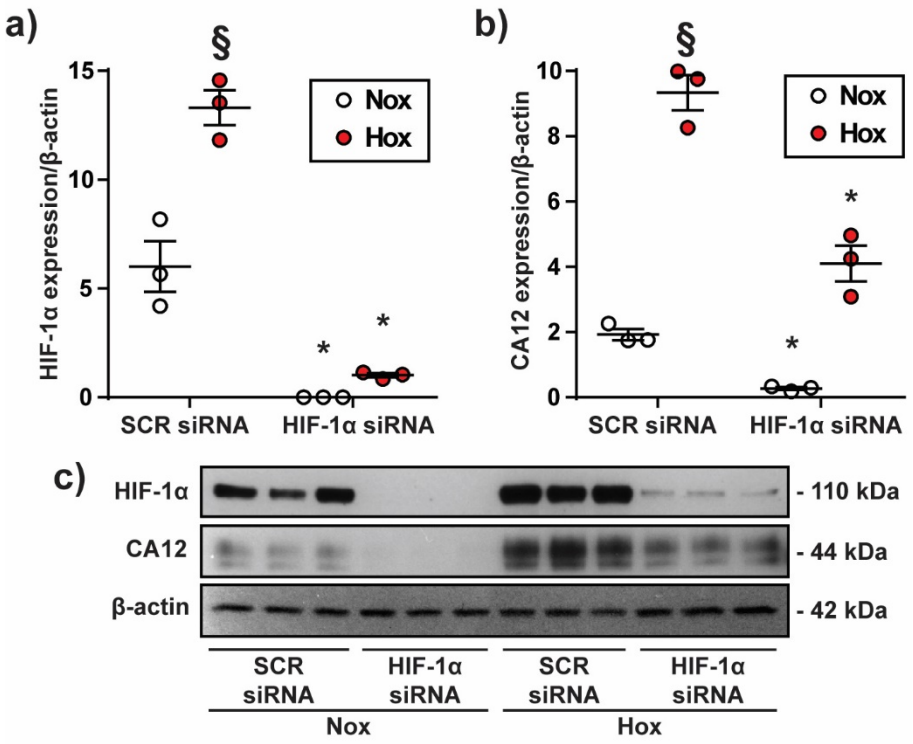

Figure 23. Effects of HIF-1α silencing on CA12 protein expression in human PASMCs after hypoxia exposure.

Densitometric analysis of **a**) HIF-1α and **b**) CA12 protein expression in hPASMCs treated with scramble siRNA (SCR siRNA) or siRNA against HIF-1α (HIF-1α siRNA) after 72 hours of 1% O_2 chronic hypoxia incubation (Hox) compared to normoxia control (Nox) and **c**) respective representative blots are shown. Data are given as the ratio of HIF-1α or CA12 to β-actin expression and presented as mean ± SEM (n=3). §$p<0.05$ compared to Nox SCR siRNA, *$p<0.05$ compared to appropriate SCR siRNA control.

3.3.3. Effect of HIF-2α knockdown on the increased CA9 and 12 protein expression in human PASMCs under chronic hypoxia incubation

In order to investigate the potential role of HIF-2α transcription factor in CA9 and 12 elevated protein expression in hPASMCs, we have performed siRNA-based knockdown of HIF-2α in human PASMCs. Transfected cells were exposed to normoxia or hypoxia conditions for 72 hours and subsequently investigated for CA9 and 12 protein expression. Silencing of HIF-1α success was evident by Western Blot analysis (Figure 24c). Hypoxia led to the significant upregulation of CA9 and 12 protein expression, compared to normoxia control (Figure 24a,b). In contrast to HIF-

1α, our investigation showed that HIF-2α knockdown did not affect CA9 and 12 increased protein expression after hypoxia exposure (Figure 24a,b).

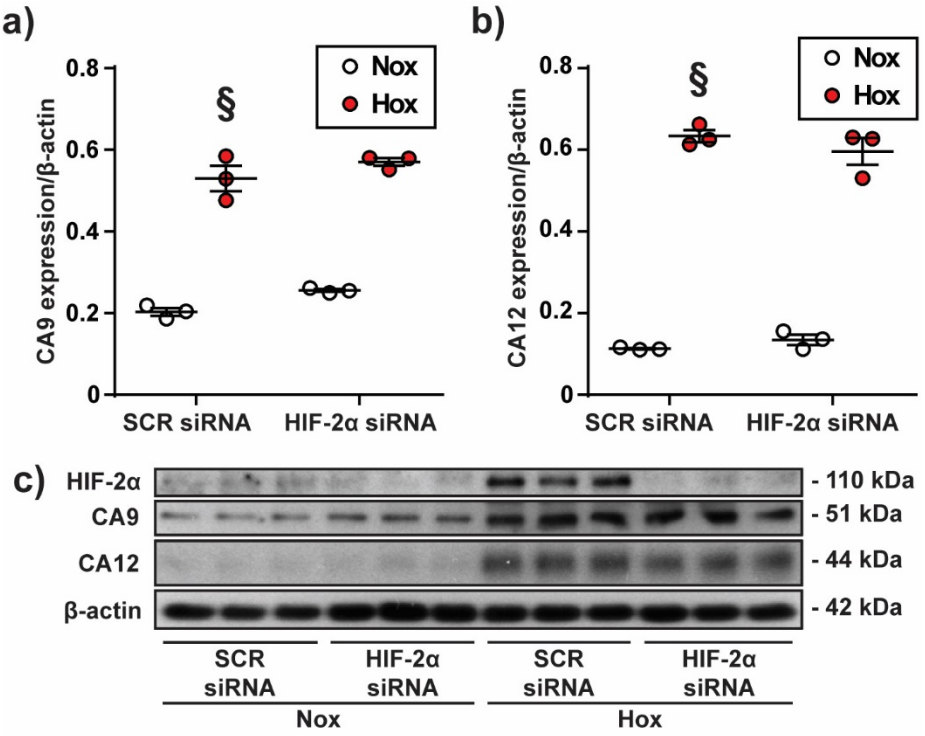

Figure 24. HIF-2α silencing effect on CA9 and 12 protein expression in human PASMCs after hypoxia exposure.

Densitometric analysis of **a**) CA9 and **b**) 12 protein expression in hPASMCs treated with scramble siRNA (SCR siRNA) or siRNA against HIF-2α (HIF-2α siRNA) after 72 hours of 1% O_2 chronic hypoxia incubation (Hox) compared to normoxia control (Nox) and **c**) respective representative blots are shown. Data are given as the ratio of CA9 or 12 to β-actin expression and presented as mean ± SEM (n=3). §$p<0.05$ compared to Nox SCR siRNA.

3.4. Role of CA9 and 12 in the proliferation and migration of PASMCs

3.4.1. Impact of CA9 and 12 inhibition on mouse PASMCs proliferation under chronic hypoxia

Precapillary PASMCs isolated from healthy mice, as described in the methods section, were exposed to hypoxia for 72 hours, resulting in a significant increase in proliferation compared to normoxia control (Figure 25a). Our results demonstrated a significant decrease of mPASMCs proliferation in hypoxia conditions upon CA9 and 12 inhibition with 50µM of S4 inhibitor (Figure

25a). Importantly, cell viability assay has revealed non-toxicity of S4 inhibitor at all doses except for 100µM (Figure 25b).

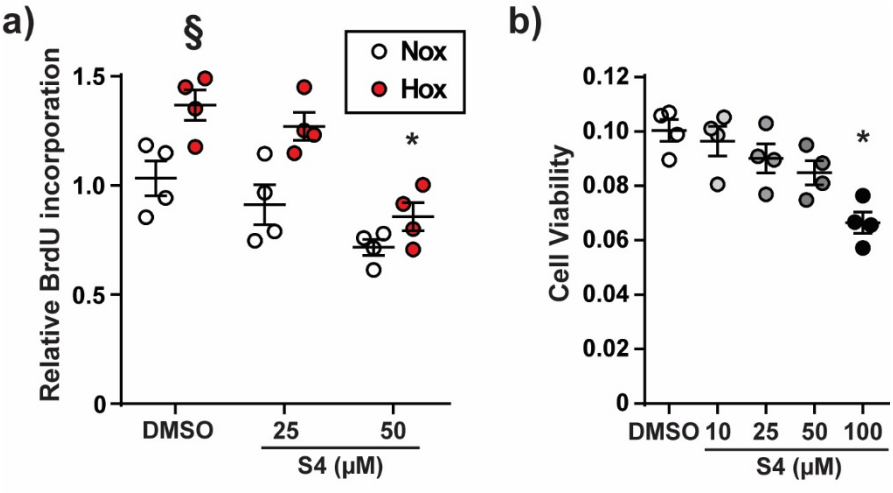

Figure 25. Effects of CA9 and 12 inhibition on the proliferation of mouse PASMCs after hypoxia exposure.

a) Proliferation of mPASMCs after 72 hours of 1% O_2 chronic hypoxia incubation (Hox) compared to normoxia control (Nox), measured by 5-bromo-2'-deoxyuridine (BrdU) incorporation assay. mPASMCs were treated with either S4 inhibitor or dimethyl sulfoxide (DMSO). **b**) Cell viability of mPASMCs treated with different concentrations of S4 inhibitor compared to DMSO control and measured by tetrazolium dye (MTT) assay. Data are given as relative absorbance measured at (a) 370 nm (reference wavelength 492 nm) or (b) 570 nm (reference wavelength 690 nm) and presented as mean ± SEM (n=4). §$p<0.05$ compared to Nox DMSO control, *$p<0.05$ compared to the appropriate DMSO control.

3.4.2. CA9 and 12 inhibition influence on the proliferation of human PASMCs after chronic hypoxic incubation

Exposure of healthy human donor PASMCs to hypoxia for three days led to a significant increase in proliferation compared to normoxia control (Figure 26a,c). Our data showed that treatment with 50µM of S4 inhibitor significantly decreased hPASMCs proliferation in both normoxia and hypoxia conditions. Interestingly, hPASMCs proliferation in hypoxia upon S4 treatment was reduced to the level of normoxia control (Figure 26a).

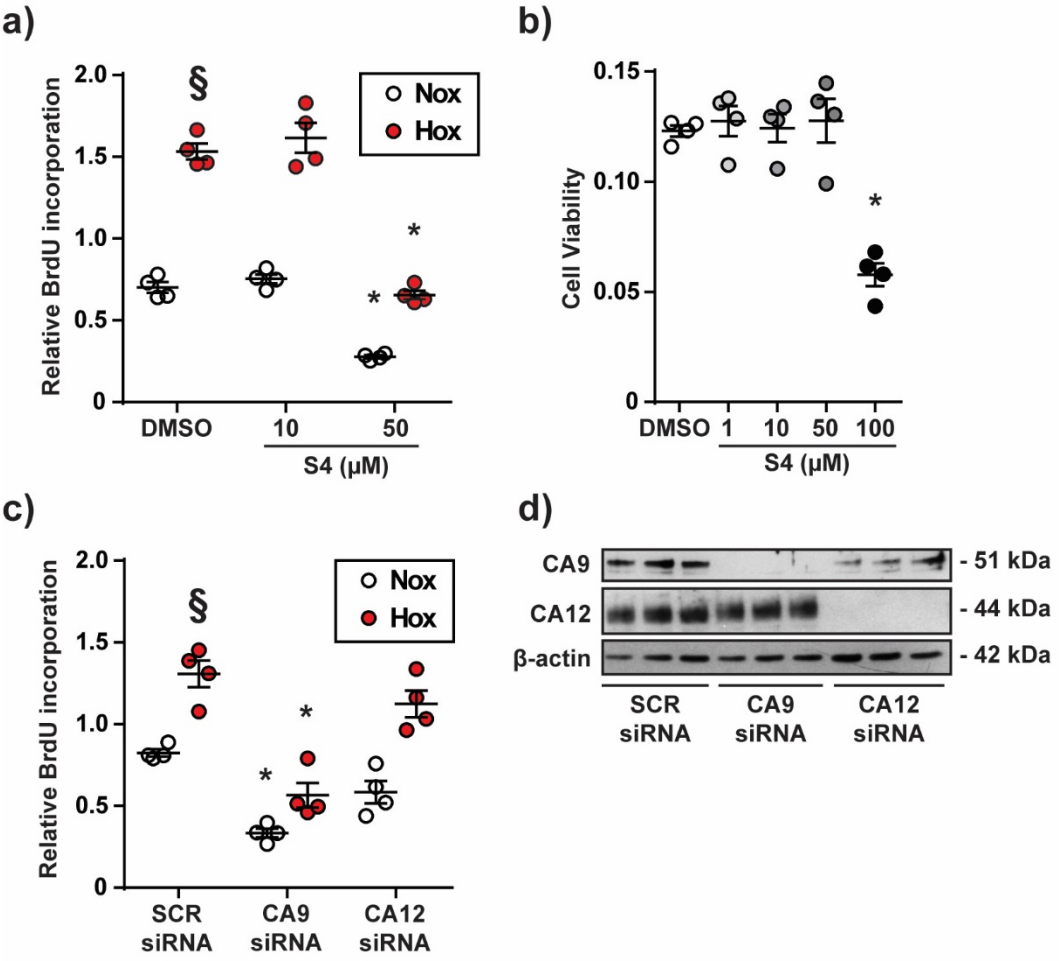

Figure 26. Effects of CA9 and 12 inhibition or silencing on the proliferation of human PASMCs after hypoxia exposure.

a) Proliferation of hPASMCs after 72 hours of 1% O_2 chronic hypoxia incubation (Hox) compared to normoxia control (Nox) was measured by 5-bromo-2'-deoxyuridine (BrdU) incorporation assay. hPASMCs were treated with S4 inhibitor or dimethyl sulfoxide (DMSO) or **c**) transfected with scramble siRNA (SCR siRNA), siRNA against CA9 (CA9 siRNA) and CA12 (CA12 siRNA). **b**) Cell viability of hPASMCs treated with different concentrations of S4 inhibitor was measured by tetrazolium dye (MTT) assay. **d**) Representative blots of CA9 and 12 gene silencing are shown. Data are given as relative absorbance measured at (a,c) 370 nm (reference wavelength 492 nm) or (b) 570 nm (reference wavelength 690 nm) and presented as mean ± SEM (n=4). §$p<0.05$ compared to Nox (a) DMSO or (c) SCR siRNA control, *$p<0.05$ compared to the appropriate DMSO or SCR siRNA control.

In addition, cell viability assay has demonstrated S4 non-toxicity at all doses except for 100μM (Figure 26b). Finally, the specific role in the proliferation of both CA9 and 12 was investigated by the siRNA knockdown approach (Figure 26d). Our results demonstrated a significant decrease in

hPASMCs proliferation upon CA9 gene silencing in both normoxia and hypoxia conditions (Figure 26c).

3.4.3. CA9 and 12 inhibition influence on the proliferation of human PASMCs after PDGF-BB stimulation

Human PASMCs stimulation with PDGF-BB for 72 hours led to a significant increase in proliferation, compared to the unstimulated control (Figure 27a-b). Our results have demonstrated that treatment with an S4 inhibitor significantly reduced PDGF-BB-induced hPAMSCs proliferation in a dose-dependent manner (Figure 27a).

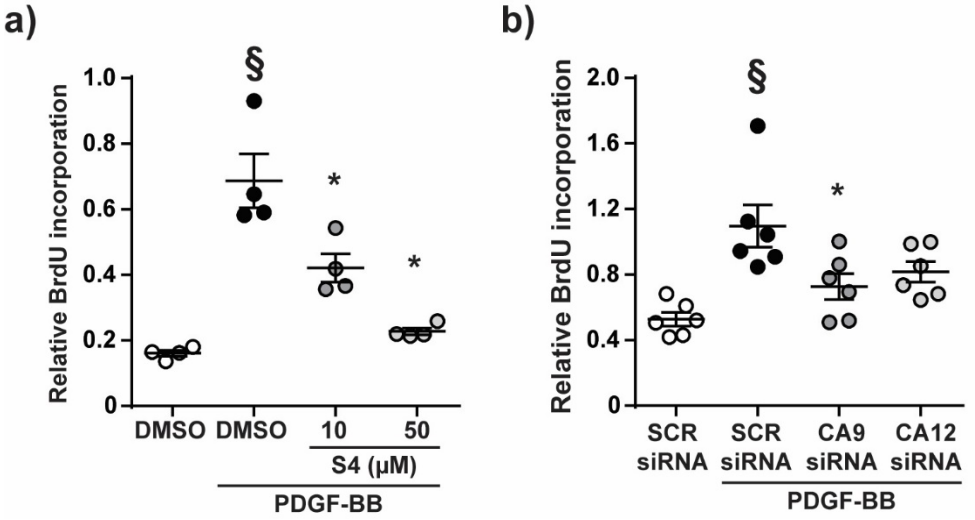

Figure 27. The impact of inhibition or silencing CA9 and 12 on the proliferation of human PASMCs following PDGF-BB stimulation.

a) Proliferation of hPASMCs after 72 hours of platelet-derived growth factor-BB (PDGF-BB) stimulation compared to unstimulated control was measured by 5-bromo-2'-deoxyuridine (BrdU) incorporation assay. hPASMCs were treated with S4 inhibitor or dimethyl sulfoxide (DMSO) or **b**) transfected with scramble siRNA (SCR siRNA), siRNA against CA9 (CA9 siRNA) or CA12 (CA12 siRNA). Data are given as relative absorbance measured at 370 nm (reference wavelength 492 nm) and presented as mean ± SEM (n=4-6). §$p<0.05$ compared to the unstimulated (a) DMSO or (b) SCR siRNA control, *$p<0.05$ compared to the appropriate DMSO or SCR siRNA control.

Additionally, we have investigated the independent role of CA9 and 12 in hPASMCs PDGF-BB-induced proliferation. Our data revealed that both CA9 and 12 gene silencing attenuated the

proliferation of hPASMCs. CA9 knockdown had a more prominent effect and reached significance (Figure 27b).

3.4.4. Impact of CA9 and 12 inhibition on human PASMCs migration under hypoxia or PDGF-BB stimulation

As described previously, the role of CA9 and 12 in the migration of hPASMCs exposed to hypoxia or PDGF-BB stimulation was investigated. Our results demonstrated that S4 treatment significantly reduced hPASMCs migration after hypoxia exposure for 12 hours (Figure 28a). Furthermore, one day of PDGF-BB stimulation led to a significant increase in hPASMCs migration (Figure 28b). Our data revealed that S4 treatment significantly reduced PDGF-BB-induced hPASMCs migration (Figure 28b).

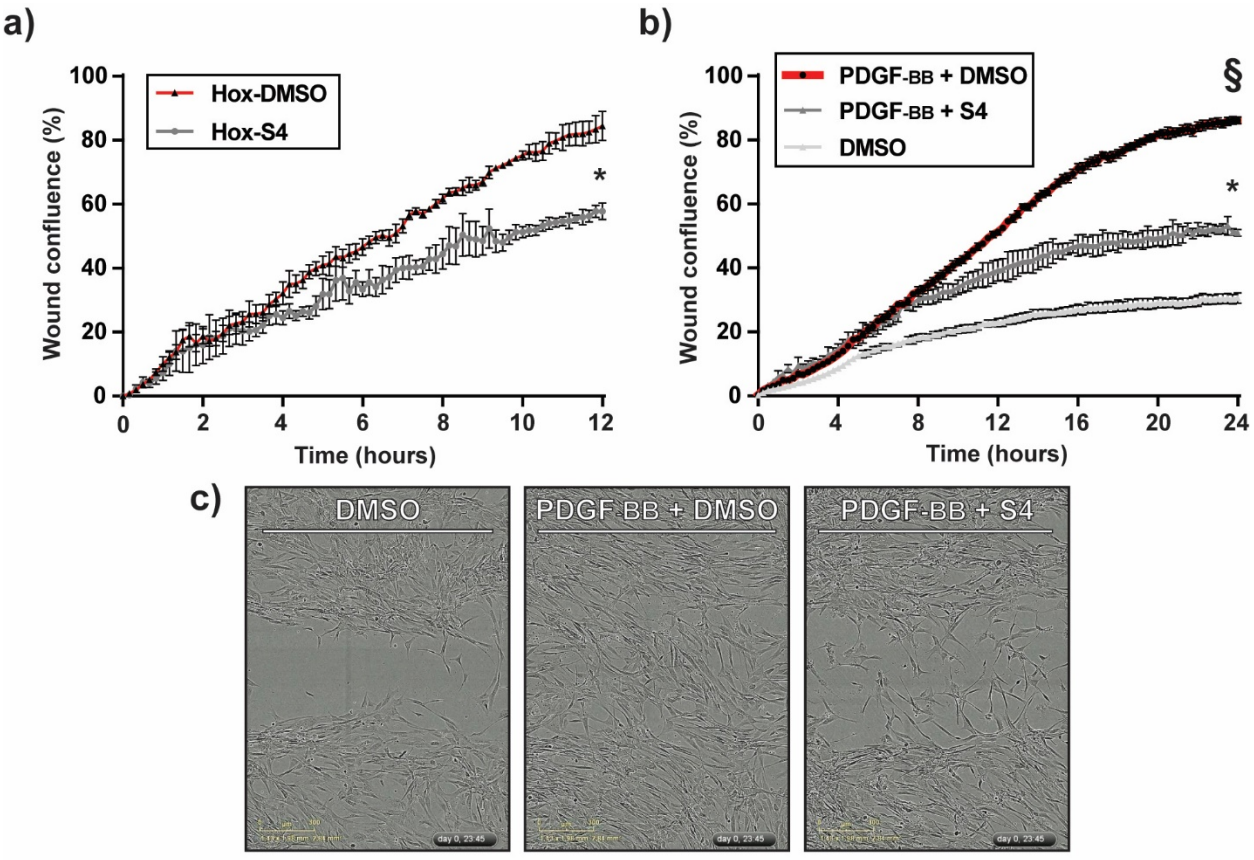

Figure 28. Effects of CA9 and 12 inhibition on the migration of human PASMCs after hypoxia or PDGF-BB stimulation.

a) Migration of hPASMCs after 12 hours of 1% O_2 hypoxia exposure (Hox) or **b**) 24 hours of platelet-derived growth factor-BB (PDGF-BB) stimulation, measured by

wound healing assay on IncuCyte live cell imaging system and **c**) respective representative pictures of PDGF-BB stimulation are presented. hPASMCs were treated with either 50 µM of S4 inhibitor or dimethyl sulfoxide (DMSO). Results are given as a percentage of wound area occupied with migrated hPASMCs (Wound Confluence (%)) at indicated time points compared to the initial wound surface and calculated by the IncuCyte ZOOM software. Live cell images were taken every 10 (a) or 15 (b) minutes. Results are given as mean ± SEM (n=4). Scale bars=300µm. §$p<0.05$ compared to the unstimulated DMSO control, *$p<0.05$ compared to (a) Hox-DMSO or (b) PDGF-BB DMSO.

3.5. Role of CA9 and 12 in PASMCs pH homeostasis

3.5.1. Effects of CA9 and 12 inhibition on the extracellular pH of human PASMCs after chronic hypoxic or PDGF-BB stimulation

The role of CA9 and 12 in the acidification of the extracellular milieu of human PASMCs after hypoxia exposure or PDGF-BB stimulation was examined as described in the methods section. Three days of hypoxia exposure resulted in a significant decrease of the hPASMCs' extracellular pH (epH), compared to normoxia control (Figure 29a). Our data showed that S4 treatment significantly elevated epH values in both normoxia and hypoxia conditions (Figure 29a).

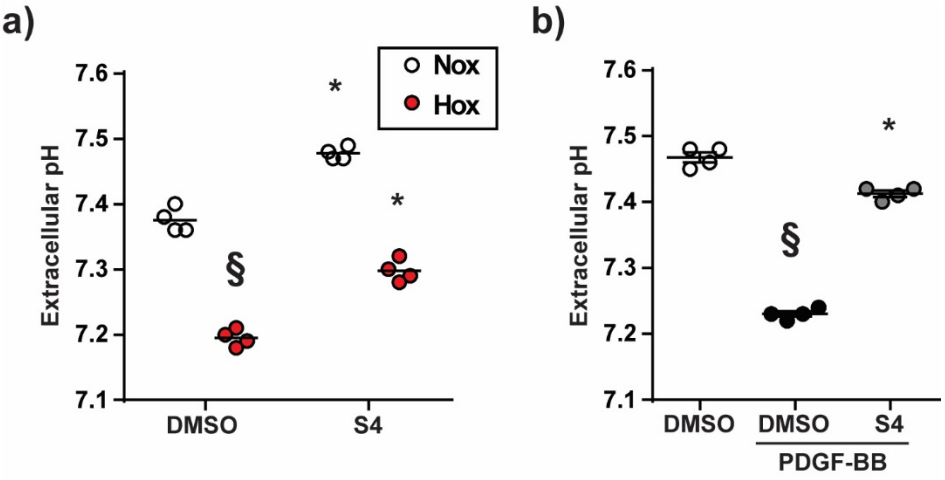

Figure 29. Impact of CA9 and 12 inhibition on the extracellular pH of human PASMCs after hypoxia exposure or PDGF-BB stimulation.

pH values of hPASMCs cell culture medium after 72 hours of **a**) 1% O_2 chronic hypoxia incubation (Hox) compared to normoxia control (Nox) or **b**) platelet-derived growth factor-BB (PDGF-BB) stimulation compared to unstimulated control are shown. pH was measured immediately upon incubation with the 766 Calimatic pH

meter. hPASMCs were treated with either 50 µM of S4 inhibitor or dimethyl sulfoxide (DMSO). Results are given as mean ± SEM (n=4). §p<0.05 compared to (a) Nox or (b) unstimulated DMSO control, *p<0.05 compared to appropriate DMSO control.

Furthermore, hPAMSCs stimulation with PDGF-BB for 72 hours significantly decreased epH values compared to unstimulated control (Figure 29b). Our investigation revealed that S4 treatment significantly reversed the PDGF-BB-induced hPASMCs extracellular acidification (Figure 29b).

3.5.2. Effects of CA9 and 12 inhibition on the intracellular pH of human PASMCs after chronic hypoxic incubation

As previously indicated, intracellular pH values (ipH) were assessed in human PASMCs. After two days of hypoxia incubation, there was a decrease in hPASMCs' ipH values, although it did not reach statistical significance (Figure 30). Importantly, treatment with the S4 inhibitor during hypoxia exposure resulted in a significant decrease of hPASMCs' ipH values compared to the hypoxia control (Figure 30).

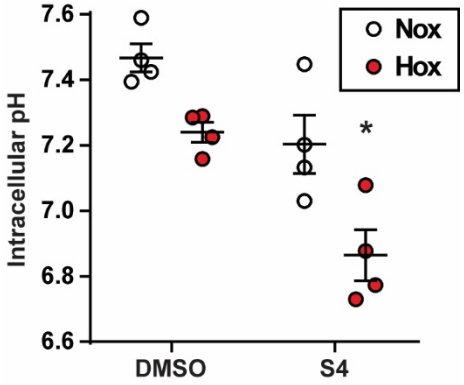

Figure 30. Impact of CA9 and 12 inhibition on the intracellular pH of human PASMCs after hypoxia exposure.

hPASMCs intracellular pH values are shown after 48 hours of 1% O_2 chronic hypoxia incubation (Hox) compared to normoxia control (Nox). Intracellular pH was measured using the pH-dependent fluorescent dye Carboxy-SNARF-1, as described in the methods section. hPASMCs were treated with either 50 µM of S4 inhibitor or dimethyl sulfoxide (DMSO). Data are given as relative fluorescence ratio of two emission wavelengths (580/640 nm) and presented as mean ± SEM (n=4). *p<0.05 compared to Hox DMSO control.

3.6. Role of CA9 and 12 in the activation of PASMCs protein kinases during chronic hypoxia

3.6.1. CA9 and 12 inhibition impact on tyrosine and serine/threonine kinome profile of human PASMCs under chronic hypoxia

Furthermore, we investigated the effect of CA9 and 12 inhibition on the kinome profile of human PASMCs after chronic hypoxia incubation as described in the methods section. In more detail, human PASMCs were exposed to normoxia or hypoxia stimulation for 72 hours, and in hypoxia conditions cells were treated either with 50 μM of S4 inhibitor or DMSO control. Finally, cell lysates were analyzed for tyrosine and serine/threonine kinase activity using the PamStation12 platform.

Heat maps of tyrosine substrate phosphorylation and a complete list of predicted upstream tyrosine kinase activity are represented in Figure 31. Our investigation showed that chronic hypoxia exposure in human PASMCs significantly increased the activity of various tyrosine kinases (Figure 31b). The highest increase of activity was detected in the following tyrosine kinases: insulin receptor (InsR) kinase, insulin like growth factor 1 receptor (IGF1R) kinase, insulin receptor-related receptor (IRR) kinase, member of TAM family of receptor tyrosine kinase (Tyro3/Sky) and member of TEC family of non-receptor tyrosine kinases (TXK). Furthermore, treatment with S4 inhibitor resulted in a significant decrease in the activity of various protein tyrosine kinases in hPASMCs after hypoxia exposure (Figure 31c). Highest decrease of activity was observed in human epidermal growth factor receptor 4 (HER4) kinase, c-Met receptor tyrosine kinase, Hematopoietic cell kinase (HCK), colony-stimulating factor 1 receptor (FmS/CSFR) kinase and tropomyosin receptor kinase B (TRKB).

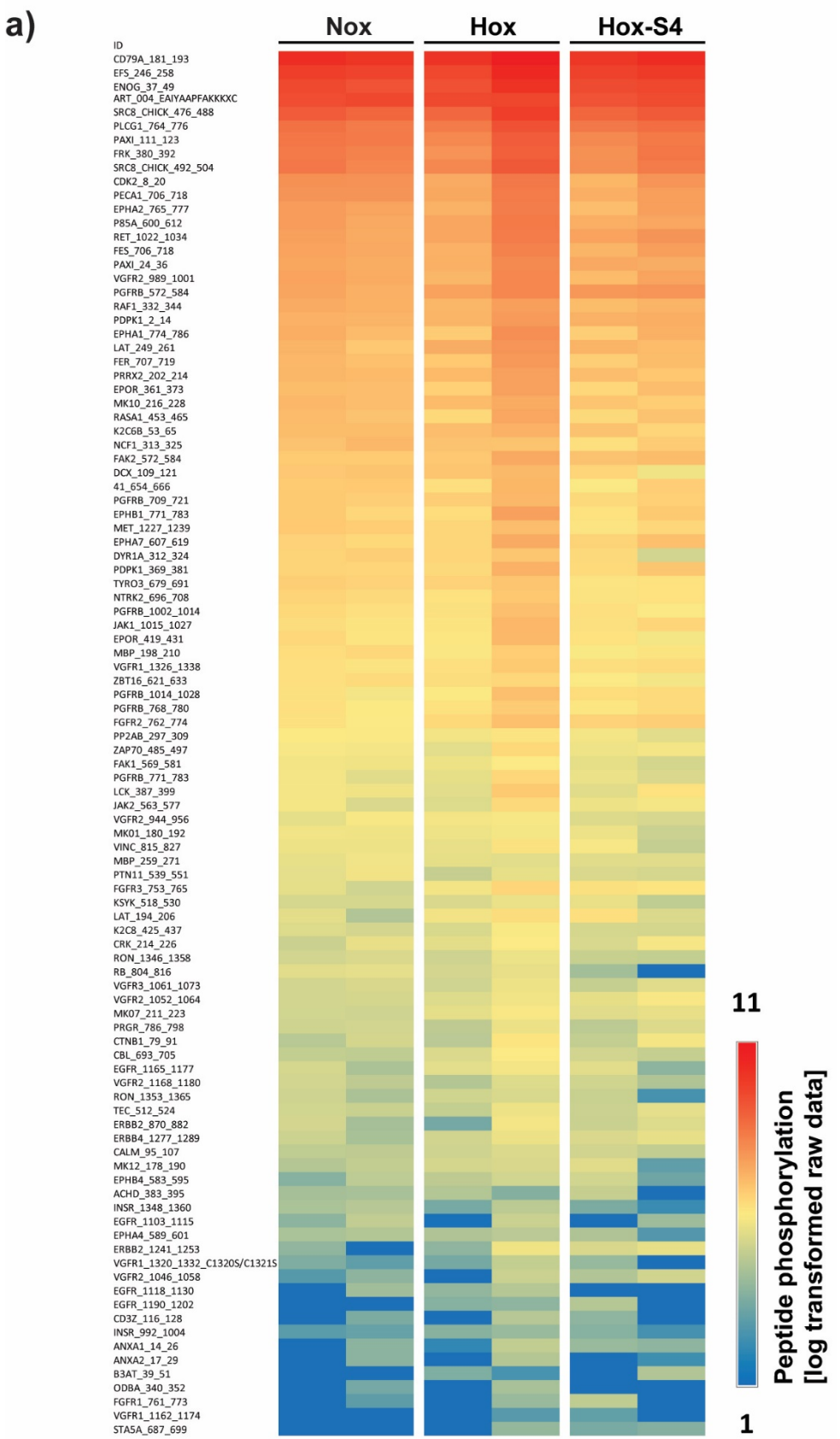
a)
Nox
Hox
Hox-S4
ID
CD79A_181_193
EFS_246_258
ENOG_37_49
ART_004_EAIYAAPFAKKKXC
SRC8_CHICK_476_488
PLCG1_764_776
PAXI_111_123
FRK_380_392
SRC8_CHICK_492_504
CDK2_8_20
PECA1_706_718
EPHA2_765_777
P85A_600_612
RET_1022_1034
FES_706_718
PAXI_24_36
VGFR2_989_1001
PGFRB_572_584
RAF1_332_344
PDPK1_2_14
EPHA1_774_786
LAT_249_261
FER_707_719
PRRX2_202_214
EPOR_361_373
MK10_216_228
RASA1_453_465
K2C6B_53_65
NCF1_313_325
FAK2_572_584
DCX_109_121
41_654_666
PGFRB_709_721
EPHB1_771_783
MET_1227_1239
EPHA7_607_619
DYR1A_312_324
PDPK1_369_381
TYRO3_679_691
NTRK2_696_708
PGFRB_1002_1014
JAK1_1015_1027
EPOR_419_431
MBP_198_210
VGFR1_1326_1338
ZBT16_621_633
PGFRB_1014_1028
PGFRB_768_780
FGFR2_762_774
PP2AB_297_309
ZAP70_485_497
FAK1_569_581
PGFRB_771_783
LCK_387_399
JAK2_563_577
VGFR2_944_956
MK01_180_192
VINC_815_827
MBP_259_271
PTN11_539_551
FGFR3_753_765
KSYK_518_530
LAT_194_206
K2C8_425_437
CRK_214_226
RON_1346_1358
RB_804_816
VGFR3_1061_1073
VGFR2_1052_1064
MK07_211_223
PRGR_786_798
CTNB1_79_91
CBL_693_705
EGFR_1165_1177
VGFR2_1168_1180
RON_1353_1365
TEC_512_524
ERBB2_870_882
ERBB4_1277_1289
CALM_95_107
MK12_178_190
EPHB4_583_595
ACHD_383_395
INSR_1348_1360
EGFR_1103_1115
EPHA4_589_601
ERBB2_1241_1253
VGFR1_1320_1332_C1320S/C1321S
VGFR2_1046_1058
EGFR_1118_1130
EGFR_1190_1202
CD3Z_116_128
INSR_992_1004
ANXA1_14_26
ANXA2_17_29
B3AT_39_51
ODBA_340_352
FGFR1_761_773
VGFR1_1162_1174
STA5A_687_699
11
1
Peptide phosphorylation
[log transformed raw data]

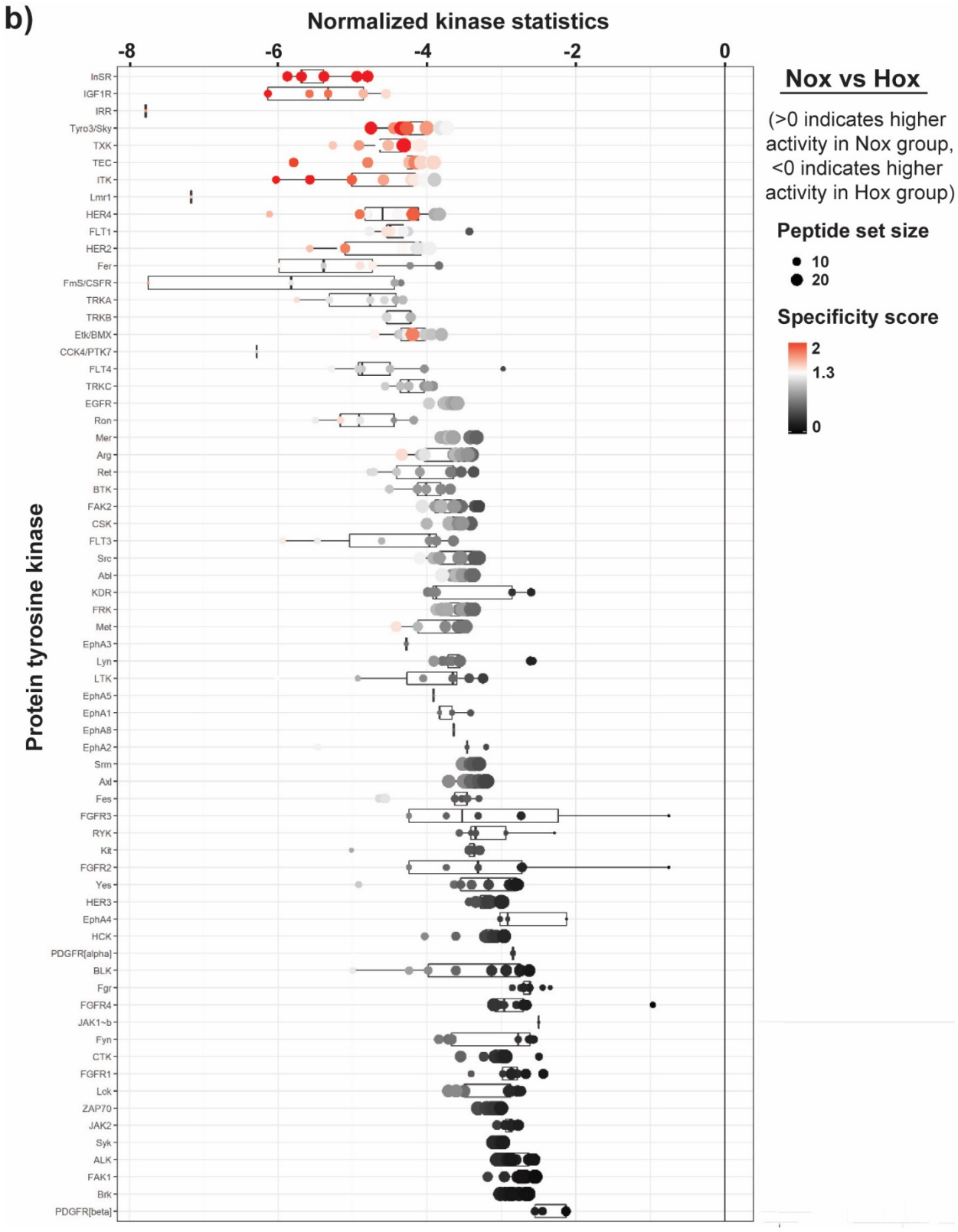
b)
Normalized kinase statistics
-8
-6
-4
-2
0
Protein tyrosine kinase
InSR
IGF1R
IRR
Tyro3/Sky
TXK
TEC
ITK
Lmr1
HER4
FLT1
HER2
Fer
FmS/CSFR
TRKA
TRKB
Etk/BMX
CCK4/PTK7
FLT4
TRKC
EGFR
Ron
Mer
Arg
Ret
BTK
FAK2
CSK
FLT3
Src
Abl
KDR
FRK
Met
EphA3
Lyn
LTK
EphA5
EphA1
EphA8
EphA2
Srm
Axl
Fes
FGFR3
RYK
Kit
FGFR2
Yes
HER3
EphA4
HCK
PDGFR[alpha]
BLK
Fgr
FGFR4
JAK1~b
Fyn
CTK
FGFR1
Lck
ZAP70
JAK2
Syk
ALK
FAK1
Brk
PDGFR[beta]
Nox vs Hox
(>0 indicates higher activity in Nox group, <0 indicates higher activity in Hox group)
Peptide set size
10
20
Specificity score
2
1.3
0

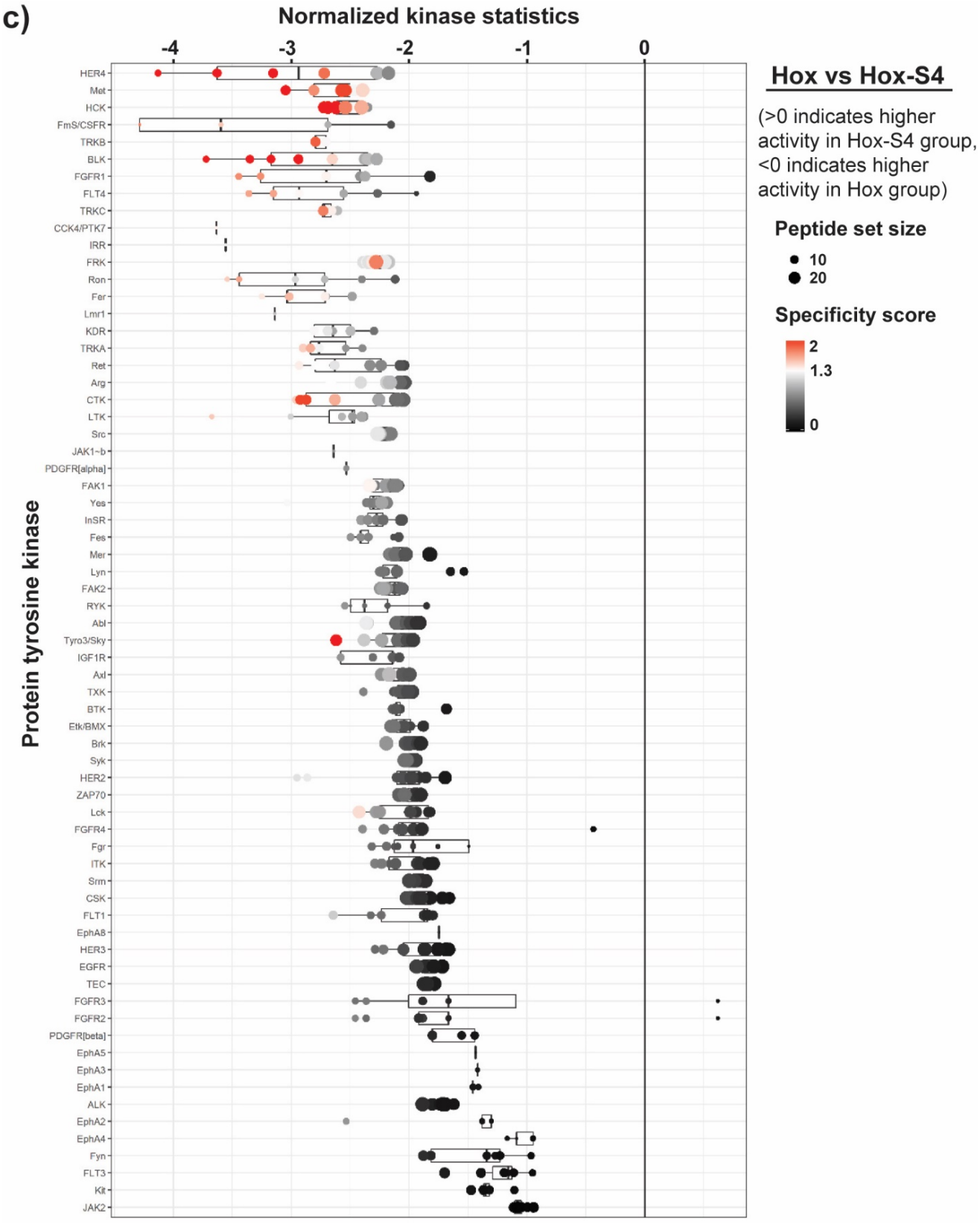
c)
Normalized kinase statistics
-4
-3
-2
-1
0
Protein tyrosine kinase
HER4
Met
HCK
FmS/CSFR
TRKB
BLK
FGFR1
FLT4
TRKC
CCK4/PTK7
IRR
FRK
Ron
Fer
Lmr1
KDR
TRKA
Ret
Arg
CTK
LTK
Src
JAK1~b
PDGFR[alpha]
FAK1
Yes
InSR
Fes
Mer
Lyn
FAK2
RYK
Abl
Tyro3/Sky
IGF1R
Axl
TXK
BTK
Etk/BMX
Brk
Syk
HER2
ZAP70
Lck
FGFR4
Fgr
ITK
Srm
CSK
FLT1
EphA8
HER3
EGFR
TEC
FGFR3
FGFR2
PDGFR[beta]
EphA5
EphA3
EphA1
ALK
EphA2
EphA4
Fyn
FLT3
Kit
JAK2
Hox vs Hox-S4
(>0 indicates higher activity in Hox-S4 group, <0 indicates higher activity in Hox group)
Peptide set size
10
20
Specificity score
2
1.3
0

Figure 31. Effects of CA9 and 12 inhibition on hPASMCs protein tyrosine kinases after chronic hypoxic incubation.

Human PASMCs were exposed to 1% O_2 chronic hypoxia incubation (Hox) for 72 hours, compared to normoxia control (Nox). Cells were treated with 50 μM of S4 inhibitor (Hox-S4) or dimethyl sulfoxide (Nox, Hox), followed by an assessment of the peptide-based tyrosine kinase activity by using the PamStation12 platform with Evolve 12 software as described in the methods section. **a**) A heat map displaying log-transformed fluorescence signals for substrate tyrosine phosphorylation, used for upstream kinase analysis and **b**) prediction of protein tyrosine kinases activity in Hox, compared to Nox or **c**) Hox-S4, compared to Hox group are shown. Normalized kinase statistics estimate relative kinase activity, while the specificity score measures prediction reliability and accuracy.

Complete list of predicted upstream serine/threonine kinase activity and heat maps of serine/threonine substrate phosphorylation are depicted in Figure 32. Our results demonstrated that chronic hypoxia exposure in human PASMCs significantly increased the activity of various serine/threonine protein kinases (Figure 32b). The highest increase of activity was detected in the following serine/threonine protein kinases: mitogen-activated protein kinase (HGK/ZC1), ribosomal protein S6 kinase like 1 (RSKL2), TRAF2 and NCK-interacting kinase (TNIK/ZC2), ribosomal protein S6 kinases (RSK3) and rapidly accelerated fibrosarcoma (RAF1) kinase. In addition, treatment with S4 inhibitor led to a significant decrease in the activity of various serine/threonine protein kinases in hPASMCs after hypoxia exposure (Figure 32c). Most prominent decrease of activity was observed in glycogen synthase kinase three beta (GSK-3β), GSK-3α, protein kinase C-related kinase 1 (PKN1/PRK1), protein kinase C beta (PKCβ) and PKCζ.

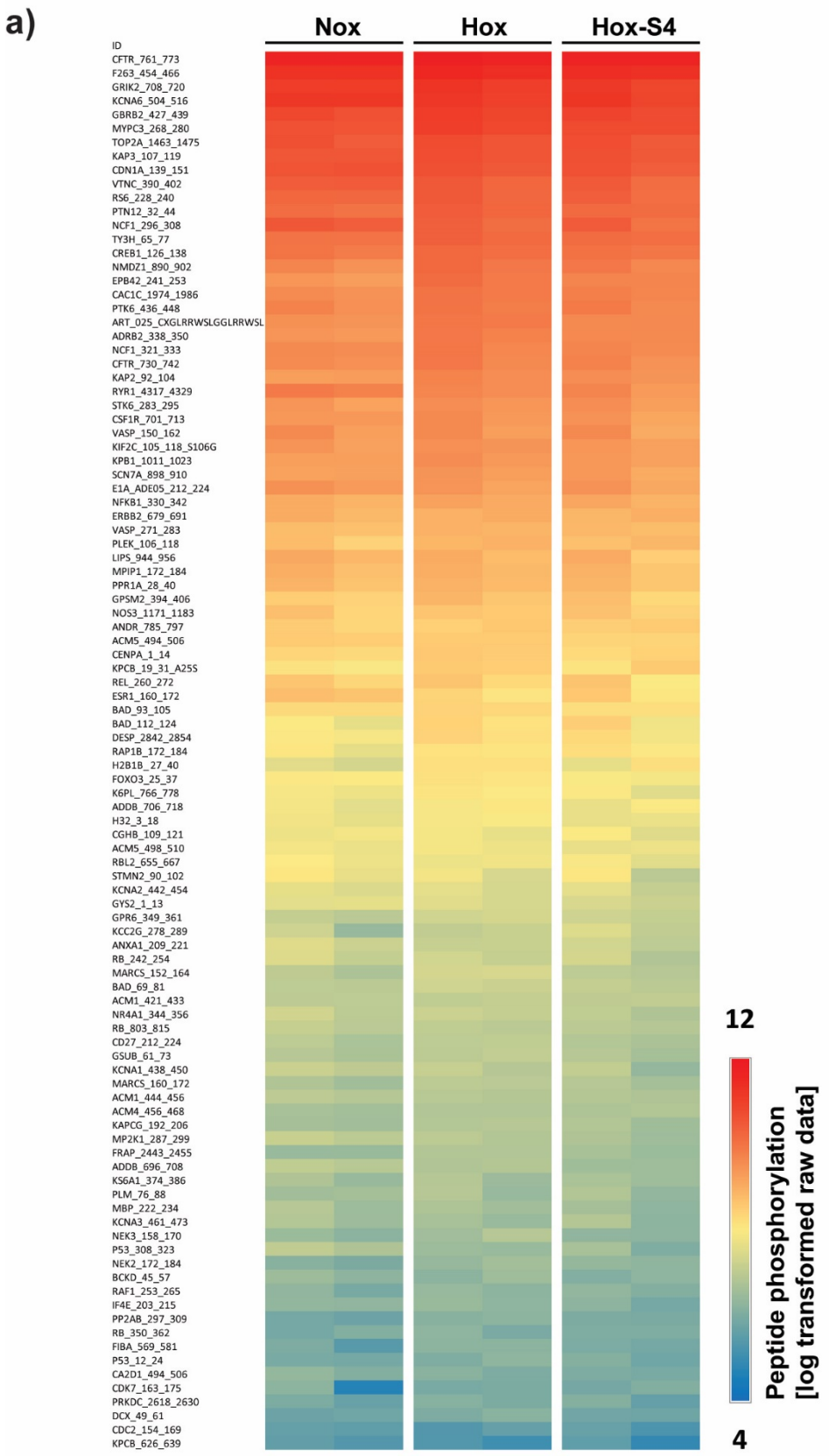
a)
Nox
Hox
Hox-S4
ID
CFTR_761_773
F263_454_466
GRIK2_708_720
KCNA6_504_516
GBRB2_427_439
MYPC3_268_280
TOP2A_1463_1475
KAP3_107_119
CDN1A_139_151
VTNC_390_402
RS6_228_240
PTN12_32_44
NCF1_296_308
TY3H_65_77
CREB1_126_138
NMDZ1_890_902
EPB42_241_253
CAC1C_1974_1986
PTK6_436_448
ART_025_CXGLRRWSLGGLRRWSL
ADRB2_338_350
NCF1_321_333
CFTR_730_742
KAP2_92_104
RYR1_4317_4329
STK6_283_295
CSF1R_701_713
VASP_150_162
KIF2C_105_118_S106G
KPB1_1011_1023
SCN7A_898_910
E1A_ADE05_212_224
NFKB1_330_342
ERBB2_679_691
VASP_271_283
PLEK_106_118
LIPS_944_956
MPIP1_172_184
PPR1A_28_40
GPSM2_394_406
NOS3_1171_1183
ANDR_785_797
ACM5_494_506
CENPA_1_14
KPCB_19_31_A25S
REL_260_272
ESR1_160_172
BAD_93_105
BAD_112_124
DESP_2842_2854
RAP1B_172_184
H2B1B_27_40
FOXO3_25_37
K6PL_766_778
ADDB_706_718
H32_3_18
CGHB_109_121
ACM5_498_510
RBL2_655_667
STMN2_90_102
KCNA2_442_454
GYS2_1_13
GPR6_349_361
KCC2G_278_289
ANXA1_209_221
RB_242_254
MARCS_152_164
BAD_69_81
ACM1_421_433
NR4A1_344_356
RB_803_815
CD27_212_224
GSUB_61_73
KCNA1_438_450
MARCS_160_172
ACM1_444_456
ACM4_456_468
KAPCG_192_206
MP2K1_287_299
FRAP_2443_2455
ADDB_696_708
K56A1_374_386
PLM_76_88
MBP_222_234
KCNA3_461_473
NEK3_158_170
P53_308_323
NEK2_172_184
BCKD_45_57
RAF1_253_265
IF4E_203_215
PP2AB_297_309
RB_350_362
FIBA_569_581
P53_12_24
CA2D1_494_506
CDK7_163_175
PRKDC_2618_2630
DCX_49_61
CDC2_154_169
KPCB_626_639
12
4
Peptide phosphorylation
[log transformed raw data]

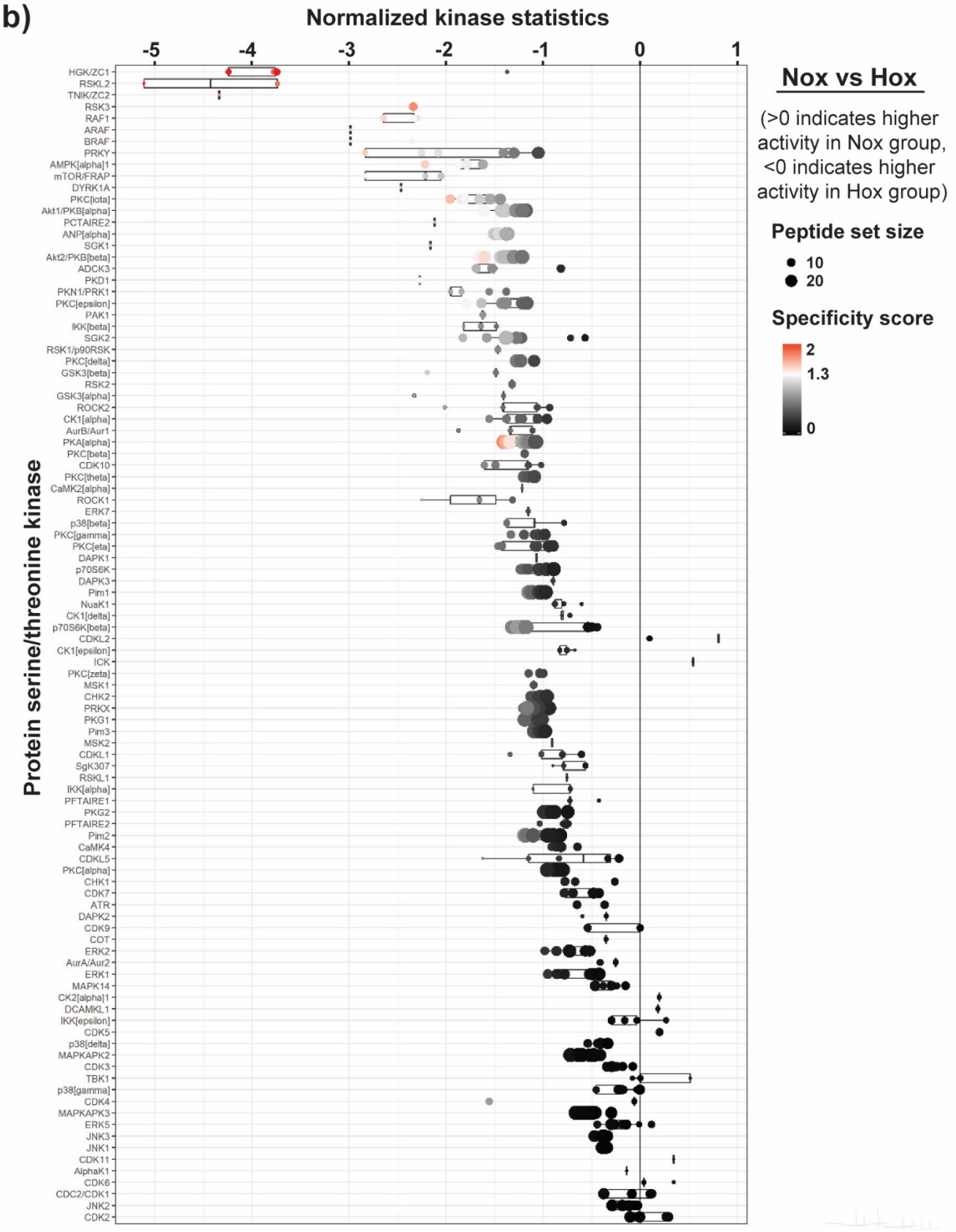
b)
Normalized kinase statistics
-5
-4
-3
-2
-1
0
1
Protein serine/threonine kinase
HGK/ZC1
RSKL2
TNIK/ZC2
RSK3
RAF1
ARAF
BRAF
PRKY
AMPK[alpha]1
mTOR/FRAP
DYRK1A
PKC[iota]
Akt1/PKB[alpha]
PCTAIRE2
ANP[alpha]
SGK1
Akt2/PKB[beta]
ADCK3
PKD1
PKN1/PRK1
PKC[epsilon]
PAK1
IKK[beta]
SGK2
RSK1/p90RSK
PKC[delta]
GSK3[beta]
RSK2
GSK3[alpha]
ROCK2
CK1[alpha]
AurB/Aur1
PKA[alpha]
PKC[beta]
CDK10
PKC[theta]
CaMK2[alpha]
ROCK1
ERK7
p38[beta]
PKC[gamma]
PKC[eta]
DAPK1
p70S6K
DAPK3
Pim1
NuaK1
CK1[delta]
p70S6K[beta]
CDKL2
CK1[epsilon]
ICK
PKC[zeta]
MSK1
CHK2
PRKX
PKG1
Pim3
MSK2
CDKL1
SgK307
RSKL1
IKK[alpha]
PFTAIRE1
PKG2
PFTAIRE2
Pim2
CaMK4
CDKL5
PKC[alpha]
CHK1
CDK7
ATR
DAPK2
CDK9
COT
ERK2
AurA/Aur2
ERK1
MAPK14
CK2[alpha]1
DCAMKL1
IKK[epsilon]
CDK5
p38[delta]
MAPKAPK2
CDK3
TBK1
p38[gamma]
CDK4
MAPKAPK3
ERK5
JNK3
JNK1
CDK11
AlphaK1
CDK6
CDC2/CDK1
JNK2
CDK2
Nox vs Hox
(>0 indicates higher activity in Nox group, <0 indicates higher activity in Hox group)
Peptide set size
10
20
Specificity score
2
1.3
0

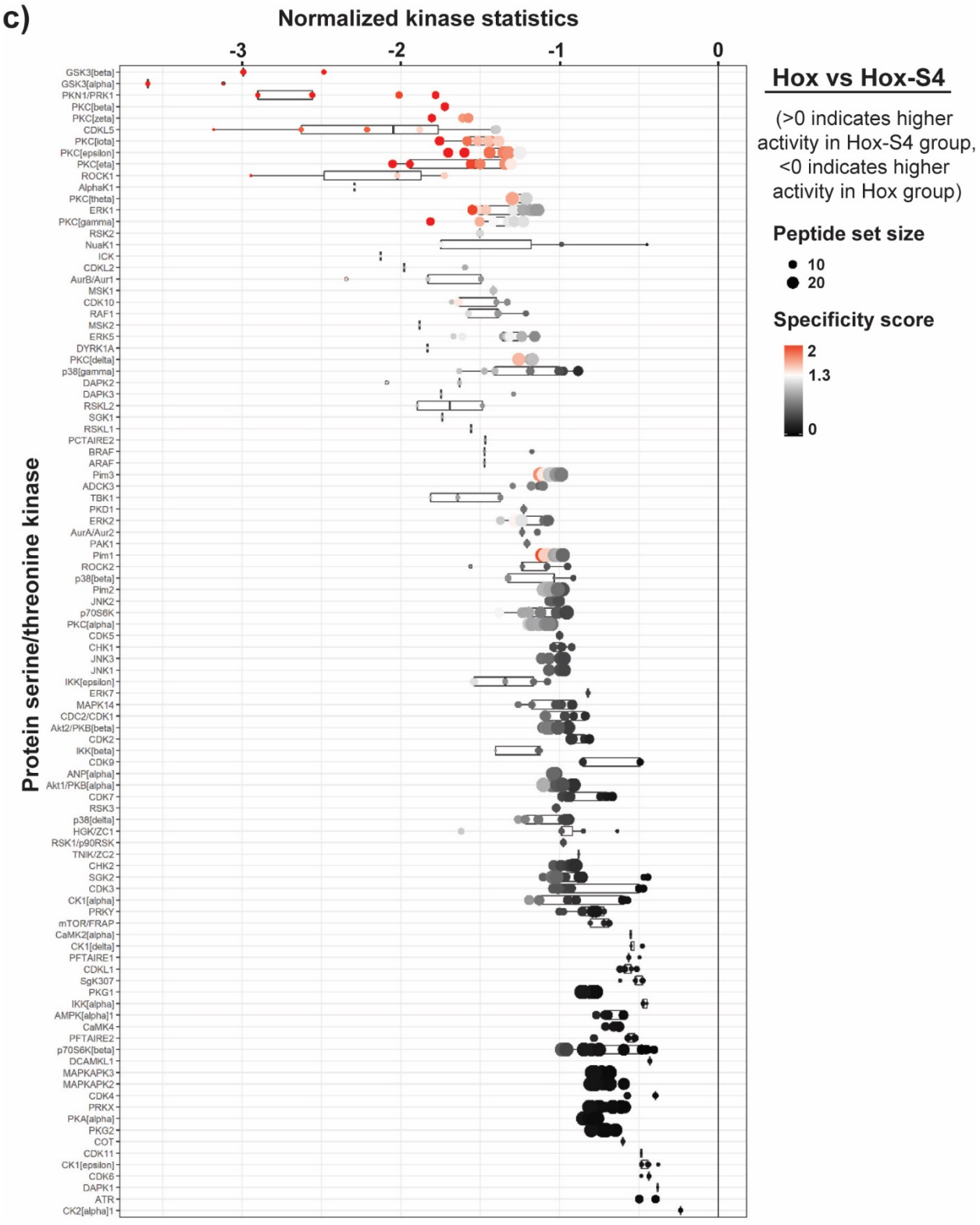
c)
Normalized kinase statistics
-3
-2
-1
0
Protein serine/threonine kinase
GSK3[beta]
GSK3[alpha]
PKN1/PRK1
PKC[beta]
PKC[zeta]
CDKL5
PKC[iota]
PKC[epsilon]
PKC[eta]
ROCK1
AlphaK1
PKC[theta]
ERK1
PKC[gamma]
RSK2
NuaK1
ICK
CDKL2
AurB/Aur1
MSK1
CDK10
RAF1
MSK2
ERK5
DYRK1A
PKC[delta]
p38[gamma]
DAPK2
DAPK3
RSKL2
SGK1
RSKL1
PCTAIRE2
BRAF
ARAF
Pim3
ADCK3
TBK1
PKD1
ERK2
AurA/Aur2
PAK1
Pim1
ROCK2
p38[beta]
Pim2
JNK2
p70S6K
PKC[alpha]
CDK5
CHK1
JNK3
JNK1
IKK[epsilon]
ERK7
MAPK14
CDC2/CDK1
Akt2/PKB[beta]
CDK2
IKK[beta]
CDK9
ANP[alpha]
Akt1/PKB[alpha]
CDK7
RSK3
p38[delta]
HGK/ZC1
RSK1/p90RSK
TNIK/ZC2
CHK2
SGK2
CDK3
CK1[alpha]
PRKY
mTOR/FRAP
CaMK2[alpha]
CK1[delta]
PFTAIRE1
CDKL1
SgK307
PKG1
IKK[alpha]
AMPK[alpha]1
CaMK4
PFTAIRE2
p70S6K[beta]
DCAMKL1
MAPKAPK3
MAPKAPK2
CDK4
PRKX
PKA[alpha]
PKG2
COT
CDK11
CK1[epsilon]
CDK6
DAPK1
ATR
CK2[alpha]1
Hox vs Hox-S4
(>0 indicates higher activity in Hox-S4 group, <0 indicates higher activity in Hox group)
Peptide set size
10
20
Specificity score
2
1.3
0

Figure 32. Effects of CA9 and 12 inhibition on hPASMCs protein serine/threonine kinases after chronic hypoxic incubation.

Human PASMCs underwent 72-hour 1% O_2 chronic hypoxia incubation (Hox) in comparison to normoxia control (Nox). Cells were subjected to either 50 μM of the S4 inhibitor (Hox-S4) or dimethyl sulfoxide (Nox, Hox) treatment. Subsequently, we assessed peptide-based serine/threonine kinase activity using the PamStation12 platform with Evolve 12 software as described in the methods section. Presented is **a**) heat map displaying log-transformed fluorescence signals related to substrate serine/threonine phosphorylation, utilized for upstream kinase analysis and **b**) the prediction of protein serine/threonine kinase activity in Hox, compared to Nox or **c**) Hox-S4 in comparison to the Hox group. Normalized kinase statistics estimate relative kinase activity, while the specificity score evaluates the reliability and accuracy of predictions.

3.6.2. CA9 and 12 influence on the activation of protein tyrosine and serine/threonine kinases during chronic hypoxia

Our results demonstrated significantly increased activity in 32 tyrosine and serine-threonine kinases in hPASMCs after hypoxia stimulation compared to normoxia control (Figures 31b, 32b and 33b). Notably, treatment with an S4 inhibitor in hypoxia significantly decreased activity in 39 tyrosine and serine-threonine kinases compared to hypoxia control (Figures 31c, 32c and 33a,b). Finally, 9 of the affected kinases were shared between the two compared conditions, with increased activity after hypoxia incubation, compared to normoxia control, and subsequently, decreased activity following the S4 treatment (Figure 33b). Affected kinases shared between the two compared conditions included protein kinase C iota type (PKCι), insulin receptor-related receptor (IRR) kinase, human epidermal growth factor receptor 4 (HER4) kinase, colony-stimulating factor 1 receptor (FmS/CSFR) kinase, tropomyosin receptor kinase A (TRKA), tropomyosin receptor kinase B (TRKB), feline sarcoma-related (Fer) kinase, colon carcinoma kinase 4 (CCK4-PTK7) and macrophage stimulating 1 receptor (Ron, MST1R) kinase.

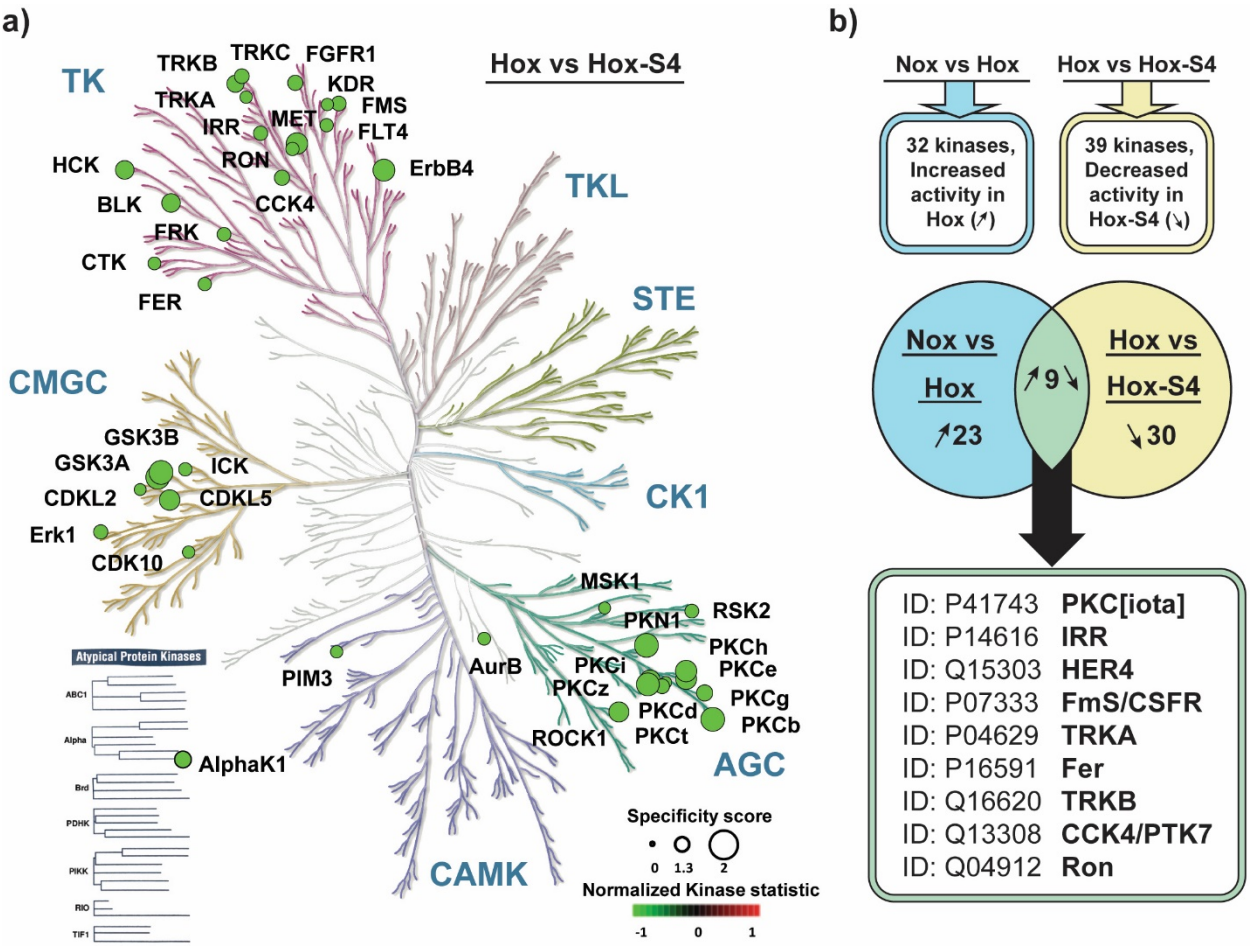

Figure 33. Effects of CA9 and 12 inhibition on hPASMCs kinome after chronic hypoxic incubation.

Human PASMCs were exposed to 1% O_2 chronic hypoxia incubation (Hox) for 72 hours, compared to normoxia control (Nox). Cells were treated with 50 µM of S4 inhibitor (Hox-S4) or dimethyl sulfoxide (Nox, Hox), followed by an assessment of the peptide-based tyrosine kinase activity by using the PamStation12 platform with Evolve 12 software as described in the methods section. **a**) Kinase three, depicting protein tyrosine and serine/threonine kinases with altered activity in hypoxia after treatment with an S4 inhibitor (Hox vs Hox-S4), is presented (green colour indicating lower kinase activity in the Hox-S4 group). The illustration reproduced courtesy of Cell Signaling Technology, Inc. In addition, **b**) a list of 9 affected kinases shared between the two compared conditions (Nox vs Hox and Hox vs Hox-S4) is shown. TK, tyrosine kinases; TKL, tyrosine kinase-like kinases; STE, STE family kinases; CK1, casein kinase 1; CMGC, CMGC family kinases; AGC, AGC family kinases; CAMK, Calmodulin-regulated kinases; PKC[iota], protein kinase C iota type; IRR, insulin receptor-related receptor; HER4, human epidermal growth factor receptor 4; FmS/CSFR, colony-stimulating factor 1 receptor; TRKA, tropomyosin receptor kinase

A; TRKB, tropomyosin receptor kinase B; Fer, feline sarcoma-related tyrosine kinase; CCK4-PTK7, colon carcinoma kinase 4; Ron, macrophage stimulating 1 receptor

3.7. CA9 and 12 inhibition effect on the development of MCT-induced pulmonary hypertension

3.7.1. Hemodynamics and RV hypertrophy effects of CA9 and 12 inhibition in MCT-induced PH in rats

Monocrotaline injection led to the development of PH, as evident by significantly increased values of RVSP and RV hypertrophy (Fulton index, RV/(LV+S)), as compared to the healthy control group (Figure 34a-b). Importantly, the treatment with an S4 inhibitor significantly ameliorated both the RVSP and Fulton index in comparison to the MCT placebo group (Figure 34a,b). MCT application significantly reduced SAP values in both placebo and S4 treated groups, as compared to the healthy control (Figure 34c). However, CAs inhibitor did not affect SAP values in comparison to the MCT-placebo group.

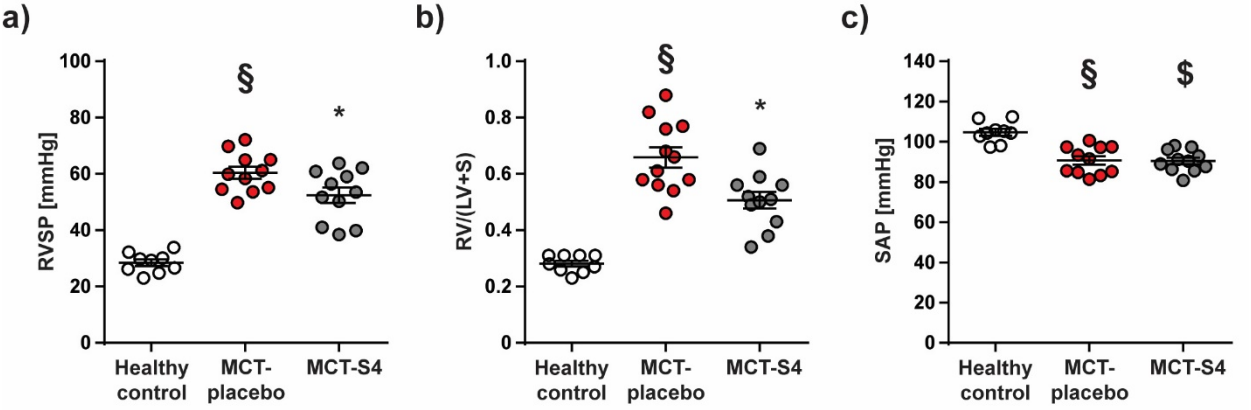

Figure 34. Effects of S4 on hemodynamics and right ventricular hypertrophy in MCT-induced pulmonary hypertension in rats.

As described in the methods section, rats were injected with either saline (Healthy control) or monocrotaline (MCT). During weeks 4 and 5 following MCT administration animals were treated with either placebo (MCT-placebo) or S4 (MCT-S4), after which hemodynamic and right ventricular hypertrophy investigation were performed. The following parameters were assessed: **a**) Right ventricular systolic pressure (RVSP), **b**) ratio of right to left ventricular plus septum weight (RV/(LV+S)), and **c**) systemic arterial pressure (SAP). Results are presented as mean ± SEM (n=9-12). $, §$p<0.05$ compared to the Healthy control, *$p<0.05$ compared to the MCT-placebo.

3.7.2. Effects of CA9 and 12 inhibition on right-heart structure and function in MCT-induced PH in rats

Monocrotaline administration affected both right heart structure and function, as evident by significantly increased echocardiographic parameters RVID and RVWT and decreased TAPSE, S´RV and CI values in comparison to the healthy control (Figure 35a-e). Notably, the treatment with S4 inhibitor significantly ameliorated RVID, TAPSE and S´RV in comparison to the MCT-placebo group (Figure 35a,c,d).

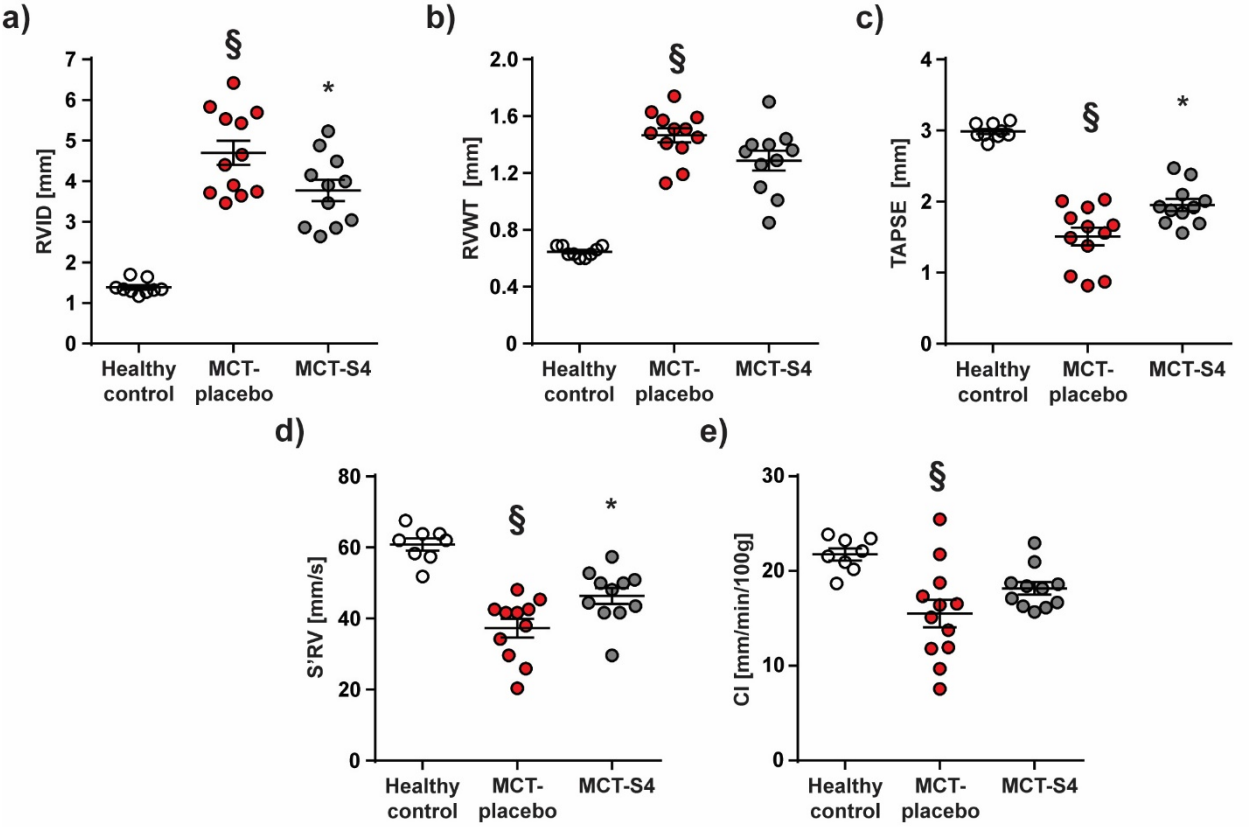

Figure 35. S4 effect on right-heart structure and function in MCT-induced pulmonary hypertension in rats.

Rats were injected with either saline (Healthy control) or monocrotaline as described in the methods section. After MCT administration, in weeks 4 and 5, rats were treated with either placebo (MCT-placebo) or S4 (MCT-S4), followed by echocardiographic assessment. The following parameters were measured: **a**) Right ventricular internal diameter (RVID), **b**) right ventricular wall thickness (RVWT), **c**) tricuspid annular plane systolic excursion (TAPSE), **d**) Pulsed tissue Doppler-derived right ventricular annular systolic excursion velocity (S´RV) and **e**) cardiac index (CI). Results are

presented as mean ± SEM (n=8-12). §p<0.05 compared to the Healthy control, *p<0.05 compared to the MCT-placebo.

3.7.3. Influence of CA9 and 12 inhibition on pulmonary vascular remodeling in MCT-induced PH in rats

Investigated degree of muscularization, a parameter of the pulmonary vascular remodeling process, revealed a significant elevation of fully-muscularized and reduction of non-muscularized pulmonary vessels in the lungs of the animals administered with MCT, compared to the healthy control (Figure 36a). In comparison to the MCT placebo group treatment with S4, a CA9 and 12 inhibitor, resulted in a significant decrease of fully-muscularized and significant increase of non-muscularized pulmonary vessels compared (Figure 36a).

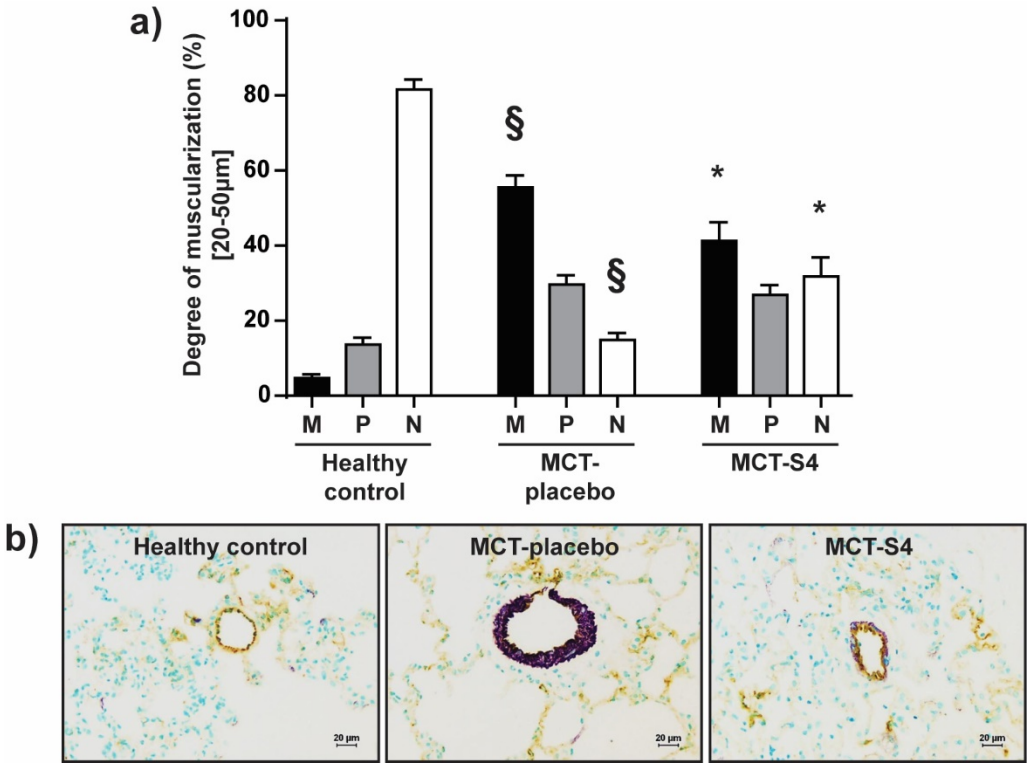

Figure 36. Effects of S4 on the degree of muscularization in MCT-induced pulmonary hypertension in rats.

As described previously, immunostaining for α-smooth muscle actin and von Willebrand factor, and subsequently, pulmonary vascular morphometry for rat lung sections was performed. The results include: **a**) percentages of fully (M), partially (P), and non-muscularized (N) vessels of total pulmonary vessel cross-sections, and **b**) representative photomicrographs for healthy control, MCT-injected rats receiving

placebo (MCT-placebo), or S4 (MCT-S4). Results are presented as mean ± SEM (n=9-11). Scale bars=20µm. §p<0.05 compared to the Healthy control, *p<0.05 compared to the MCT-placebo.

3.8. CA9 and 12 inhibition impact on the development of chronic hypoxia-induced pulmonary hypertension

3.8.1. Hemodynamics and RV hypertrophy effects of CA9 and 12 inhibition in chronic hypoxia-induced PH in mice

In comparison to the mice exposed to normoxia conditions, chronic hypoxia exposure led to the induction of PH in mice, as demonstrated by significantly elevated RVSP and RV hypertrophy (assessed by the Fulton index, RV/(LV+S)) (Figure 37a,b). Treatment with S4, a CA9 and 12 inhibitor, significantly decreased RVSP compared to the hypoxic placebo group (Figure 37a). Furthermore, there were no alterations in SAP values between different experimental groups (Figure 37c).

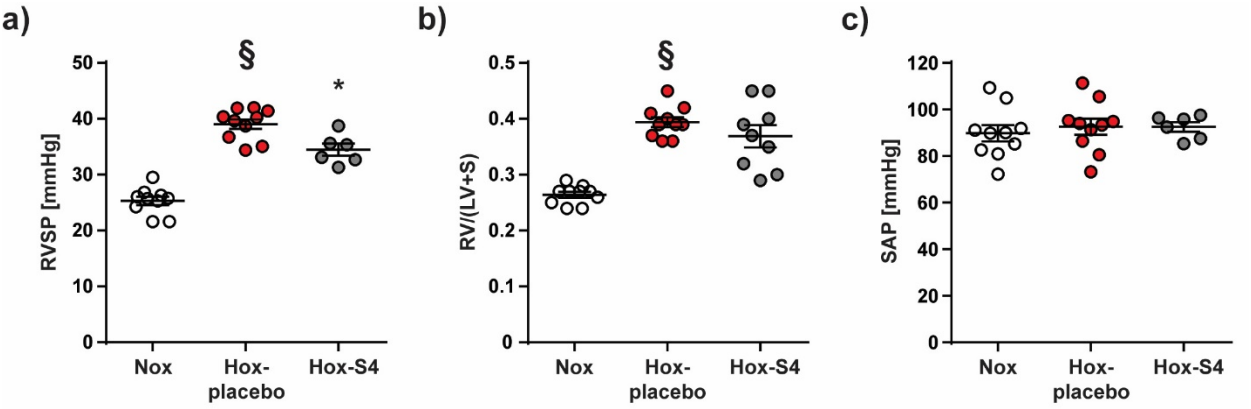

Figure 37. Effects of S4 on hemodynamics and right ventricular hypertrophy in chronic hypoxia-induced pulmonary hypertension in mice.

As described in the methods section, mice were exposed for five weeks to normoxia (Nox) or chronic hypoxia conditions. During weeks 4 and 5, hypoxia-exposed animals were treated with either a placebo (Hox-placebo) or S4 (Hox-S4), and subsequently hemodynamic and right ventricular hypertrophy investigations were conducted. The following parameters were assessed **a**) right ventricular systolic pressure (RVSP), **b**) right to left ventricular plus septum weight ratio (RV/(LV+S)), and **c**) systemic arterial pressure (SAP). Results are presented as mean ± SEM (n=6-10). §p<0.05 compared to Nox, *p<0.05 compared to Hox-placebo.

3.8.2. Effects of CA9 and 12 inhibition on right-heart structure and function in chronic hypoxia-induced PH in mice

Furthermore, chronic hypoxic exposure affected the mice right heart structure and function, based on significantly elevated RVID and RVWT and decreased TAPSE, S´RV and CI values, compared to the normoxia group (Figure 38a-e). Treatment with S4 in hypoxia led to a significant decrease of RVID and RVWT compared to the placebo mice group (Figure 38a, b). At the same time, there was no improvement in right heart functional parameters (Figure 38c-e).

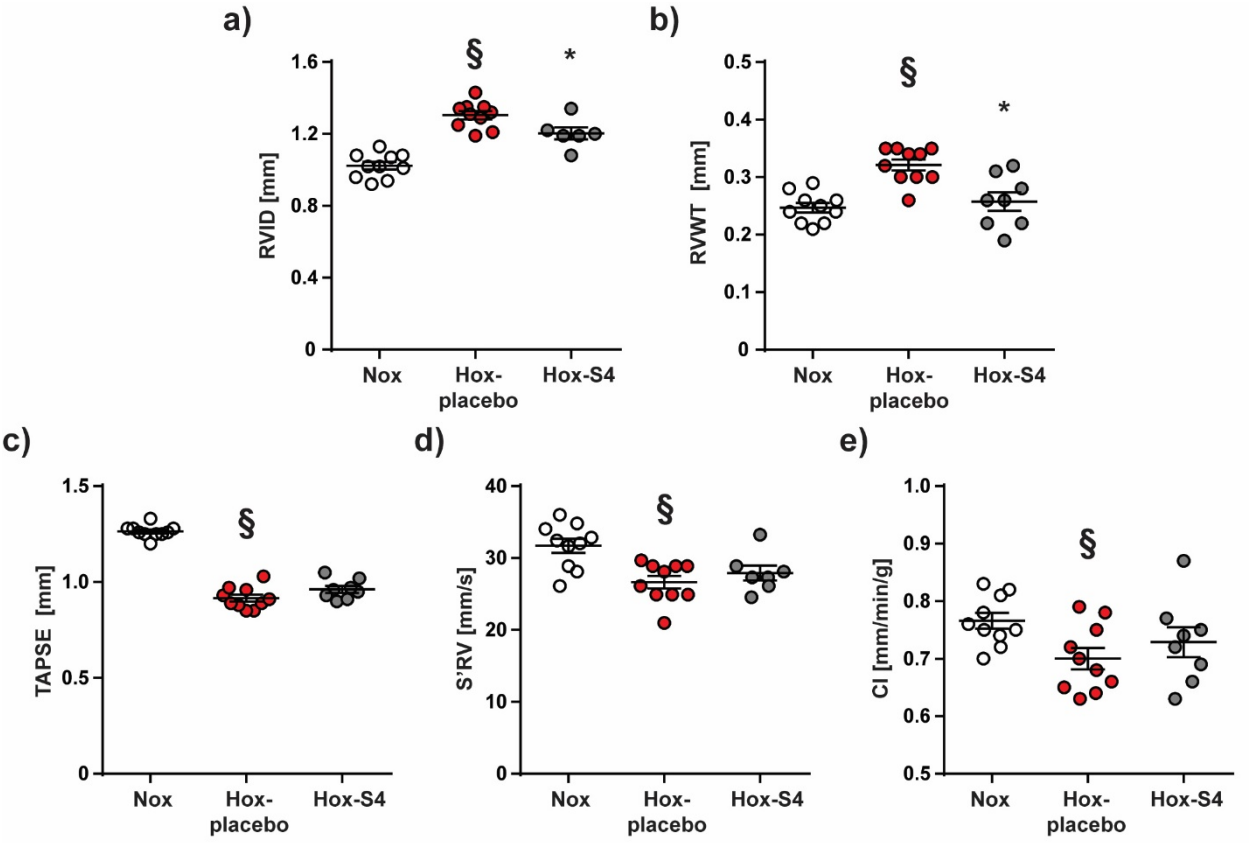

Figure 38. Effects of S4 on right-heart structure and function in chronic hypoxia-induced pulmonary hypertension in mice.

C57BL/6 J mice were exposed for five weeks to either normoxia (Nox) or chronic hypoxia conditions, as described previously. Hypoxia-exposed animals were treated with either a placebo (Hox-placebo) or S4 (Hox-S4) for two weeks from day 21 after the onset of hypoxia exposure, followed by echocardiographic assessment. **a**) Right ventricular internal diameter (RVID), **b**) right ventricular wall thickness (RVWT), **c**) tricuspid annular plane systolic excursion (TAPSE), **d**) Pulsed tissue Doppler-derived right ventricular annular systolic excursion velocity (S´RV) and **e**) cardiac index (CI)

are shown. Results are presented as mean ± SEM (n=6-10). §p<0.05 compared to Nox, *p<0.05 compared to Hox-placebo.

3.8.3. CA9 and 12 inhibition influence on pulmonary vascular remodeling in chronic hypoxia-induced PH in mice

Analysis of the pulmonary vascular remodeling in mice after exposure to chronic hypoxia revealed a significant reduction of non-muscularized and augmentation of fully-muscularized pulmonary vessels, as compared to the normoxia mice (Figure 39a). Importantly, the S4 treatment in chronically hypoxic mice resulted in a significant decrease in fully-muscularized and an increase in non-muscularized pulmonary vessels in comparison with the placebo group (Figure 39a).

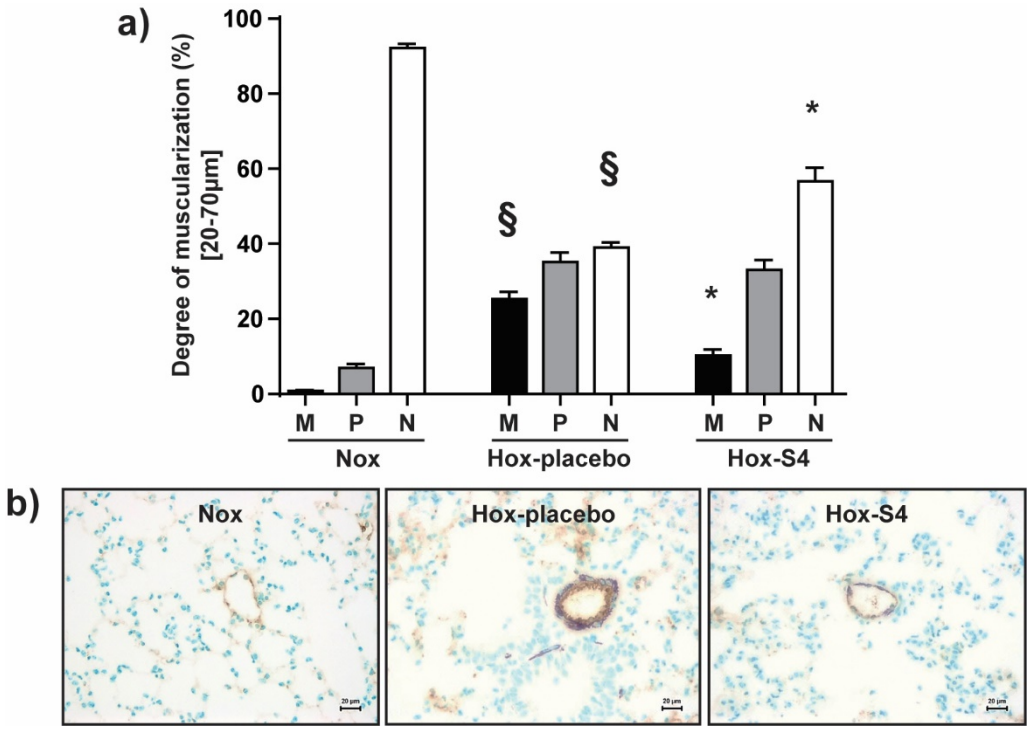

Figure 39. Effects of S4 on the degree of muscularization in chronic hypoxia-induced pulmonary hypertension in mice.

As described above, immunostaining for α-smooth muscle actin and von Willebrand factor was conducted, with subsequent pulmonary vascular morphometry performed on mice lung sections. The results include: **a**) percentages of fully- (M), partially- (P) and non- (N) muscularized vessels of the total pulmonary vessel cross-section, and **b**) representative photomicrographs for mice exposed to either normoxia (Nox) or chronic hypoxia conditions, and treated with either a placebo (Hox-placebo) or S4 (Hox-S4).

Results are presented as mean ± SEM (n=9-11). Scale bars=20µm. §p<0.05 compared to the Nox, *p<0.05 compared to the Hox-placebo.

3.9. CA9 circulating levels in PH patients

3.9.1. Characterization of PH patients with coupled and uncoupled right heart function

In order to investigate potential biomarker properties, circulating levels of CA9 were measured by enzyme-linked immunosorbent assay in the plasma samples of PH patients who underwent conductance right heart catheterization as described previously. Based on assessed RV-arterial coupling, a ratio of end-systolic to arterial elastance (Ees/Ea), subjects were affiliated with the coupled (Ees/Ea>0.8) or uncoupled (Ees/Ea<0.8) group. Demographic and clinical characteristics of involved human subjects, such as age, gender ratio and mPAP, are presented in Table 4.

Table 4. Demographic and clinical data of PH patients.

PH	Age (Years)	Gender ratio m/f (%)	BMI (kg/m²)	Ees/Ea ratio	mPAP (mmHg)	PVR (dyn*sec/ cm^5)	TAPSE (mm)	BNP (pg/ml)
Coupled	56.9 ± 3.1	25/75	27.6 ± 1.4	1.28 ± 0.1	32.5 ± 2.3	378.3 ± 46.1	23.3 ± 1.1	112.5 ± 39.4
Uncoupled	50.3 ± 3.2	64.3/35.7	25.5 ± 1.5	0.45 ± 0.04*	52.6 ± 4.5*	746.3 ± 88.5*	18.7 ± 0.9*	296 ± 74.1*

Abbreviations: f - female; m - male; BMI – body mass index; Ees - end-systolic elastance; Ea - arterial elastance; mPAP - mean pulmonary arterial pressure; PVR - pulmonary vascular resistance; TAPSE - tricuspid annular plane systolic excursion; BNP - brain natriuretic peptide. Data are presented as mean ± SEM (n=20 (Coupled), 14 (Uncoupled)) *p<0.05 compared to Coupled.

3.9.2. CA9 circulating levels in PH patients with coupled and uncoupled right heart function

CA9 levels were assessed in plasma samples collected from PH patients who went through conductance right heart catheterization, following the manufacturer instructions described in the methods section. Based on the Ees/Ea ratio, subjects were affiliated with the coupled (Ees/Ea>0.8) or uncoupled (Ees/Ea<0.8) group. Our investigation demonstrated an increase in CA9 circulating levels in the uncoupled group compared to the coupled group of PH patients, although the change did not reach significance (Figure 40).

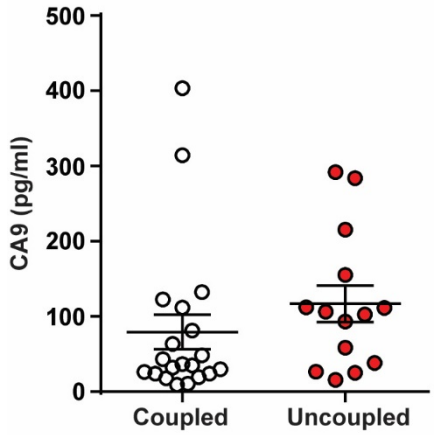

Figure 40. CA9 circulating levels in PH patients.

Plasma samples were collected from the PH patients who underwent conductance right heart catheterization with subsequent pressure-volume measurements. Depending on the end-systolic to arterial elastance (Ees/Ea) ratio, subjects were affiliated with the Coupled (Ees/Ea>0.8) or Uncoupled (Ees/Ea<0.8) group. CA9 circulating levels in PH patients with coupled and uncoupled RV function, evaluated by enzyme-linked immunosorbent assay (ELISA), are shown. Ees - end-systolic elastance; Ea - arterial elastance. Results are presented as mean ± SEM (n=20 (Coupled), 14 (Uncoupled)).

3.9.3. Correlation of CA9 circulating levels with PH patients' clinical characteristics

Finally, correlations of circulating CA9 levels with various clinical parameters were investigated (Figure 41). Our results showed a significant correlation between circulating CA9 levels and end-systolic to arterial elastance ratio (Figure 41a) and between circulating CA9 and BNP levels (Figure 41b). In the case of mPAP and PVR parameters of PH patients, there was no significant correlation with CA9 circulating levels (Figure 41c, d).

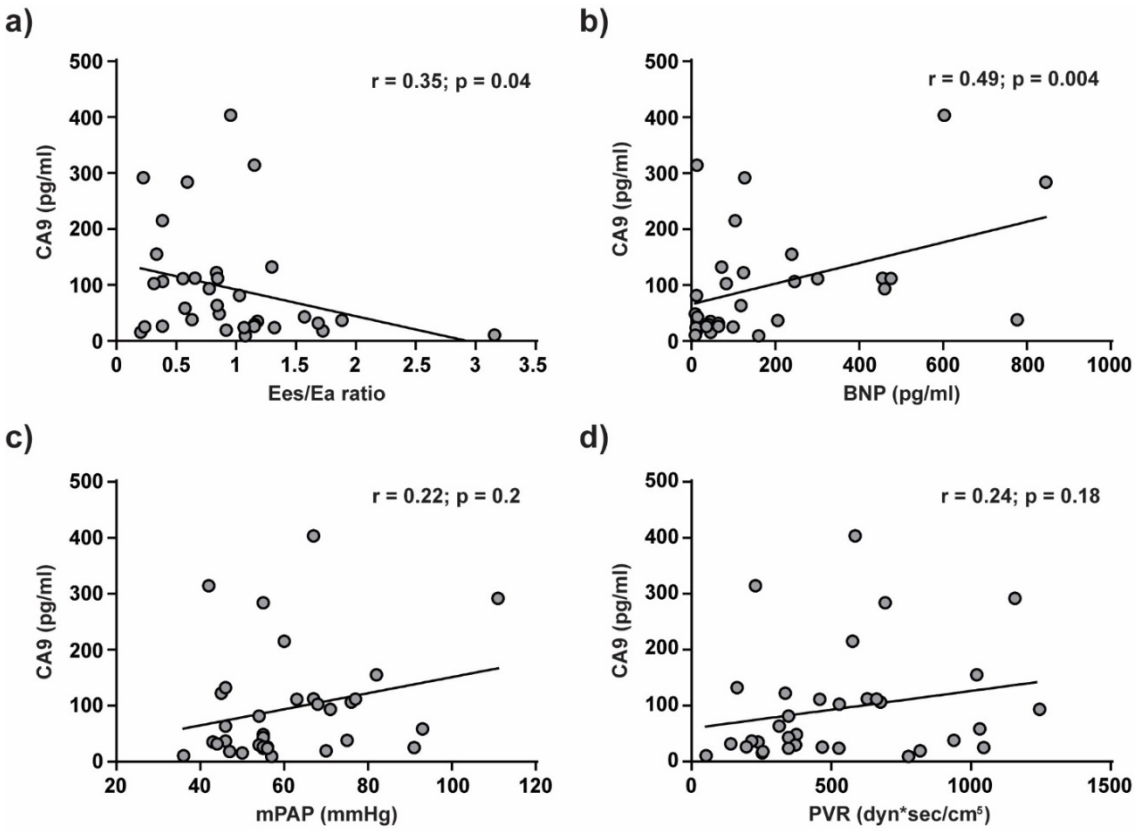

Figure 41. Soluble CA9 levels association with various clinical parameters in PH patients.

Plasma samples were collected from the PH patients who underwent conductance right heart catheterization with subsequent pressure-volume measurements. CA9 circulating levels in PH patients were investigated by enzyme-linked immunosorbent assay (ELISA). Correlation linear regression analysis of circulating CA9 levels and **a**) Ees/Ea ratio, **b**) circulating BNP levels, **c**) mPAP and **d**) PVR are shown. Ees - end-systolic elastance; Ea - arterial elastance; mPAP - mean pulmonary arterial pressure; PVR - pulmonary vascular resistance; BNP - brain natriuretic peptide. Data are presented as scatter plots showing relationship between CA9 circulating levels and Ees/Ea ratio, BNP circulating levels, mPAP and PVR (n=34 (Ees/Ea ratio, mPAP and PVR), 31 (BNP)), r - correlation coefficient.

4. Discussion

Pulmonary vascular remodeling, a hallmark of pulmonary hypertension, is characterized by several cancer-like features, such as dysregulated proliferation and migration of pulmonary vascular cells[17, 18, 21]. In addition, numerous extrapulmonary tissues and cell types are affected, including remodeled right ventricle of the heart and cardiomyocytes, skeletal muscle and immune cells[67, 68]. Interestingly, all of the affected tissues and cell types are depicted by metabolic shift in glucose metabolism from oxidative phosphorylation to glycolysis, a hallmark of malignant cell transformation[70]. Therefore, PH is considered as a syndrome with multiorgan involvement, and mitochondrial function is central, characterized by suppressed glucose oxidation and activation of glycolysis.

Carbonic anhydrases, especially transmembrane isoforms CA9 and 12 have recently become highly intriguing topics in cancer research because they are overexpressed in many tumors and often are associated with disease progression and response to therapy[113, 115, 133]. CA9 and 12 play a crucial role in cancer cells' pH regulation system allowing cancer cells to maintain pH homeostasis and highly proliferative phenotype[112, 119, 121]. In addition, CA9 and 12 are important factors in various functional properties of cancer cells, including adhesion, migration, invasion and metastasis[118].

Despite the substantial progressions and advances over the last 20 years in PH therapy, there is still no successful option for curing the disease and the development of novel therapeutic strategies remains desired[15, 16, 18]. Metabolic-modulating therapies that aim to decrease glycolysis may be effective against both proliferative PASMCs and PAECs in the pulmonary artery wall of patients with severe pulmonary hypertension. Based on described background, this study aimed to investigate the role of CA9 and 12 in hypoxia and non-hypoxia induced PH development and CA9 and 12 potential as novel therapeutic targets in PH.

In general, the major findings of the present study are:

1) CA9 and 12 expression profile was upregulated in IPAH patients, *in vivo* and *in vitro* models of hypoxia and non-hypoxia induced PH, driven by the HIF-1α transcription factor.

2) CA9 and 12 play important role in the proliferation and migration of PASMCs upon hypoxia and non-hypoxia stimuli.

3) CA9 and 12 play a role in human PASMCs intracellular pH homeostasis and subsequently activation of the protein kinases upon hypoxia exposure.

4) pharmacological inhibition of CA9 and 12 significantly ameliorated development of PH in monocrotaline-induced PH in rats and chronic hypoxia-induced PH in mice experimental models.

5) circulating CA9 levels were elevated in PH patients with uncoupled RV-arterial coupling compared to the coupled group.

Our study suggests both hypoxia and non-hypoxia driven upregulation of CA9 and 12, and their involvement in PASMC intracellular pH homeostasis, migration and highly proliferative phenotype in PH. Additionally, CA9 and 12 play a role in animal models of this severe and life-threatening pulmonary vascular disease.

4.1. CA9 and 12 expression in hypoxia and non-hypoxia induced PH

Pulmonary hypertension, in several aspects, is described as a cancer-like disease[17, 18, 21]. Expression of transmembrane CA9 and 12 is upregulated in various types of cancer, including those affecting the brain, head/neck, breast, lung, bladder, cervix uteri, colon/rectum, and kidney[207]. Besides diagnostic purposes, the detection of CA9 expression carries significant prognostic implications, as elevated CA9 expression is associated with poor clinical outcomes in cervical[208], rectal[209], breast[210], lung[211], and brain[212] tumors. Among normal tissues, CA9 and 12 have only limited distribution, making them promising therapeutic targets[123-125]. CA9 expression is exclusive to the

epithelia of the stomach, gallbladder, pancreas, and intestine, while CA12 expression in normal tissues is limited to the kidney, intestine, reproductive epithelia, and eye. Additionally, CA9-deficient mice are characterized by mild phenotypic changes, most prominently gastric hyperplasia[126, 127]. In the field of pulmonary hypertension, elevated CA9 protein expression has been reported in pulmonary hypertensive endothelial cells, but only as a marker of activated HIF1-α transcription factor[184]. No studies investigating the specific roles of CA9 and 12 have been performed in pulmonary hypertension.

To investigate CA9 and 12 expression profiles in PH, we began by measuring the mRNA expression of all CA isoforms in IPAH patients. Our results revealed significantly increased CA9 and 12 mRNA expression in IPAH patients compared to donors (Figure 11). Next, we examined CA9 and 12 protein expression in an experimental model of PH, chronic hypoxia-induced PH in mice. Our analysis demonstrated a significant augmentation of CA12 and a noticeable trend in augmented CA9 protein levels in the lungs of mice with chronic hypoxia-induced PH compared to normoxia controls (Figure 17). Furthermore, we evaluated CA9 and 12 expression profiles in hypoxia and non-hypoxia-induced *in vitro* models of PH. Hypoxia exposure resulted in elevated CA9 and 12 mRNA and protein expression in human (Figures 13 and 19) and mouse (Figures 12 and 18) PASMCs compared to normoxia controls. Additionally, non-hypoxia stimuli previously implicated in PH pathophysiology[17, 18], including various growth and inflammatory factors such as TNF-α, PDGF, TGF-β, IL-1, and IL-6, also led to an augmented CA9 and 12 expression profile (Figures 14-16, 20, and 21).

In contrast to CA12, the transcription of the CA9 gene, as one of the most sensitive HIF-1α activity sensors, has been widely investigated[132]. HIF-1α binding to the hypoxia-responsive element in the CA9 promoter drives the complex action of CA9 gene transcription[133, 134]. The CA9 core promoter contains five cis-acting elements in addition to the HRE. Some non-hypoxia stimuli, such as inflammatory and growth factor stimuli, also positively influence CA9 transcription through hypoxia-independent induction and stabilization of HIF-1α[141-144]. Although CA9 has been exclusively responsive to HIF-1α in all the cell types investigated so far, it has been demonstrated that HIF-2α can bind to the CA9 promoter HRE[138]. In addition to the well-described role of the HIF-1α transcription factor in PH, recent studies have suggested an important role for HIF-2α as

well in the development of PH[26-28]. Our study demonstrated the importance of HIF-1α binding to the CA9 promoter HRE in the A549 cell line upon hypoxia exposure (Figure 22). Additionally, the effect of HIF-1α knockdown on the decrease in CA12 protein expression upon hypoxia stimulation was shown (Figure 23). In contrast, our results showed that elevated CA9 and 12 protein expression upon hypoxia exposure in human PASMCs is HIF-2α independent (Figure 24).

4.2. Role of CA9 and 12 on functional properties of PASMCs

4.2.1. Effect of CA9 and 12 silencing and inhibition on proliferation and migration of PASMCs

Increased proliferation and migration of PASMCs are crucial events in the pulmonary vascular remodeling process and the development of pulmonary hypertension[3, 17, 18]. In this study, we investigated the role of CA9 and 12 in these important functional properties of PASMCs using siRNA-based knockdown and pharmacological inhibition approaches. One of the biggest challenges in designing CA inhibitors as potential therapeutic drugs in the cancer field has been achieving selectivity for tumor-related CA9 and 12 with extracellular catalytic activity without inhibiting ubiquitous intracellular CAs[115, 125, 130]. S4, a ureidosulfamate, is a promising CA inhibitor with high affinity for transmembrane CA9 and 12 and low affinity for cytosolic CA1 and 2 isoforms[175-177]. Treatment with S4 ameliorated the metastatic tumor burden in the lungs of mice bearing orthotropic eGFP-MDA-MB-231 tumors and inhibited the proliferation and migration of MDA-MB-231 cells *in vitro*[175].

Our study demonstrated the important role of CA9 and 12 in the proliferation of mouse and human PASMCs upon hypoxia and non-hypoxia stimulation. Treatment with S4, a CA9 and 12 small molecular inhibitor, led to a significant decrease in PDGF-BB and hypoxia-induced proliferation in mouse and human PASMCs and reversed proliferation to the levels of the appropriate controls (Figures 25, 26a, and 27a). Additionally, we investigated the specific role of CA9 or CA12 isoforms in the hypoxia and PDGF-BB-induced proliferation of human PASMCs by means of siRNA knockdown targeting against CA9 or CA12. In both hypoxia and non-hypoxia-induced proliferation of human PASMCs, silencing of the CA9 isoform had a more prominent effect on proliferation (Figures 26c and 27b). Furthermore, our study demonstrated the important role of CA9 and 12 in the hypoxia and non-hypoxia induced migration of human PASMCs (Figure 28).

Treatment with S4 significantly reduced hypoxia and PDGF-BB-induced migration of human PASMCs.

4.2.2. Effect of CA9 and 12 inhibition on human PAMSCs pH homeostasis

CA9 and 12 play a crucial role in cancer cell pH regulation system[112, 119-122]. The metabolic shift from oxidative phosphorylation to glycolysis, a hallmark of malignant cell transformation, leads to the accumulation of lactate and protons, the end-products of glycolysis. Cancer cells activate their pH regulation system to maintain intracellular pH homeostasis and a hyperproliferative phenotype[112]. Consequently, protons and lactate are extruded outside of cancer cells, leading to the acidification of the extracellular milieu, which favors cancer cell spreading and invasiveness. Previous report has indicated that activation of Na+/H+ exchanger-1, another member of the pH regulation system, is activated in a chronic hypoxia-induced PH model in mice, and that NHE-1 inhibition resulted in decreased intracellular pH values in mouse PASMCs[213].

In this study, we investigated the role of CA9 and 12 in the intracellular pH homeostasis of human PASMCs and the acidification of their extracellular milieu. Our results demonstrated the important role of CA9 and 12 in hypoxia and non-hypoxia induced acidification of the extracellular milieu of human PASMCs (Figure 29). Treatment with S4 in human PASMCs significantly increased extracellular pH values after hypoxia and PDGF-BB-induced acidification. Furthermore, our study successfully demonstrated the involvement of CA9 and 12 in intracellular pH homeostasis in human PASMCs (Figure 30). Treatment with the S4 inhibitor in human PASMCs upon hypoxia exposure resulted in a significant decrease in intracellular pH values below the optimum range (pHi=7.2-7.4) necessary for the cells' normal functional properties[178].

4.2.3. Role of CA9 and 12 in the activation of the human PASMCs protein kinases in hypoxia

The importance of pH homeostasis for normal cellular function has been well established[178, 180-182]. Decreasing intracellular pH below the optimum range can impact a variety of proteins and enzymes, interfering through proposed conformational changes with their functional properties, such as phosphorylation, and subsequently, their activation or inactivation. pH-sensitive targets affect numerous cellular functions, including ion homeostasis, signal transduction, cell shape,

contractility, and metabolism[178]. The activation of various kinases, such as cyclin-dependent kinases[200] and PDGF receptor kinases[37], plays a crucial role in the development of PH.

In this study, we successfully demonstrated the crucial role of CA9 and 12 in the activation of human PASMCs' tyrosine and serine/threonine kinases upon hypoxia stimulation (Figures 31-33). Hypoxia exposure led to a significant increase in the activity of 32 kinases compared to normoxia control, while treatment with S4 in hypoxia resulted in a significantly decreased activity of 39 kinases. Nine of the affected tyrosine and serine/threonine kinases were shared between the two conditions compared (Figure 33), including protein kinases already described in PH pathophysiology, such as protein kinase C iota type (PKCι), human epidermal growth factor receptor 4 (HER4), and tropomyosin receptor kinase A (TRKA). Besides PKCι, treatment with S4 decreased the activity of numerous PKC isoforms, including PKCα, PKCβ, PKCγ, PKCθ, PKCε, and PKCδ (Figure 32c). Previously, it has been described that activated PKC causes pulmonary vasoconstriction[214, 215] and cytokines production[216]. Additionally, polydatin attenuates PH development and reverses remodeling through PKC mechanisms in chronic hypoxia-induced PH in rats[217]. Elevated circulating levels of HER4 have been reported in patients with heart failure and related pulmonary hypertension[218]. HER4 levels were decreased after heart transplantation and reflected decreased volume overload and improved cardiac function. Furthermore, the role of TRKA has been reported in the chronic hypoxia model of PH in rats, and activated TRKA pathway was associated with increased proliferation and migration and decreased apoptosis in rat PASMCs upon hypoxia exposure[219]. Furthermore, our study demonstrated that glycogen synthase kinase 3 beta (GSK3β) and alpha (GSK3α) were the two serine/threonine protein kinases with the most significant decrease in activity upon S4 treatment in hypoxia. Although their activity was increased in hypoxia compared to normoxia, it didn't reach statistical significance. It has been reported that activated GSK3β contributes to the proliferation of rat PASMCs in a PDGF-dependent manner[220].

4.3. CA9 and 12 inhibition in MCT-induced and chronic hypoxia-induced PH

Several studies have investigated the effect of acetazolamide, a non-selective CA inhibitor, on the pathophysiology of PH[185-190]. Treatment with ACZ reduced hypoxic pulmonary vasoconstriction in isolated perfused rabbit lungs[186] and conscious, spontaneously breathing dogs[187]. In another study, acetazolamide treatment ameliorated the effects of chronic hypoxia on PVR and CO in rats exposed to chronic hypoxia[188]. Recently, it has been shown that ACZ diminished Sugen 5416/hypoxia-induced PH in rats[185]. Importantly, previous studies demonstrated that the effects of ACZ on vasodilation during hypoxia and inhibition of hypoxia-induced calcium responses are independent of CA enzymatic activity[189, 190]. To date, the specific role of CA9 and 12 in experimental models of PH has not been studied.

To investigate the therapeutic potential of a specific CA9 and 12 inhibitor, independent of the cause of the disease, we performed chronic treatment studies in experimental pulmonary hypertension induced by MCT injection in rats and chronic hypoxia in mice. We successfully demonstrated that S4 improved pulmonary hypertension, right ventricular hypertrophy, structure, and function, as well as pulmonary vascular remodeling in MCT-induced pulmonary hypertension in rats, as evident from significantly ameliorated RVSP, RV/(LV+S), RVID, TAPSE, S'RV, and degree of muscularization of peripheral pulmonary vessels (Figures 34-36). MCT injection significantly reduced SAP values in both placebo and S4-treated groups, although S4 treatment did not affect SAP values compared to the MCT-placebo group (Figure 34c). Furthermore, we demonstrated that S4 treatment ameliorated pulmonary hypertension, right heart structure, and pulmonary vascular remodeling in chronic hypoxia-induced pulmonary hypertension in mice, as evident from significantly reduced RVSP, RVID, RVWT, and degree of muscularization of peripheral pulmonary vessels (Figures 37-39). In addition, the CA inhibitor visibly improved right ventricular hypertrophy, although the effect did not reach statistical significance (Figure 37b). Our study showed that S4 treatment had a more prominent effect in MCT-induced PH in rats compared to chronic hypoxia-induced PH in mice. This can be explained by the difference in the severity of the developed disease between the two animal models, with MCT-induced PH being the more severe experimental model of PH. Taken together, this study strongly suggests beneficial therapeutic effects of CA9 and 12 inhibition in PH, independent of the cause of the disease.

4.4. CA9 circulating levels in PH patients

The extracellular domain of CA9 is shed in tumor cells by ADAM 10 and ADAM 17[150, 151]. Besides its expression in tumor tissues, soluble CA9 is detectable in cancer patients' plasma and has been extensively investigated in various types of cancer, including clear cell renal cell carcinoma, hepatocellular carcinoma, non-small cell lung, head and neck, gastric, and castration-resistant prostate cancer (Table 2)[152-167]. Elevated circulating CA9 levels are often indicative of a poor prognosis in cancer patients. RV-arterial coupling reflects right ventricular adaptation to elevated afterload and stands as a significant prognostic factor in PH patients[7-9]. The biggest challenge in assessing RV-arterial coupling is the invasive nature of pressure-volume relationship analysis, and new non-invasive methods, including biomarker approaches, are desirable for future establishment[10-12].

In our previous study, we demonstrated significantly increased circulating levels of CA9 in IPAH patients compared to the non-PH control group (unpublished data). Additionally, a significant correlation was observed between CA9 circulating levels and several clinical parameters of IPAH patients, such as cardiac index, six-minute walking distance, and circulating BNP levels. In this study, we investigated plasma samples obtained from patients who underwent conductance right heart catheterization and RV-arterial coupling assessment. We demonstrated an elevation in CA9 circulating levels in the uncoupled group compared to the coupled group of PH patients, although the change did not reach significance (Figure 40). Furthermore, soluble CA9 levels were significantly correlated with the end-systolic to arterial elastance ratio and circulating BNP levels, while there was no significant correlation with mPAP and PVR parameters of PH patients (Figure 41). Although this study suggests circulating CA9 as a prognostic marker, involvement of a higher number of researched subjects is needed to further investigate soluble CA9 biomarker potential for RV-arterial coupling in PH patients.

4.5. Conclusion

This study provides evidence for the role of CA9 and 12 in PASMCs pH homeostasis, leading to the development of hypoxia and non-hypoxia-induced pulmonary hypertension and unravels possible up- and downstream signaling mechanisms. A short summary of this study is depicted in Figure 42. Hypoxia and non-hypoxia stimuli lead to the HIF-1α-driven upregulation of CA9 and

12 expression profile in highly proliferative PASMCs, characterized by a metabolic shift from oxidative phosphorylation to glycolysis as the main source of energy production (Figure 42a). Subsequently, upregulated glucose uptake and glycolysis lead to the cellular accumulation of lactate and protons, the end-products of glycolysis. CA9 and 12 play a role in PASMCs' intracellular pH regulation system through the carbon dioxide bicarbonate buffer system, resulting in extruded protons outside the cell, extracellular milieu acidification, and intracellular pH homeostasis. Keeping the intracellular pH values in the optimum range is a crucial event for the cell's normal functions, such as phosphorylation of various enzymes and, subsequently, maintenance of the highly proliferative phenotype of PASMCs leading to pulmonary vascular remodeling and PH development. CA9 and 12 inhibition disrupted PASMCs' extrusion of protons, intracellular pH homeostasis, acidification of the extracellular milieu, and activation of various protein kinases, resulting in decreased proliferation and migration (Figure 42b). Additionally, CA9 and 12 inhibition in two experimental models of PH improved pulmonary hypertension, right ventricular hypertrophy, and pulmonary vascular remodeling (Figures 34-39). Finally, circulating CA9 showed potential as a prognostic biomarker in PH patients (Figures 40, 41).

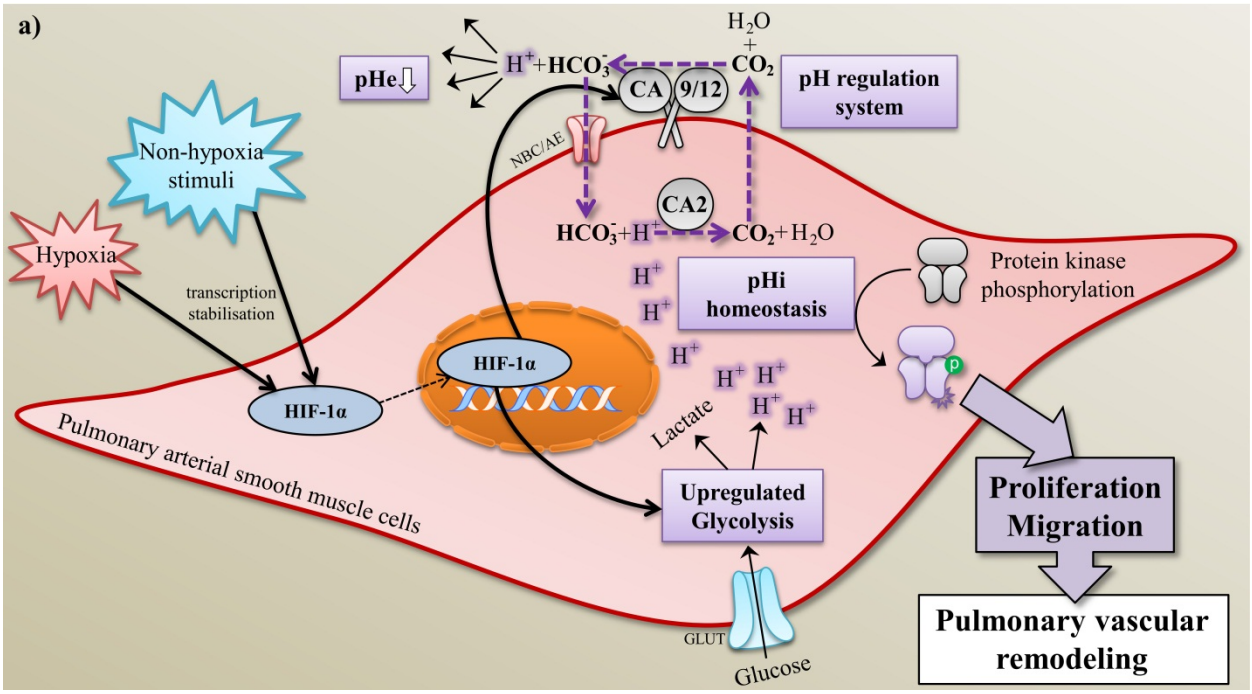

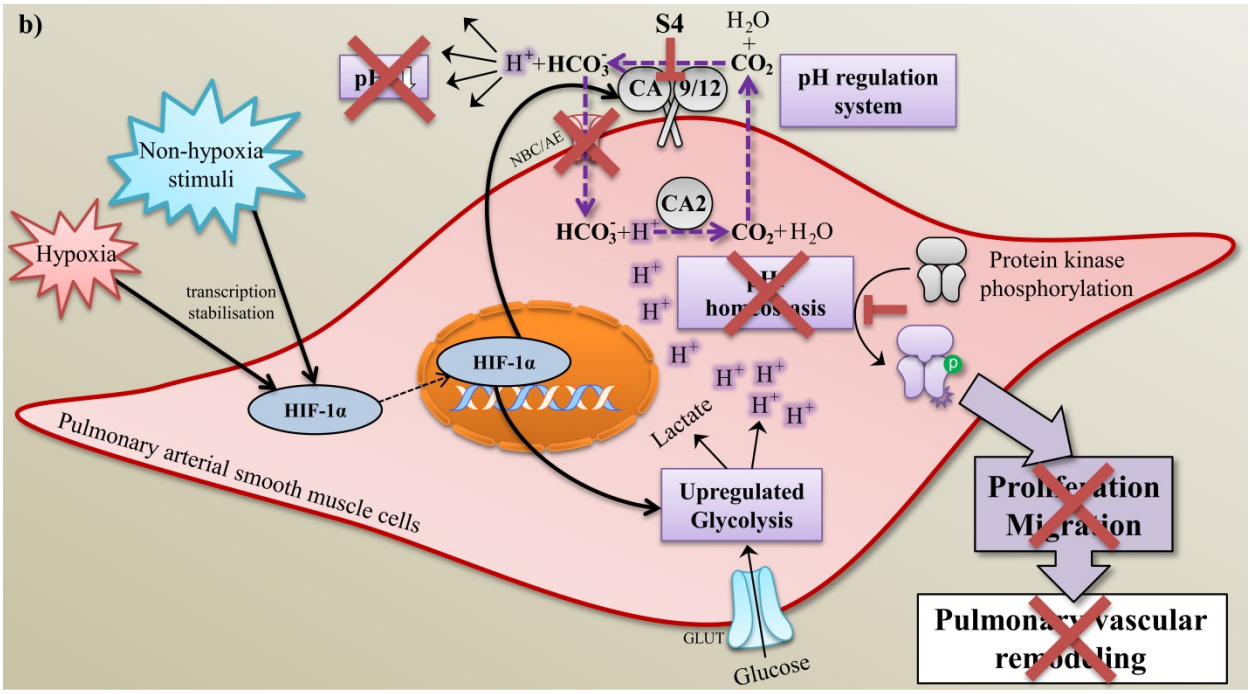

Figure 42. Proposed role of CA9 and 12 in PASMCs pH homeostasis and pulmonary vascular remodeling during PH.

a) Hypoxia and non-hypoxia stimuli, such as PDGF-BB, TGF-β, TNF-α, IL-1, and IL-6, elevate PASMCs CA9 and 12 expression profiles in a HIF-1α-dependent manner. The metabolic shift towards glycolysis in highly proliferative PH PASMCs results in the accumulation of lactate and protons inside the cells. CA9 and 12 play a role in PASMCs' pH regulation system, which extrudes protons outside of the cells, leading to pHi homeostasis and extracellular acidification. pH homeostasis is necessary for PASMCs to maintain functional properties, such as the phosphorylation of various protein kinases, resulting in continuous proliferation and migration, and ultimately, pulmonary vascular remodeling and the development of pulmonary hypertension. **b**) CA9 and 12 inhibition leads to the disrupted PASMCs' pH regulation system, accumulation of protons inside the cells, decrease of extracellular acidification, and discontinued intracellular pH homeostasis, resulting in decreased phosphorylation of various protein kinases, and subsequently, decreased PASMCs proliferation and migration, and ameliorated pulmonary vascular remodeling.

Abbreviations: GLUT - glucose transporter; HIF-1α - hypoxia-inducible factor 1 alpha; NBC - Na^+-dependent HCO_3^- cotransporter; AE - Cl^-/HCO_3^- anion exchanger; pHe - extracellular pH; pHi - intracellular pH; PDGF-BB - platelet-derived growth factor-BB; TNF-α - tumor necrosis factor-alpha; TGF-β - transforming growth factor beta; IL-1/6 - interleukin-1/6.

5. Summary

Pulmonary hypertension (PH) is a severe and incurable disease characterized by a progressive elevation of pulmonary arterial pressure, ultimately resulting in right ventricle failure and death. Pulmonary vascular remodeling is a crucial event in the disease development and its portrayed by several cancer-like features, such as increased proliferation, migration and resistance to apoptosis of pulmonary vascular cells. Additionally, a metabolic shift from oxidative phosphorylation to glycolysis, a hallmark of malignant cell transformation, has been described in pulmonary vascular cells. Carbonic anhydrases (CAs), especially CA9 and 12, have become intriguing topics in cancer research due to their overexpression in various tumors and limited expression in normal tissues. Elevated CA9 plasma levels are described in various cancers and often associated with disease progression. They play a crucial role in cancer cells' intracellular pH regulation, hyperproliferative phenotype, and various functional aspects, such as adhesion, migration, invasion and metastasis. Despite significant progress in pulmonary hypertension therapy, new treatment strategies are needed. Metabolic-modulating therapies targeting glycolysis could be effective against proliferative cells in the pulmonary artery wall.

Our study aimed to investigate the role of CA9 and 12 in hypoxia and non-hypoxia induced PH. We have successfully demonstrated an elevated CA9 and 12 expression profile in idiopathic pulmonary arterial hypertension (IPAH) patients, *in vivo* and *in vitro* models of hypoxia and non-hypoxia induced PH, driven by the HIF-1α transcription factor. This study strongly indicates the important role of CA9 and 12 in hypoxia and non-hypoxia induced proliferation and migration of pulmonary arterial smooth muscle cells (PASMCs). Furthermore, CA9 and 12 are involved in PASMCs intracellular pH homeostasis and acidification of their extracellular milieu, subsequently activating numerous protein kinases upon hypoxia exposure. Additionally, this study demonstrated the beneficial therapeutic effect of CA9 and 12 pharmacological inhibition in two experimental models of PH, the monocrotaline model in rats and the chronic hypoxia model in mice. Finally, this study revealed an increase in circulating CA9 levels in PH patients with uncoupled right ventricle-arterial coupling compared to the coupled group.

In conclusion, CA9 and 12 play an important role in hypoxia and non-hypoxia induced PH by contributing to the pulmonary vascular remodeling and may represent novel therapeutic targets for the treatment of pulmonary hypertension in the future.

6. Zusammenfassung

Pulmonale Hypertonie (PH) ist eine schwere und unheilbare Krankheit, die durch eine progressive Erhöhung des pulmonal arteriellen Drucks gekennzeichnet ist und zu einem Versagen des rechten Ventrikels und letztendlich zum Tod führt. Die Umstrukturierung der pulmonalen Gefäße ist ein entscheidendes Ereignis in der Entwicklung der Krankheit und wird durch mehrere krebsähnliche Merkmale, wie erhöhte Proliferation, Migration und Resistenz gegenüber der Apoptose von pulmonalen Gefäßzellen, dargestellt. Zusätzlich wurde ein Wechsel von oxidativer Phosphorylierung zur Glykolyse, als ein charakteristisches Merkmal der malignen Zelltransformation, in pulmonalen Gefäßzellen beschrieben. Carboanhydrasen (CAs), insbesondere CA9 und 12, sind aufgrund ihrer Überexpression in verschiedenen Tumoren und ihrer begrenzten Expression in normalen Geweben zu interessanten Themen in der Krebsforschung geworden. Erhöhte CA9-Plasmaspiegel werden in verschiedenen Krebsarten beschrieben und sind oft mit dem Krankheitsverlauf verbunden. Sie spielen eine entscheidende Rolle bei der intrazellulären pH-Regulation von Krebszellen, ihrem hyperproliferativen Phänotyp und verschiedenen funktionalen Aspekten wie Adhäsion, Migration, Invasion und Metastasierung. Trotz bedeutender Fortschritte in der Therapie der pulmonalen Hypertonie sind neue Behandlungsstrategien erforderlich. Stoffwechselmodulierende Therapien, die auf die Glykolyse abzielen, könnten gegen proliferative Zellen in der Pulmonalarterienwand wirksam sein.

Unsere Studie hatte zum Ziel, die Rolle von CA9 und 12 bei Hypoxie- und Nicht-Hypoxie-induzierter PH zu untersuchen. Wir haben erfolgreich ein erhöhtes Expressionsprofil von CA9 und 12 bei Patienten mit idiopathischer pulmonal arterieller Hypertonie (IPAH) sowie in in vivo- und in vitro-Modellen Hypoxie- und Nicht-Hypoxie-induzierter PH nachgewiesen, die durch den Transkriptionsfaktor HIF-1α gesteuert werden. Diese Studie deutet stark auf die wichtige Rolle von CA9 und 12 bei der Hypoxie- und Nicht-Hypoxie-induzierten Proliferation und Migration glatter Muskelzellen in den Pulmonalarterien (PASMCs) hin. Darüber hinaus sind CA9 und 12 an der intrazellulären pH-Homöostase von PASMCs und der Azidifizierung ihrer extrazellulären Umgebung beteiligt, wodurch bei Hypoxieeinwirkung zahlreiche Proteinkinasen aktiviert werden. Darüber hinaus zeigte diese Studie einen vorteilhaften therapeutischen Effekt der

pharmakologischen Hemmung von CA9 und 12 in zwei experimentellen Modellen von PH, dem Monocrotalin-Modell in Ratten und dem chronischen Hypoxie-Modell in Mäusen. Schließlich zeigte diese Studie einen Anstieg des zirkulierenden CA9-Spiegels bei PH-Patienten mit entkoppelter rechtsventrikulär-arterieller Kopplung im Vergleich zur gekoppelten Gruppe.

Zusammenfassend spielen CA9 und 12 eine wichtige Rolle bei der Hypoxie- und Nicht-Hypoxie-induzierten PH, indem sie zur Umstrukturierung der pulmonalen Gefäße beitragen und möglicherweise neuartige therapeutische Ziele für die Behandlung der pulmonalen Hypertonie in der Zukunft darstellen.

7. Index of figures

8. Index of tables

9. Declaration

I declare that I have independently completed this dissertation, without any unauthorized assistance from others, and have only utilized acknowledged support as outlined within. I have properly recognized and cited all passages directly or indirectly sourced from published or unpublished materials, as well as any information pertaining to verbal exchanges. Throughout the research presented in this dissertation, I have adhered to the ethical standards established in the charter of the Justus Liebig University of Giessen.

Aleksandar Petrovic

10. References

1. Humbert M, Guignabert C, Bonnet S, Dorfmüller P, Klinger JR, Nicolls MR, Olschewski AJ, Pullamsetti SS, Schermuly RT, Stenmark KR and Rabinovitch M. Pathology and pathobiology of pulmonary hypertension: state of the art and research perspectives. *The European respiratory journal*. 2019;53.

2. Simonneau G, Montani D, Celermajer DS, Denton CP, Gatzoulis MA, Krowka M, Williams PG and Souza R. Haemodynamic definitions and updated clinical classification of pulmonary hypertension. *The European respiratory journal*. 2019;53.

3. Humbert M, Kovacs G, Hoeper MM, Badagliacca R, Berger RMF, Brida M, Carlsen J, Coats AJS, Escribano-Subias P, Ferrari P, Ferreira DS, Ghofrani HA, Giannakoulas G, Kiely DG, Mayer E, Meszaros G, Nagavci B, Olsson KM, Pepke-Zaba J, Quint JK, Rådegran G, Simonneau G, Sitbon O, Tonia T, Toshner M, Vachiery JL, Vonk Noordegraaf A, Delcroix M and Rosenkranz S. 2022 ESC/ERS Guidelines for the diagnosis and treatment of pulmonary hypertension. *The European respiratory journal*. 2023;61.

4. Hatano Si. Primary pulmonary hypertension report on a WHO meeting, Geneva, 15-17 October 1973. Geneva: Geneva, WHO; 1975.

5. Kovacs G and Olschewski H. The definition of pulmonary hypertension: history, practical implications and current controversies. *Breathe*. 2021;17:210076.

6. Galiè N, McLaughlin VV, Rubin LJ and Simonneau G. An overview of the 6th World Symposium on Pulmonary Hypertension. *The European respiratory journal*. 2019;53.

7. Tello K, Seeger W, Naeije R, Vanderpool R, Ghofrani HA, Richter M, Tedford RJ and Bogaard HJ. Right heart failure in pulmonary hypertension: Diagnosis and new perspectives on vascular and direct right ventricular treatment. *British journal of pharmacology*. 2021;178:90-107.

8. Tello K, Gall H, Richter M, Ghofrani A and Schermuly R. Right ventricular function in pulmonary (arterial) hypertension. *Herz*. 2019;44:509-516.

9. Richter MJ, Hsu S, Yogeswaran A, Husain-Syed F, Vadász I, Ghofrani HA, Naeije R, Harth S, Grimminger F, Seeger W, Gall H, Tedford RJ and Tello K. Right ventricular pressure-volume loop shape and systolic pressure change in pulmonary hypertension. *American journal of physiology Lung cellular and molecular physiology*. 2021;320:L715-l725.

10. Tello K, Axmann J, Ghofrani HA, Naeije R, Narcin N, Rieth A, Seeger W, Gall H and Richter MJ. Relevance of the TAPSE/PASP ratio in pulmonary arterial hypertension. *International journal of cardiology*. 2018;266:229-235.

11. Richter MJ, Yogeswaran A, Husain-Syed F, Vadász I, Rako Z, Mohajerani E, Ghofrani HA, Naeije R, Seeger W, Herberg U, Rieth A, Tedford RJ, Grimminger F, Gall H and Tello K. A novel non-

invasive and echocardiography-derived method for quantification of right ventricular pressure-volume loops. *European heart journal Cardiovascular Imaging*. 2022;23:498-507.

12. Keranov S, Dörr O, Jafari L, Liebetrau C, Keller T, Troidl C, Kriechbaum S, Voss S, Richter M, Tello K, Gall H, Ghofrani HA, Mayer E, Seeger W, Hamm CW and Nef H. SPARCL1 as a biomarker of maladaptive right ventricular remodelling in pulmonary hypertension. *Biomarkers: biochemical indicators of exposure, response, and susceptibility to chemicals*. 2020;25:290-295.

13. McGoon MD, Ferrari P, Armstrong I, Denis M, Howard LS, Lowe G, Mehta S, Murakami N and Wong BA. The importance of patient perspectives in pulmonary hypertension. *The European respiratory journal*. 2019;53.

14. Frost A, Badesch D, Gibbs JSR, Gopalan D, Khanna D, Manes A, Oudiz R, Satoh T, Torres F and Torbicki A. Diagnosis of pulmonary hypertension. *The European respiratory journal*. 2019;53.

15. Sitbon O, Gomberg-Maitland M, Granton J, Lewis MI, Mathai SC, Rainisio M, Stockbridge NL, Wilkins MR, Zamanian RT and Rubin LJ. Clinical trial design and new therapies for pulmonary arterial hypertension. *The European respiratory journal*. 2019;53.

16. O'Callaghan DS, Savale L, Montani D, Jaïs X, Sitbon O, Simonneau G and Humbert M. Treatment of pulmonary arterial hypertension with targeted therapies. *Nature reviews Cardiology*. 2011;8:526-38.

17. Schermuly RT, Ghofrani HA, Wilkins MR and Grimminger F. Mechanisms of disease: pulmonary arterial hypertension. *Nature reviews Cardiology*. 2011;8:443-55.

18. Pullamsetti SS, Savai R, Seeger W and Goncharova EA. Translational advances in the field of pulmonary hypertension. From cancer biology to new pulmonary arterial hypertension therapeutics. Targeting cell growth and proliferation signaling hubs. *American journal of respiratory and critical care medicine*. 2017;195:425-437.

19. de Jesus Perez VA. Molecular pathogenesis and current pathology of pulmonary hypertension. *Heart failure reviews*. 2016;21:239-57.

20. Lau EMT, Giannoulatou E, Celermajer DS and Humbert M. Epidemiology and treatment of pulmonary arterial hypertension. *Nature reviews Cardiology*. 2017;14:603-614.

21. Tuder RM. Pulmonary vascular remodeling in pulmonary hypertension. *Cell and tissue research*. 2017;367:643-649.

22. McLaughlin VV, Shah SJ, Souza R and Humbert M. Management of pulmonary arterial hypertension. *Journal of the American College of Cardiology*. 2015;65:1976-97.

23. Hansmann G and Zamanian RT. PPARgamma activation: a potential treatment for pulmonary hypertension. *Science translational medicine*. 2009;1:12ps14.

24. Veith C, Schermuly RT, Brandes RP and Weissmann N. Molecular mechanisms of hypoxia-inducible factor-induced pulmonary arterial smooth muscle cell alterations in pulmonary hypertension. *The Journal of physiology*. 2016;594:1167-77.

25. Bonnet S, Michelakis ED, Porter CJ, Andrade-Navarro MA, Thébaud B, Bonnet S, Haromy A, Harry G, Moudgil R, McMurtry MS, Weir EK and Archer SL. An abnormal mitochondrial-hypoxia inducible factor-1alpha-Kv channel pathway disrupts oxygen sensing and triggers pulmonary arterial hypertension in fawn hooded rats: similarities to human pulmonary arterial hypertension. *Circulation*. 2006;113:2630-41.

26. Tan Q, Kerestes H, Percy MJ, Pietrofesa R, Chen L, Khurana TS, Christofidou-Solomidou M, Lappin TR and Lee FS. Erythrocytosis and pulmonary hypertension in a mouse model of human HIF2A gain of function mutation. *The Journal of biological chemistry*. 2013;288:17134-44.

27. Kapitsinou PP, Rajendran G, Astleford L, Michael M, Schonfeld MP, Fields T, Shay S, French JL, West J and Haase VH. The Endothelial Prolyl-4-Hydroxylase Domain 2/Hypoxia-Inducible Factor 2 Axis Regulates Pulmonary Artery Pressure in Mice. *Molecular and cellular biology*. 2016;36:1584-94.

28. Cowburn AS, Crosby A, Macias D, Branco C, Colaço RD, Southwood M, Toshner M, Crotty Alexander LE, Morrell NW, Chilvers ER and Johnson RS. HIF2α-arginase axis is essential for the development of pulmonary hypertension. *Proceedings of the National Academy of Sciences of the United States of America*. 2016;113:8801-6.

29. Piao L, Sidhu VK, Fang YH, Ryan JJ, Parikh KS, Hong Z, Toth PT, Morrow E, Kutty S, Lopaschuk GD and Archer SL. FOXO1-mediated upregulation of pyruvate dehydrogenase kinase-4 (PDK4) decreases glucose oxidation and impairs right ventricular function in pulmonary hypertension: therapeutic benefits of dichloroacetate. *Journal of molecular medicine*. 2013;91:333-46.

30. Savai R, Al-Tamari HM, Sedding D, Kojonazarov B, Muecke C, Teske R, Capecchi MR, Weissmann N, Grimminger F, Seeger W, Schermuly RT and Pullamsetti SS. Pro-proliferative and inflammatory signaling converge on FoxO1 transcription factor in pulmonary hypertension. *Nature medicine*. 2014;20:1289-300.

31. Yu Y, Keller SH, Remillard CV, Safrina O, Nicholson A, Zhang SL, Jiang W, Vangala N, Landsberg JW, Wang JY, Thistlethwaite PA, Channick RN, Robbins IM, Loyd JE, Ghofrani HA, Grimminger F, Schermuly RT, Cahalan MD, Rubin LJ and Yuan JX. A functional single-nucleotide polymorphism in the TRPC6 gene promoter associated with idiopathic pulmonary arterial hypertension. *Circulation*. 2009;119:2313-22.

32. Christman BW, McPherson CD, Newman JH, King GA, Bernard GR, Groves BM and Loyd JE. An imbalance between the excretion of thromboxane and prostacyclin metabolites in pulmonary hypertension. *The New England journal of medicine*. 1992;327:70-5.

33. Giaid A and Saleh D. Reduced expression of endothelial nitric oxide synthase in the lungs of patients with pulmonary hypertension. *The New England journal of medicine*. 1995;333:214-21.

34. Rabinovitch M. Molecular pathogenesis of pulmonary arterial hypertension. *The Journal of clinical investigation*. 2008;118:2372-9.

35. Yi ES, Kim H, Ahn H, Strother J, Morris T, Masliah E, Hansen LA, Park K and Friedman PJ. Distribution of obstructive intimal lesions and their cellular phenotypes in chronic pulmonary hypertension. A morphometric and immunohistochemical study. *American journal of respiratory and critical care medicine*. 2000;162:1577-86.

36. Meyrick B and Reid L. Hypoxia-induced structural changes in the media and adventitia of the rat hilar pulmonary artery and their regression. *The American journal of pathology*. 1980;100:151-78.

37. Schermuly RT, Dony E, Ghofrani HA, Pullamsetti S, Savai R, Roth M, Sydykov A, Lai YJ, Weissmann N, Seeger W and Grimminger F. Reversal of experimental pulmonary hypertension by PDGF inhibition. *The Journal of clinical investigation*. 2005;115:2811-21.

38. Grimminger F and Schermuly RT. PDGF receptor and its antagonists: role in treatment of PAH. *Advances in experimental medicine and biology*. 2010;661:435-46.

39. Rabinovitch M, Guignabert C, Humbert M and Nicolls MR. Inflammation and immunity in the pathogenesis of pulmonary arterial hypertension. *Circulation research*. 2014;115:165-75.

40. Nicod LP. The endothelium and genetics in pulmonary arterial hypertension. *Swiss medical weekly*. 2007;137:437-42.

41. Jones PL, Cowan KN and Rabinovitch M. Tenascin-C, proliferation and subendothelial fibronectin in progressive pulmonary vascular disease. *The American journal of pathology*. 1997;150:1349-60.

42. Yamashita J, Itoh H, Hirashima M, Ogawa M, Nishikawa S, Yurugi T, Naito M, Nakao K and Nishikawa S. Flk1-positive cells derived from embryonic stem cells serve as vascular progenitors. *Nature*. 2000;408:92-6.

43. Pak O, Janssen W, Ghofrani HA, Seeger W, Grimminger F, Schermuly RT and Weissmann N. Animal models of pulmonary hypertension: role in translational research. *Drug Discovery Today: Disease Models*. 2010;7:89-97.

44. Stenmark KR, Meyrick B, Galie N, Mooi WJ and McMurtry IF. Animal models of pulmonary arterial hypertension: the hope for etiological discovery and pharmacological cure. *American journal of physiology Lung cellular and molecular physiology*. 2009;297:L1013-32.

45. Lalich JJ and Merkow L. Pulmonary arteritis produced in rat by feeding Crotalaria spectabilis. *Laboratory investigation; a journal of technical methods and pathology*. 1961;10:744-50.

46. Reid MJ, Lamé MW, Morin D, Wilson DW and Segall HJ. Monocrotaline metabolism and distribution in Fisher 344 and Sprague-Dawley rats. *Comparative biochemistry and physiology Part B, Biochemistry & molecular biology*. 1997;117:115-23.

47. Reid MJ, Lamé MW, Morin D, Wilson DW and Segall HJ. Involvement of cytochrome P450 3A in the metabolism and covalent binding of 14C-monocrotaline in rat liver microsomes. *Journal of biochemical and molecular toxicology*. 1998;12:157-66.

48. Nogueira-Ferreira R, Vitorino R, Ferreira R and Henriques-Coelho T. Exploring the monocrotaline animal model for the study of pulmonary arterial hypertension: A network approach. *Pulmonary pharmacology & therapeutics*. 2015;35:8-16.

49. Simonneau G, Robbins IM, Beghetti M, Channick RN, Delcroix M, Denton CP, Elliott CG, Gaine SP, Gladwin MT, Jing ZC, Krowka MJ, Langleben D, Nakanishi N and Souza R. Updated clinical classification of pulmonary hypertension. *Journal of the American College of Cardiology*. 2009;54:S43-s54.

50. Singh N, Dorfmüller P, Shlobin OA and Ventetuolo CE. Group 3 pulmonary hypertension: from bench to bedside. *Circulation research*. 2022;130:1404-1422.

51. McGettrick M and Peacock A. Group 3 pulmonary hypertension: challenges and opportunities. *Global cardiology science & practice*. 2020;2020:e202006.

52. Prins KW, Rose L, Archer SL, Pritzker M, Weir EK, Kazmirczak F, Misialek JR and Thenappan T. Disproportionate right ventricular dysfunction and poor survival in group 3 pulmonary hypertension. *American journal of respiratory and critical care medicine*. 2018;197:1496-1499.

53. Wilkins MR, Ghofrani HA, Weissmann N, Aldashev A and Zhao L. Pathophysiology and treatment of high-altitude pulmonary vascular disease. *Circulation*. 2015;131:582-90.

54. Elwing J and Panos RJ. Pulmonary hypertension associated with COPD. *International journal of chronic obstructive pulmonary disease*. 2008;3:55-70.

55. Mannino DM. COPD: epidemiology, prevalence, morbidity and mortality, and disease heterogeneity. *Chest*. 2002;121:121s-126s.

56. West JB. The physiologic basis of high-altitude diseases. *Annals of internal medicine*. 2004;141:789-800.

57. Sommer N, Dietrich A, Schermuly RT, Ghofrani HA, Gudermann T, Schulz R, Seeger W, Grimminger F and Weissmann N. Regulation of hypoxic pulmonary vasoconstriction: basic mechanisms. *The European respiratory journal*. 2008;32:1639-51.

58. Myatt L. Control of vascular resistance in the human placenta. *Placenta*. 1992;13:329-41.

59. Campian ME, Hardziyenka M, Michel MC and Tan HL. How valid are animal models to evaluate treatments for pulmonary hypertension? *Naunyn-Schmiedeberg's archives of pharmacology*. 2006;373:391-400.

60. Stenmark KR, Fagan KA and Frid MG. Hypoxia-induced pulmonary vascular remodeling: cellular and molecular mechanisms. *Circulation research*. 2006;99:675-91.

61. Stenmark KR, Gerasimovskaya E, Nemenoff RA and Das M. Hypoxic activation of adventitial fibroblasts: role in vascular remodeling. *Chest*. 2002;122:326s-334s.

62. Weissmann N, Grimminger F and Seeger W. Hypoxia in lung vascular biology and disease. *Cardiovascular research*. 2006;71:618-9.

63. Mittal M, Roth M, König P, Hofmann S, Dony E, Goyal P, Selbitz AC, Schermuly RT, Ghofrani HA, Kwapiszewska G, Kummer W, Klepetko W, Hoda MA, Fink L, Hänze J, Seeger W, Grimminger F, Schmidt HH and Weissmann N. Hypoxia-dependent regulation of nonphagocytic NADPH oxidase subunit NOX4 in the pulmonary vasculature. *Circulation research*. 2007;101:258-67.

64. Schermuly RT, Stasch JP, Pullamsetti SS, Middendorff R, Müller D, Schlüter KD, Dingendorf A, Hackemack S, Kolosionek E, Kaulen C, Dumitrascu R, Weissmann N, Mittendorf J, Klepetko W, Seeger W, Ghofrani HA and Grimminger F. Expression and function of soluble guanylate cyclase in pulmonary arterial hypertension. *The European respiratory journal*. 2008;32:881-91.

65. Schermuly RT, Pullamsetti SS, Kwapiszewska G, Dumitrascu R, Tian X, Weissmann N, Ghofrani HA, Kaulen C, Dunkern T, Schudt C, Voswinckel R, Zhou J, Samidurai A, Klepetko W, Paddenberg R, Kummer W, Seeger W and Grimminger F. Phosphodiesterase 1 upregulation in pulmonary arterial hypertension: target for reverse-remodeling therapy. *Circulation*. 2007;115:2331-9.

66. Dresdale DT, Schultz M and Michtom RJ. Primary pulmonary hypertension. I. Clinical and hemodynamic study. *The American journal of medicine*. 1951;11:686-705.

67. Sutendra G and Michelakis ED. The metabolic basis of pulmonary arterial hypertension. *Cell metabolism*. 2014;19:558-73.

68. Paulin R and Michelakis ED. The metabolic theory of pulmonary arterial hypertension. *Circulation research*. 2014;115:148-64.

69. Harvey LD and Chan SY. Emerging metabolic therapies in pulmonary arterial hypertension. *Journal of clinical medicine*. 2017;6.

70. Chan SY and Rubin LJ. Metabolic dysfunction in pulmonary hypertension: from basic science to clinical practice. *European respiratory review : an official journal of the European Respiratory Society*. 2017;26.

71. Bradley EA and Bradley D. Pulmonary arterial hypertension and insulin resistance. *Journal of molecular and genetic medicine: an international journal of biomedical research*. 2014;2.

72. Zamanian RT, Hansmann G, Snook S, Lilienfeld D, Rappaport KM, Reaven GM, Rabinovitch M and Doyle RL. Insulin resistance in pulmonary arterial hypertension. *The European respiratory journal*. 2009;33:318-24.

73. West J, Niswender KD, Johnson JA, Pugh ME, Gleaves L, Fessel JP and Hemnes AR. A potential role for insulin resistance in experimental pulmonary hypertension. *The European respiratory journal*. 2013;41:861-71.

74. Pearce EL, Poffenberger MC, Chang CH and Jones RG. Fueling immunity: insights into metabolism and lymphocyte function. *Science*. 2013;342:1242454.

75. Devaraj S and Jialal I. Dysfunctional endothelial progenitor cells in metabolic syndrome. *Experimental diabetes research*. 2012;2012:585018.

76. Weir EK, López-Barneo J, Buckler KJ and Archer SL. Acute oxygen-sensing mechanisms. *The New England journal of medicine*. 2005;353:2042-55.

77. Ward PS and Thompson CB. Metabolic reprogramming: a cancer hallmark even warburg did not anticipate. *Cancer cell*. 2012;21:297-308.

78. Dromparis P and Michelakis ED. Mitochondria in vascular health and disease. *Annual review of physiology*. 2013;75:95-126.

79. Dromparis P, Paulin R, Stenson TH, Haromy A, Sutendra G and Michelakis ED. Attenuating endoplasmic reticulum stress as a novel therapeutic strategy in pulmonary hypertension. *Circulation*. 2013;127:115-25.

80. Dromparis P, Sutendra G and Michelakis ED. The role of mitochondria in pulmonary vascular remodeling. *Journal of molecular medicine*. 2010;88:1003-10.

81. Stacpoole PW. Therapeutic targeting of the pyruvate dehydrogenase complex/pyruvate dehydrogenase kinase (PDC/PDK) axis in cancer. *Journal of the National Cancer Institute.* 2017;109.

82. Woolbright BL, Rajendran G, Harris RA and Taylor JA, 3rd. Metabolic flexibility in cancer: targeting the pyruvate dehydrogenase kinase: pyruvate dehydrogenase axis. *Molecular cancer therapeutics*. 2019;18:1673-1681.

83. Semenza GL. Hypoxia-inducible factors in physiology and medicine. *Cell*. 2012;148:399-408.

84. Kim JW, Tchernyshyov I, Semenza GL and Dang CV. HIF-1-mediated expression of pyruvate dehydrogenase kinase: a metabolic switch required for cellular adaptation to hypoxia. *Cell metabolism*. 2006;3:177-85.

85. Papandreou I, Cairns RA, Fontana L, Lim AL and Denko NC. HIF-1 mediates adaptation to hypoxia by actively downregulating mitochondrial oxygen consumption. *Cell metabolism*. 2006;3:187-97.

86. Michelakis ED, McMurtry MS, Wu XC, Dyck JR, Moudgil R, Hopkins TA, Lopaschuk GD, Puttagunta L, Waite R and Archer SL. Dichloroacetate, a metabolic modulator, prevents and reverses chronic hypoxic pulmonary hypertension in rats: role of increased expression and activity of voltage-gated potassium channels. *Circulation*. 2002;105:244-50.

87. McMurtry MS, Bonnet S, Wu X, Dyck JR, Haromy A, Hashimoto K and Michelakis ED. Dichloroacetate prevents and reverses pulmonary hypertension by inducing pulmonary artery smooth muscle cell apoptosis. *Circulation research*. 2004;95:830-40.

88. Rizzuto R, Duchen MR and Pozzan T. Flirting in little space: the ER/mitochondria Ca_2^+ liaison. *Science's STKE: signal transduction knowledge environment*. 2004;2004:1.

89. Szabadkai G and Duchen MR. Mitochondria: the hub of cellular Ca_2^+ signaling. *Physiology*. 2008;23:84-94.

90. Simoneau JA and Kelley DE. Altered glycolytic and oxidative capacities of skeletal muscle contribute to insulin resistance in NIDDM. *Journal of applied physiology*. 1997;83:166-71.

91. Flamment M, Hajduch E, Ferré P and Foufelle F. New insights into ER stress-induced insulin resistance. *Trends in endocrinology and metabolism*. 2012;23:381-90.

92. Piao L, Fang YH, Cadete VJ, Wietholt C, Urboniene D, Toth PT, Marsboom G, Zhang HJ, Haber I, Rehman J, Lopaschuk GD and Archer SL. The inhibition of pyruvate dehydrogenase kinase improves impaired cardiac function and electrical remodeling in two models of right ventricular hypertrophy: resuscitating the hibernating right ventricle. *Journal of molecular medicine*. 2010;88:47-60.

93. Liu D, Qin S, Su D, Wang K, Huang Y, Huang Y and Pang Y. Metabolic reprogramming of the right ventricle and pulmonary arteries in a flow-associated pulmonary arterial hypertension rat model. *ACS omega*. 2022;7:1273-1287.

94. Fang YH, Piao L, Hong Z, Toth PT, Marsboom G, Bache-Wiig P, Rehman J and Archer SL. Therapeutic inhibition of fatty acid oxidation in right ventricular hypertrophy: exploiting Randle's cycle. *Journal of molecular medicine*. 2012;90:31-43.

95. Shi LZ, Wang R, Huang G, Vogel P, Neale G, Green DR and Chi H. HIF1alpha-dependent glycolytic pathway orchestrates a metabolic checkpoint for the differentiation of TH17 and Treg cells. *The Journal of experimental medicine*. 2011;208:1367-76.

96. Lunt SY and Vander Heiden MG. Aerobic glycolysis: meeting the metabolic requirements of cell proliferation. *Annual review of cell and developmental biology*. 2011;27:441-64.

97. Lenna S, Farina AG, Martyanov V, Christmann RB, Wood TA, Farber HW, Scorza R, Whitfield ML, Lafyatis R and Trojanowska M. Increased expression of endoplasmic reticulum stress and unfolded protein response genes in peripheral blood mononuclear cells from patients with limited cutaneous systemic sclerosis and pulmonary arterial hypertension. *Arthritis and rheumatism*. 2013;65:1357-66.

98. Xu W, Koeck T, Lara AR, Neumann D, DiFilippo FP, Koo M, Janocha AJ, Masri FA, Arroliga AC, Jennings C, Dweik RA, Tuder RM, Stuehr DJ and Erzurum SC. Alterations of cellular bioenergetics in pulmonary artery endothelial cells. *Proceedings of the National Academy of Sciences of the United States of America*. 2007;104:1342-7.

99. Warburg O, Wind F and Negelein E. The metabolism of tumors in the body. *The Journal of general physiology*. 1927;8:519-30.

100. Pasteur L. Mémoire sur la fermentation appelée lactique (Extrait par l'auteur). *Molecular Medicine*. 1995;1:599-601.

101. Vaupel P and Multhoff G. Revisiting the Warburg effect: historical dogma versus current understanding. *The Journal of physiology*. 2021;599:1745-1757.

102. DeBerardinis RJ and Chandel NS. We need to talk about the Warburg effect. *Nature metabolism*. 2020;2:127-129.

103. Pokharel MD, Marciano DP, Fu P, Franco MC, Unwalla H, Tieu K, Fineman JR, Wang T and Black SM. Metabolic reprogramming, oxidative stress, and pulmonary hypertension. *Redox biology*. 2023;64:102797.

104. Abdel-Haleem AM, Lewis NE, Jamshidi N, Mineta K, Gao X and Gojobori T. The emerging facets of non-cancerous Warburg effect. *Frontiers in endocrinology*. 2017;8:279.

105. Sun H, Chen L, Cao S, Liang Y and Xu Y. Warburg effects in cancer and normal proliferating cells: two tales of the same name. *Genomics, proteomics & bioinformatics*. 2019;17:273-286.

106. Frost SC, McKenna R. Carbonic anhydrase: mechanism, regulation, links to disease, and industrial applications. *Ohio Library and Information Network.* 2014.

107. Forster RE. Remarks on the discovery of carbonic anhydrase. *Experientia Supplementum*. 2000:1-11.

108. Mishra CB, Tiwari M and Supuran CT. Progress in the development of human carbonic anhydrase inhibitors and their pharmacological applications: Where are we today? *Medicinal research reviews*. 2020;40:2485-2565.

109. Lindskog S and Silverman DN. The catalytic mechanism of mammalian carbonic anhydrases. *Experientia Supplementum*. 2000:175-95.

110. Imtaiyaz Hassan M, Shajee B, Waheed A, Ahmad F and Sly WS. Structure, function and applications of carbonic anhydrase isozymes. *Bioorganic & medicinal chemistry*. 2013;21:1570-82.

111. Frost SC. Physiological functions of the alpha class of carbonic anhydrases. *Sub-cellular biochemistry*. 2014;75:9-30.

112. Chiche J, Ilc K, Brahimi-Horn MC and Pouysségur J. Membrane-bound carbonic anhydrases are key pH regulators controlling tumor growth and cell migration. *Advances in enzyme regulation*. 2010;50:20-33.

113. Pastorekova S and Gillies RJ. The role of carbonic anhydrase IX in cancer development: links to hypoxia, acidosis, and beyond. *Cancer metastasis reviews*. 2019;38:65-77.

114. Pastorek J and Pastorekova S. Hypoxia-induced carbonic anhydrase IX as a target for cancer therapy: from biology to clinical use. *Seminars in cancer biology*. 2015;31:52-64.

115. Supuran CT. Carbonic anhydrases: novel therapeutic applications for inhibitors and activators. *Nature reviews Drug discovery*. 2008;7:168-81.

116. Hsieh MJ, Chen KS, Chiou HL and Hsieh YS. Carbonic anhydrase XII promotes invasion and migration ability of MDA-MB-231 breast cancer cells through the p38 MAPK signaling pathway. *European journal of cell biology*. 2010;89:598-606.

117. Lounnas N, Rosilio C, Nebout M, Mary D, Griessinger E, Neffati Z, Chiche J, Spits H, Hagenbeek TJ, Asnafi V, Poulsen SA, Supuran CT, Peyron JF and Imbert V. Pharmacological inhibition of carbonic anhydrase XII interferes with cell proliferation and induces cell apoptosis in T-cell lymphomas. *Cancer letters*. 2013;333:76-88.

118. Daunys S and Petrikaitė V. The roles of carbonic anhydrases IX and XII in cancer cell adhesion, migration, invasion and metastasis. *Biology of the cell*. 2020;112:383-397.

119. Swietach P, Vaughan-Jones RD and Harris AL. Regulation of tumor pH and the role of carbonic anhydrase 9. *Cancer metastasis reviews*. 2007;26:299-310.

120. Chiche J, Brahimi-Horn MC and Pouysségur J. Tumour hypoxia induces a metabolic shift causing acidosis: a common feature in cancer. *Journal of cellular and molecular medicine*. 2010;14:771-94.

121. Becker HM. Carbonic anhydrase IX and acid transport in cancer. *British journal of cancer*. 2020;122:157-167.

122. Corbet C and Feron O. Tumour acidosis: from the passenger to the driver's seat. *Nature reviews Cancer*. 2017;17:577-593.

123. Benej M, Pastorekova S and Pastorek J. Carbonic anhydrase IX: regulation and role in cancer. *Subcellular biochemistry*. 2014;75:199-219.

124. Zamanova S, Shabana AM, Mondal UK and Ilies MA. Carbonic anhydrases as disease markers. *Expert opinion on therapeutic patents*. 2019;29:509-533.

125. Nocentini A and Supuran CT. Carbonic anhydrase inhibitors as antitumor/antimetastatic agents: a patent review (2008-2018). *Expert opinion on therapeutic patents*. 2018;28:729-740.

126. Gut MO, Parkkila S, Vernerová Z, Rohde E, Závada J, Höcker M, Pastorek J, Karttunen T, Gibadulinová A, Závadová Z, Knobeloch KP, Wiedenmann B, Svoboda J, Horak I and Pastoreková S. Gastric hyperplasia in mice with targeted disruption of the carbonic anhydrase gene Car9. *Gastroenterology*. 2002;123:1889-903.

127. Leppilampi M, Karttunen TJ, Kivelä J, Gut MO, Pastoreková S, Pastorek J and Parkkila S. Gastric pit cell hyperplasia and glandular atrophy in carbonic anhydrase IX knockout mice: studies on two strains C57/BL6 and BALB/C. *Transgenic research*. 2005;14:655-63.

128. Opavský R, Pastoreková S, Zelník V, Gibadulinová A, Stanbridge EJ, Závada J, Kettmann R and Pastorek J. Human MN/CA9 gene, a novel member of the carbonic anhydrase family: structure and exon to protein domain relationships. *Genomics*. 1996;33:480-7.

129. Nakagawa Y, Uemura H, Hirao Y, Yoshida K, Saga S and Yoshikawa K. Radiation hybrid mapping of the human MN/CA9 locus to chromosome band 9p12-p13. *Genomics*. 1998;53:118-9.

130. Kciuk M, Gielecińska A, Mujwar S, Mojzych M, Marciniak B, Drozda R and Kontek R. Targeting carbonic anhydrase IX and XII isoforms with small molecule inhibitors and monoclonal antibodies. *Journal of enzyme inhibition and medicinal chemistry*. 2022;37:1278-1298.

131. Waheed A and Sly WS. Carbonic anhydrase XII functions in health and disease. *Gene*. 2017;623:33-40.

132. Kaluz S, Kaluzová M, Liao SY, Lerman M and Stanbridge EJ. Transcriptional control of the tumor- and hypoxia-marker carbonic anhydrase 9: A one transcription factor (HIF-1) show? *Biochimica et biophysica acta*. 2009;1795:162-72.

133. Wykoff CC, Beasley NJ, Watson PH, Turner KJ, Pastorek J, Sibtain A, Wilson GD, Turley H, Talks KL, Maxwell PH, Pugh CW, Ratcliffe PJ and Harris AL. Hypoxia-inducible expression of tumor-associated carbonic anhydrases. *Cancer research*. 2000;60:7075-83.

134. Kaluz S, Kaluzová M and Stanbridge EJ. Rational design of minimal hypoxia-inducible enhancers. *Biochemical and biophysical research communications*. 2008;370:613-8.

135. Kaluz S, Kaluzová M, Opavský R, Pastoreková S, Gibadulinová A, Dequiedt F, Kettmann R and Pastorek J. Transcriptional regulation of the MN/CA 9 gene coding for the tumor-associated

carbonic anhydrase IX. Identification and characterization of a proximal silencer element. *The Journal of biological chemistry*. 1999;274:32588-95.

136. Kaluz S, Kaluzová M and Stanbridge EJ. Expression of the hypoxia marker carbonic anhydrase IX is critically dependent on SP1 activity. Identification of a novel type of hypoxia-responsive enhancer. *Cancer research*. 2003;63:917-22.

137. Kaluzová M, Pastoreková S, Svastová E, Pastorek J, Stanbridge EJ and Kaluz S. Characterization of the MN/CA 9 promoter proximal region: a role for specificity protein (SP) and activator protein 1 (AP1) factors. *The Biochemical journal*. 2001;359:669-77.

138. Lau KW, Tian YM, Raval RR, Ratcliffe PJ and Pugh CW. Target gene selectivity of hypoxia-inducible factor-alpha in renal cancer cells is conveyed by post-DNA-binding mechanisms. *British journal of cancer*. 2007;96:1284-92.

139. Kaluz S, Kaluzová M, Chrastina A, Olive PL, Pastoreková S, Pastorek J, Lerman MI and Stanbridge EJ. Lowered oxygen tension induces expression of the hypoxia marker MN/carbonic anhydrase IX in the absence of hypoxia-inducible factor 1 alpha stabilization: a role for phosphatidylinositol 3'-kinase. *Cancer research*. 2002;62:4469-77.

140. Ihnatko R, Kubes M, Takacova M, Sedlakova O, Sedlak J, Pastorek J, Kopacek J and Pastorekova S. Extracellular acidosis elevates carbonic anhydrase IX in human glioblastoma cells via transcriptional modulation that does not depend on hypoxia. *International journal of oncology*. 2006;29:1025-33.

141. Yildirim H and Köçkar F. TGF-beta upregulates tumor-associated carbonic anhydrase IX gene expression in Hep3B cells. *Cell biology international*. 2009;33:1002-7.

142. Haddad JJ and Harb HL. Cytokines and the regulation of hypoxia-inducible factor (HIF)-1alpha. *International immunopharmacology*. 2005;5:461-83.

143. Stiehl DP, Jelkmann W, Wenger RH and Hellwig-Bürgel T. Normoxic induction of the hypoxia-inducible factor 1alpha by insulin and interleukin-1beta involves the phosphatidylinositol 3-kinase pathway. *FEBS letters*. 2002;512:157-62.

144. Kockar F, Yildrim H, Sagkan RI, Hagemann C, Soysal Y, Anacker J, Hamza AA, Vordermark D, Flentje M and Said HM. Hypoxia and cytokines regulate carbonic anhydrase 9 expression in hepatocellular carcinoma cells in vitro. *World journal of clinical oncology*. 2012;3:82-91.

145. Barathova M, Takacova M, Holotnakova T, Gibadulinova A, Ohradanova A, Zatovicova M, Hulikova A, Kopacek J, Parkkila S, Supuran CT, Pastorekova S and Pastorek J. Alternative splicing variant of the hypoxia marker carbonic anhydrase IX expressed independently of hypoxia and tumour phenotype. *British journal of cancer*. 2008;98:129-36.

146. Ditte P, Dequiedt F, Svastova E, Hulikova A, Ohradanova-Repic A, Zatovicova M, Csaderova L, Kopacek J, Supuran CT, Pastorekova S and Pastorek J. Phosphorylation of carbonic anhydrase IX

controls its ability to mediate extracellular acidification in hypoxic tumors. *Cancer research*. 2011;71:7558-67.

147. Christianson HC, Menard JA, Indira Chandran V, Bourseau-Guilmain E, Shevela D, Lidfeldt J, Månsson AS, Pastorekova S, Messinger J and Belting M. Tumor antigen glycosaminoglycan modification regulates antibody-drug conjugate delivery and cytotoxicity. *Oncotarget*. 2017;8:66960-66974.

148. Pastorek J, Pastoreková S, Callebaut I, Mornon JP, Zelník V, Opavský R, Zat'ovicová M, Liao S, Portetelle D, Stanbridge EJ and et al. Cloning and characterization of MN, a human tumor-associated protein with a domain homologous to carbonic anhydrase and a putative helix-loop-helix DNA binding segment. *Oncogene*. 1994;9:2877-88.

149. Di Fiore A, Supuran CT, Scaloni A and De Simone G. Human carbonic anhydrases and post-translational modifications: a hidden world possibly affecting protein properties and functions. *Journal of enzyme inhibition and medicinal chemistry*. 2020;35:1450-1461.

150. Zatovicova M, Sedlakova O, Svastova E, Ohradanova A, Ciampor F, Arribas J, Pastorek J and Pastorekova S. Ectodomain shedding of the hypoxia-induced carbonic anhydrase IX is a metalloprotease-dependent process regulated by TACE/ADAM17. *British journal of cancer*. 2005;93:1267-76.

151. Zatovicova M, Kajanova I, Takacova M, Jelenska L, Sedlakova O, Labudova M and Pastorekova S. ADAM10 mediates shedding of carbonic anhydrase IX ectodomain non‐redundantly to ADAM17. *Oncology reports*. 2023;49.

152. Ilie M, Mazure NM, Hofman V, Ammadi RE, Ortholan C, Bonnetaud C, Havet K, Venissac N, Mograbi B, Mouroux J, Pouysségur J and Hofman P. High levels of carbonic anhydrase IX in tumour tissue and plasma are biomarkers of poor prognostic in patients with non-small cell lung cancer. *British journal of cancer*. 2010;102:1627-35.

153. Ostheimer C, Bache M, Güttler A, Kotzsch M and Vordermark D. A pilot study on potential plasma hypoxia markers in the radiotherapy of non-small cell lung cancer. Osteopontin, carbonic anhydrase IX and vascular endothelial growth factor. *Strahlentherapie und Onkologie*. 2014;190:276-82.

154. Schütze D, Milde-Langosch K, Witzel I, Rody A, Karn T, Schmidt M, Choschzick M, Jänicke F and Müller V. Relevance of cellular and serum carbonic anhydrase IX in primary breast cancer. *Journal of cancer research and clinical oncology*. 2013;139:747-54.

155. Brown-Glaberman U, Marron M, Chalasani P, Livingston R, Iannone M, Specht J and Stopeck AT. Circulating carbonic anhydrase IX and antiangiogenic therapy in breast cancer. *Disease markers*. 2016;2016:9810383.

156. Rosenberg V, Pastorekova S, Zatovicova M, Vidlickova I, Jelenska L and Slezak P. High serum carbonic anhydrase IX predicts shorter survival in head and neck cancer. *Bratislavske lekarske listy*. 2016;117:201-4.

157. Kalavska K, Chovanec M, Zatovicova M, Takacova M, Gronesova P, Svetlovska D, Baratova M, Miskovska V, Obertova J, Palacka P, Rajec J, Sycova-Mila Z, Cierna Z, Kajo K, Spanik S, Babal P, Mardiak J, Pastorekova S and Mego M. Prognostic value of serum carbonic anhydrase IX in testicular germ cell tumor patients. *Oncology letters*. 2016;12:2590-2598.

158. Woelber L, Mueller V, Eulenburg C, Schwarz J, Carney W, Jaenicke F, Milde-Langosch K and Mahner S. Serum carbonic anhydrase IX during first-line therapy of ovarian cancer. *Gynecologic oncology*. 2010;117:183-8.

159. Kock L, Mahner S, Choschzick M, Eulenburg C, Milde-Langosch K, Schwarz J, Jaenicke F, Müller V and Woelber L. Serum carbonic anhydrase IX and its prognostic relevance in vulvar cancer. *International journal of gynecological cancer*. 2011;21:141-8.

160. Hektoen HH, Flatmark K, Andersson Y, Dueland S, Redalen KR and Ree AH. Early increase in circulating carbonic anhydrase IX during neoadjuvant treatment predicts favourable outcome in locally advanced rectal cancer. *BMC cancer*. 2015;15:543.

161. Woelber L, Kress K, Kersten JF, Choschzick M, Kilic E, Herwig U, Lindner C, Schwarz J, Jaenicke F, Mahner S, Milde-Langosch K, Mueller V and Ihnen M. Carbonic anhydrase IX in tumor tissue and sera of patients with primary cervical cancer. *BMC cancer*. 2011;11:12.

162. Finkelmeier F, Canli Ö, Peiffer KH, Walter D, Tal A, Koch C, Pession U, Vermehren J, Trojan J, Zeuzem S, Piiper A, Greten FR, Grammatikos G and Waidmann O. Circulating hypoxia marker carbonic anhydrase IX (CA9) in patients with hepatocellular carcinoma and patients with cirrhosis. *PLOS one*. 2018;13:e0200855.

163. Fidan E, Mentese A, Ozdemir F, Deger O, Kavgaci H, Caner Karahan S and Aydin F. Diagnostic and prognostic significance of CA IX and suPAR in gastric cancer. *Medical oncology*. 2013;30:540.

164. Yang JS, Chen MK, Yang SF, Chang YC, Su SC, Chiou HL, Chien MH and Lin CW. Increased expression of carbonic anhydrase IX in oral submucous fibrosis and oral squamous cell carcinoma. *Clinical chemistry and laboratory medicine*. 2014;52:1367-77.

165. Smith AD, Truong M, Bristow R, Yip P, Milosevic MF and Joshua AM. The utility of serum CA9 for prognostication in prostate cancer. *Anticancer research*. 2016;36:4489-92.

166. Zhou GX, Ireland J, Rayman P, Finke J and Zhou M. Quantification of carbonic anhydrase IX expression in serum and tissue of renal cell carcinoma patients using enzyme-linked immunosorbent assay: prognostic and diagnostic potentials. *Urology*. 2010;75:257-61.

167. Takacova M, Bartosova M, Skvarkova L, Zatovicova M, Vidlickova I, Csaderova L, Barathova M, Breza J, Jr., Bujdak P, Pastorek J, Breza J, Sr. and Pastorekova S. Carbonic anhydrase IX is a clinically significant tissue and serum biomarker associated with renal cell carcinoma. *Oncology letters*. 2013;5:191-197.

168. Mahon BP, Pinard MA and McKenna R. Targeting carbonic anhydrase IX activity and expression. *Molecules*. 2015;20:2323-48.

169. Chamie K, Donin NM, Klöpfer P, Bevan P, Fall B, Wilhelm O, Störkel S, Said J, Gambla M, Hawkins RE, Jankilevich G, Kapoor A, Kopyltsov E, Staehler M, Taari K, Wainstein AJA, Pantuck AJ and Belldegrun AS. Adjuvant weekly girentuximab following nephrectomy for high-risk renal cell carcinoma: The ARISER randomized clinical trial. *JAMA oncology*. 2017;3:913-920.

170. Siebels M, Rohrmann K, Oberneder R, Stahler M, Haseke N, Beck J, Hofmann R, Kindler M, Kloepfer P and Stief C. A clinical phase I/II trial with the monoclonal antibody cG250 (RENCAREX®) and interferon-alpha-2a in metastatic renal cell carcinoma patients. *World journal of urology*. 2011;29:121-6.

171. Davis ID, Liu Z, Saunders W, Lee FT, Spirkoska V, Hopkins W, Smyth FE, Chong G, Papenfuss AT, Chappell B, Poon A, Saunder TH, Hoffman EW, Old LJ and Scott AM. A pilot study of monoclonal antibody cG250 and low dose subcutaneous IL-2 in patients with advanced renal cell carcinoma. *Cancer immunity*. 2007;7:14.

172. Lou Y, McDonald PC, Oloumi A, Chia S, Ostlund C, Ahmadi A, Kyle A, Auf dem Keller U, Leung S, Huntsman D, Clarke B, Sutherland BW, Waterhouse D, Bally M, Roskelley C, Overall CM, Minchinton A, Pacchiano F, Carta F, Scozzafava A, Touisni N, Winum JY, Supuran CT and Dedhar S. Targeting tumor hypoxia: suppression of breast tumor growth and metastasis by novel carbonic anhydrase IX inhibitors. *Cancer research*. 2011;71:3364-76.

173. Pacchiano F, Carta F, McDonald PC, Lou Y, Vullo D, Scozzafava A, Dedhar S and Supuran CT. Ureido-substituted benzenesulfonamides potently inhibit carbonic anhydrase IX and show antimetastatic activity in a model of breast cancer metastasis. *Journal of medicinal chemistry*. 2011;54:1896-902.

174. McDonald PC, Chia S, Bedard PL, Chu Q, Lyle M, Tang L, Singh M, Zhang Z, Supuran CT, Renouf DJ and Dedhar S. A Phase 1 Study of SLC-0111, a Novel inhibitor of carbonic anhydrase IX, in patients with advanced solid tumors. *American journal of clinical oncology*. 2020;43:484-490.

175. Gieling RG, Babur M, Mamnani L, Burrows N, Telfer BA, Carta F, Winum JY, Scozzafava A, Supuran CT and Williams KJ. Antimetastatic effect of sulfamate carbonic anhydrase IX inhibitors in breast carcinoma xenografts. *Journal of medicinal chemistry*. 2012;55:5591-600.

176. Bryant JL, Gieling RG, Meredith SL, Allen TJ, Walker L, Telfer BA, Supuran CT, Williams KJ and White A. Novel carbonic anhydrase IX-targeted therapy enhances the anti-tumour effects of cisplatin in small cell lung cancer. *International journal of cancer*. 2018;142:191-201.

177. Gul HI, Kucukoglu K, Yamali C, Bilginer S, Yuca H, Ozturk I, Taslimi P, Gulcin I and Supuran CT. Synthesis of 4-(2-substituted hydrazinyl)benzenesulfonamides and their carbonic anhydrase inhibitory effects. *Journal of enzyme inhibition and medicinal chemistry*. 2016;31:568-73.

178. Casey JR, Grinstein S and Orlowski J. Sensors and regulators of intracellular pH. *Nature reviews Molecular cell biology*. 2010;11:50-61.

179. Cox S and Taylor SS. Kinetic analysis of cAMP-dependent protein kinase: mutations at histidine 87 affect peptide binding and pH dependence. *Biochemistry*. 1995;34:16203-9.

180. Yahuaca P, Ek-Vitorin JF, Rush P, Delmar M and Taffet SM. Identification of a protein kinase activity that phosphorylates connexin43 in a pH-dependent manner. *Brazilian journal of medical and biological research*. 2000;33:399-406.

181. Erecińska M, Deas J and Silver IA. The effect of pH on glycolysis and phosphofructokinase activity in cultured cells and synaptosomes. *Journal of neurochemistry*. 1995;65:2765-72.

182. Mansour TE and Ahlfors CE. Studies on heart phosphofructokinase. Some kinetic and physical properties of the crystalline enzyme. *The Journal of biological chemistry*. 1968;243:2523-33.

183. Becker HM and Deitmer JW. Transport metabolons and acid/base balance in tumor cells. *Cancers*. 2020;12.

184. Fijalkowska I, Xu W, Comhair SA, Janocha AJ, Mavrakis LA, Krishnamachary B, Zhen L, Mao T, Richter A, Erzurum SC and Tuder RM. Hypoxia inducible-factor1alpha regulates the metabolic shift of pulmonary hypertensive endothelial cells. *The American journal of pathology*. 2010;176:1130-8.

185. Hudalla H, Michael Z, Christodoulou N, Willis GR, Fernandez-Gonzalez A, Filatava EJ, Dieffenbach P, Fredenburgh LE, Stearman RS, Geraci MW, Kourembanas S and Christou H. Carbonic anhydrase inhibition ameliorates inflammation and experimental pulmonary hypertension. *American journal of respiratory cell and molecular biology*. 2019;61:512-524.

186. Deem S, Hedges RG, Kerr ME and Swenson ER. Acetazolamide reduces hypoxic pulmonary vasoconstriction in isolated perfused rabbit lungs. *Respiration physiology*. 2000;123:109-19.

187. Höhne C, Krebs MO, Seiferheld M, Boemke W, Kaczmarczyk G and Swenson ER. Acetazolamide prevents hypoxic pulmonary vasoconstriction in conscious dogs. *Journal of applied physiology*. 2004;97:515-21.

188. Pichon A, Connes P, Quidu P, Marchant D, Brunet J, Levy BI, Vilar J, Safeukui I, Cymbalista F, Maignan M, Richalet JP and Favret F. Acetazolamide and chronic hypoxia: effects on haemorheology and pulmonary haemodynamics. *The European respiratory journal*. 2012;40:1401-9.

189. Höhne C, Pickerodt PA, Francis RC, Boemke W and Swenson ER. Pulmonary vasodilation by acetazolamide during hypoxia is unrelated to carbonic anhydrase inhibition. *American journal of physiology Lung cellular and molecular physiology*. 2007;292:L178-84.

190. Shimoda LA, Luke T, Sylvester JT, Shih HW, Jain A and Swenson ER. Inhibition of hypoxia-induced calcium responses in pulmonary arterial smooth muscle by acetazolamide is independent of carbonic anhydrase inhibition. *American journal of physiology Lung cellular and molecular physiology*. 2007;292:L1002-12.

191. Shukralla AA, Dolan E and Delanty N. Acetazolamide: Old drug, new evidence? *Epilepsia open*. 2022;7:378-392.

192. Dahal BK, Kosanovic D, Pamarthi PK, Sydykov A, Lai YJ, Kast R, Schirok H, Stasch JP, Ghofrani HA, Weissmann N, Grimminger F, Seeger W and Schermuly RT. Therapeutic efficacy of azaindole-1 in experimental pulmonary hypertension. *The European respiratory journal*. 2010;36:808-18.

193. Dahal BK, Cornitescu T, Tretyn A, Pullamsetti SS, Kosanovic D, Dumitrascu R, Ghofrani HA, Weissmann N, Voswinckel R, Banat GA, Seeger W, Grimminger F and Schermuly RT. Role of epidermal growth factor inhibition in experimental pulmonary hypertension. *American journal of respiratory and critical care medicine*. 2010;181:158-67.

194. Sommer N, Alebrahimdehkordi N, Pak O, Knoepp F, Strielkov I, Scheibe S, Dufour E, Andjelković A, Sydykov A, Saraji A, Petrovic A, Quanz K, Hecker M, Kumar M, Wahl J, Kraut S, Seeger W, Schermuly RT, Ghofrani HA, Ramser K, Braun T, Jacobs HT, Weissmann N and Szibor M. Bypassing mitochondrial complex III using alternative oxidase inhibits acute pulmonary oxygen sensing. *Science advances*. 2020;6:eaba0694.

195. Veith C, Vartürk-Özcan I, Wujak M, Hadzic S, Wu CY, Knoepp F, Kraut S, Petrovic A, Gredic M, Pak O, Brosien M, Heimbrodt M, Wilhelm J, Weisel FC, Malkmus K, Schäfer K, Gall H, Tello K, Kosanovic D, Sydykov A, Sarybaev A, Günther A, Brandes RP, Seeger W, Grimminger F, Ghofrani HA, Schermuly RT, Kwapiszewska G, Sommer N and Weissmann N. SPARC, a novel regulator of vascular cell function in pulmonary hypertension. *Circulation*. 2022;145:916-933.

196. Heitmeier T, Sydykov A, Lukas C, Vroom C, Korfei M, Petrovic A, Klingel K, Günther A, Eickelberg O, Weissmann N, Ghofrani HA, Seeger W, Grimminger F, Schermuly RT, Meiners S and Kosanovic D. Altered proteasome function in right ventricular hypertrophy. *Cardiovascular research*. 2020;116:406-415.

197. Pichl A, Sommer N, Bednorz M, Seimetz M, Hadzic S, Kuhnert S, Kraut S, Roxlau ET, Kojonazarov B, Wilhelm J, Gredic M, Gall H, Tello K, Richter MJ, Pak O, Petrovic A, Hecker M, Schermuly RT, Grimminger F, Seeger W, Ghofrani HA and Weissmann N. Riociguat for treatment of pulmonary hypertension in COPD: a translational study. *The European respiratory journal*. 2019;53.

198. Sydykov A, Luitel H, Mamazhakypov A, Wygrecka M, Pradhan K, Pak O, Petrovic A, Kojonazarov B, Weissmann N, Seeger W, Grimminger F, Ghofrani HA, Kosanovic D and

Schermuly RT. Genetic deficiency and pharmacological stabilization of mast cells ameliorate pressure overload-induced maladaptive right ventricular remodeling in mice. *International journal of molecular sciences*. 2020;21.

199. Mamazhakypov A, Weiß A, Zukunft S, Sydykov A, Kojonazarov B, Wilhelm J, Vroom C, Petrovic A, Kosanovic D, Weissmann N, Seeger W, Fleming I, Iglarz M, Grimminger F, Ghofrani HA, Pullamsetti SS and Schermuly RT. Effects of macitentan and tadalafil monotherapy or their combination on the right ventricle and plasma metabolites in pulmonary hypertensive rats. *Pulmonary circulation*. 2020;10:2045894020947283.

200. Weiss A, Neubauer MC, Yerabolu D, Kojonazarov B, Schlueter BC, Neubert L, Jonigk D, Baal N, Ruppert C, Dorfmuller P, Pullamsetti SS, Weissmann N, Ghofrani HA, Grimminger F, Seeger W and Schermuly RT. Targeting cyclin-dependent kinases for the treatment of pulmonary arterial hypertension. *Nature communications*. 2019;10:2204.

201. Kosanovic D, Luitel H, Dahal BK, Cornitescu T, Janssen W, Danser AH, Garrelds IM, De Mey JG, Fazzi G, Schiffers P, Iglarz M, Fischli W, Ghofrani HA, Weissmann N, Grimminger F, Seeger W, Reiss I and Schermuly RT. Chymase: a multifunctional player in pulmonary hypertension associated with lung fibrosis. *The European respiratory journal*. 2015;46:1084-94.

202. Dahal BK, Kosanovic D, Kaulen C, Cornitescu T, Savai R, Hoffmann J, Reiss I, Ghofrani HA, Weissmann N, Kuebler WM, Seeger W, Grimminger F and Schermuly RT. Involvement of mast cells in monocrotaline-induced pulmonary hypertension in rats. *Respiratory research*. 2011;12:60.

203. Sommer N, Pak O, Schörner S, Derfuss T, Krug A, Gnaiger E, Ghofrani HA, Schermuly RT, Huckstorf C, Seeger W, Grimminger F and Weissmann N. Mitochondrial cytochrome redox states and respiration in acute pulmonary oxygen sensing. *The European respiratory journal*. 2010;36:1056-66.

204. Fink L, Kohlhoff S, Stein MM, Hänze J, Weissmann N, Rose F, Akkayagil E, Manz D, Grimminger F, Seeger W and Bohle RM. cDNA array hybridization after laser-assisted microdissection from nonneoplastic tissue. *The American journal of pathology*. 2002;160:81-90.

205. Tello K, Dalmer A, Axmann J, Vanderpool R, Ghofrani HA, Naeije R, Roller F, Seeger W, Sommer N, Wilhelm J, Gall H and Richter MJ. Reserve of right ventricular-arterial coupling in the setting of chronic overload. *Circulation Heart failure*. 2019;12:e005512.

206. Richter MJ, Peters D, Ghofrani HA, Naeije R, Roller F, Sommer N, Gall H, Grimminger F, Seeger W and Tello K. Evaluation and prognostic relevance of right ventricular-arterial coupling in pulmonary hypertension. *American journal of respiratory and critical care medicine*. 2020;201:116-119.

207. Ivanov S, Liao SY, Ivanova A, Danilkovitch-Miagkova A, Tarasova N, Weirich G, Merrill MJ, Proescholdt MA, Oldfield EH, Lee J, Zavada J, Waheed A, Sly W, Lerman MI and Stanbridge EJ. Expression of hypoxia-inducible cell-surface transmembrane carbonic anhydrases in human cancer. *The American journal of pathology*. 2001;158:905-19.

208. Liao SY, Darcy KM, Randall LM, Tian C, Monk BJ, Burger RA, Fruehauf JP, Peters WA, Stock RJ and Stanbridge EJ. Prognostic relevance of carbonic anhydrase-IX in high-risk, early-stage cervical cancer: a gynecologic oncology group study. *Gynecologic oncology*. 2010;116:452-8.

209. Korkeila E, Talvinen K, Jaakkola PM, Minn H, Syrjänen K, Sundström J and Pyrhönen S. Expression of carbonic anhydrase IX suggests poor outcome in rectal cancer. *British journal of cancer*. 2009;100:874-80.

210. Hussain SA, Ganesan R, Reynolds G, Gross L, Stevens A, Pastorek J, Murray PG, Perunovic B, Anwar MS, Billingham L, James ND, Spooner D, Poole CJ, Rea DW and Palmer DH. Hypoxia-regulated carbonic anhydrase IX expression is associated with poor survival in patients with invasive breast cancer. *British journal of cancer*. 2007;96:104-9.

211. Simi L, Venturini G, Malentacchi F, Gelmini S, Andreani M, Janni A, Pastorekova S, Supuran CT, Pazzagli M and Orlando C. Quantitative analysis of carbonic anhydrase IX mRNA in human non-small cell lung cancer. *Lung cancer*. 2006;52:59-66.

212. Järvelä S, Parkkila S, Bragge H, Kähkönen M, Parkkila AK, Soini Y, Pastorekova S, Pastorek J and Haapasalo H. Carbonic anhydrase IX in oligodendroglial brain tumors. *BMC cancer*. 2008;8:1.

213. Rios EJ, Fallon M, Wang J and Shimoda LA. Chronic hypoxia elevates intracellular pH and activates Na^+/H^+ exchange in pulmonary arterial smooth muscle cells. *American journal of physiology Lung cellular and molecular physiology*. 2005;289:L867-74.

214. Weissmann N, Voswinckel R, Hardebusch T, Rosseau S, Ghofrani HA, Schermuly R, Seeger W and Grimminger F. Evidence for a role of protein kinase C in hypoxic pulmonary vasoconstriction. *The American journal of physiology*. 1999;276:L90-5.

215. Goirand F, Bardou M, Guerard P, Dumas JP, Rochette L and Dumas M. ETA, mixed ETA/ETB receptor antagonists, and protein kinase C inhibitor prevent acute hypoxic pulmonary vasoconstriction: influence of potassium channels. *Journal of cardiovascular pharmacology*. 2003;41:117-25.

216. Tsai BM, Wang M, Pitcher JM, Meldrum KK and Meldrum DR. Hypoxic pulmonary vasoconstriction and pulmonary artery tissue cytokine expression are mediated by protein kinase C. *American journal of physiology Lung cellular and molecular physiology*. 2004;287:L1215-9.

217. Miao Q, Shi XP, Ye MX, Zhang J, Miao S, Wang SW, Li B, Jiang XX, Zhang S, Hu N, Li J and Zhang J. Polydatin attenuates hypoxic pulmonary hypertension and reverses remodeling through protein kinase C mechanisms. *International journal of molecular sciences*. 2012;13:7776-7787.

218. Ahmed S, Ahmed A, Säleby J, Bouzina H, Lundgren J and Rådegran G. Elevated plasma tyrosine kinases VEGF-D and HER4 in heart failure patients decrease after heart transplantation in association with improved haemodynamics. *Heart and vessels*. 2020;35:786-799.

219. He Y, Cao X, Liu X, Li X, Xu Y, Liu J and Shi J. Quercetin reverses experimental pulmonary arterial hypertension by modulating the TrkA pathway. *Experimental cell research*. 2015;339:122-34.

220. Sklepkiewicz P, Schermuly RT, Tian X, Ghofrani HA, Weissmann N, Sedding D, Kashour T, Seeger W, Grimminger F and Pullamsetti SS. Glycogen synthase kinase 3beta contributes to proliferation of arterial smooth muscle cells in pulmonary hypertension. *PLOS one*. 2011;6:e18883.

11. Acknowledgements

As I embarked on the journey of this doctoral thesis, I quickly realized the importance of guidance, collaboration, and the collective wisdom of peers, mentors, and loved ones. Thus, as I stand on the threshold of completion, it is with deep humility and gratitude that I acknowledge the indispensable role played by numerous individuals in shaping this scholarly endeavor.

I would like to begin by expressing my profound gratitude to my supervisor Professor Dr. Ralph Schermuly, for the invaluable opportunity to work within his esteemed research group at the Laboratory for Pulmonary Pharmacotherapy, Excellence Cluster Cardio Pulmonary Institute, Department of Internal Medicine, Justus Liebig University Giessen. His unwavering commitment to excellence, coupled with boundless patience and encouragement, propelled me forward even in the face of formidable challenges. I extend my sincerest thanks for his guidance, wisdom, and unwavering belief in me.

I am deeply grateful to my first supervisor, Prof. Dr. Ivan Manzini, for their exceptional support and mentorship throughout the course of this project. Their expertise and unwavering commitment have played a pivotal role in shaping the outcome of this work. Furthermore, their encouragement and insightful feedback have fostered my personal and academic development in invaluable ways.

I am indebted to my postdoctoral mentor, Dr. Djuro Kosanovic, whose guidance illuminated the path I now proudly tread. Working alongside him has been an enriching experience, and I am grateful for his mentorship and friendship. *Hvala šefe!* I also extend my gratitude to Dr. Oleg Pak for his unconditional sharing of scientific knowledge and creative insights during our discussions.

Special thanks are due to Professor Dr. Norbert Weissmann and Professor Dr. Katja Sträßer, whose suggestions, support, and professional commitment were instrumental in bringing this thesis to fruition, as well as to Professor Dr. Werner Seeger, Director of the Medical Clinic II and Chairmen of the German Centre for Lung Research (DZL), for providing a stimulating international research environment.

I am deeply appreciative of the faculty and administrative members of the GGL and MBML Graduate Programs for their significant influence on my scientific progression and the development of crucial career-building skills.

I extend my gratitude to the individuals listed below for their valuable exchange of opinions and practical assistance: Dr. Akylbek Sydykov, Prof. Dr. Natascha Sommer, Prof. Dr. Hossein Ardeschir Ghofrani, Prof. Dr. Henning Gall, Prof. Dr. Khodr Tello, Dr. Argen Mamazhakypov, Dr. Astrid Weiss, Prof. Dr. Friedrich Grimminger, Prof. Dr. Elie El Agha, Dr. Baktybek Kojonazarov, Dr. Nabham Rai, Dr. Swathi Veeroju, Dr. Ingrid Henneke, Dr. Thomas Sontag, Dr. Simone Kraut, Jan Ewert, Franz Loeffler, Daniel Gerd Bermes, Dr. Simon Platzek, Julia Faupel, Edma Loku and Anis Cilic.

Special thanks also go to Nils Schupp, Carmen Homberger, Ingrid Breitenborn-Müller, Sophia Hattesohl and Miriam Wessendorf for their unwavering support and technical assistance.

To my dear friends and colleagues, including: Christina Pilz, Karin Quanz, Elizabeta Krstic, Dr. Stefan Hadzic, Dr. Marija Gredic, Dr. Cheng-Yu Wu, Dr. Mira Y. Gökyildirim, Dr. Claudio Nardiello, Dr. Claudia Fernanda Garcia Castro, Dr. Ipek Vartürk-Özcan and Prof. Dr. Malgorzata Wygrecka, your presence has brought joy and warmth to my academic journey. I am grateful for the smiles, laughter, and camaraderie we shared.

Lastly, I express heartfelt gratitude to my parents, Slavica and Milomir, and my sister, Aleksandra, for their boundless love, trust, and unwavering support. Thank you for being my pillars of strength. Hvala!